Natural Product Reports

# Vibrational Optical Activity for Structural Characterization of Natural products

| | |
|---|---|
| Journal: | *Natural Product Reports* |
| Manuscript ID | NP-REV-05-2020-000025.R1 |
| Article Type: | Review Article |
| Date Submitted by the Author: | 21-Jun-2020 |
| Complete List of Authors: | Polavarapu, Prasad; Vanderbilt University,<br>Santoro, Ernesto; Università della Basilicata, Dipartimento di Scienze |
| | |

# Vibrational Optical Activity for Structural Characterization of Natural products

Prasad L Polavarapu* and Ernesto Santoro

Department of Chemistry, Vanderbilt University, Nashville, TN 37235

## Abstract

This review presents the recent progress towards elucidating the structures of chiral natural products and applications using vibrational optical activity (VOA) spectroscopy. Vibrational circular dichroism (VCD) and vibrational Raman optical activity (VROA) are two separate branches of VOA spectroscopy, providing independent and complementary structural information. While determining the absolute configuration (AC) of a given natural product is the primary goal, the determination or assessment of major conformations associated with each diastereomer is also a significant part of this enquiry. The latest developments in experimental and computational aspects of VOA spectroscopies and their applications for inferring the AC and predominant conformations of natural products are summarized. The prospects and limitations in the application of VOA spectroscopy to new natural products are summarized.

## 7. Acknowledgments

## 8. Notes and References

# 1. Introduction

The structures of chiral molecules can be elucidated from the interaction between chiral molecules and circularly polarized light. This branch of research, referred to as chiroptical spectroscopy, is comprised of different phenomena.[1, 2] One is circular dichroism (CD), a measure of differential absorption of left and right circularly polarized incident light. Electronic circular dichroism (ECD) deals with CD originating from molecular electronic transitions. The second is optical rotatory dispersion (ORD) in the visible spectral region, also derived from molecular electronic transitions. ECD and ORD are interdependent, due to Kramers-Kronig relationship between them,[3] and are collectively referred to as electronic optical activity (EOA). A newer research area, evolving since early 1970s, is vibrational circular dichroism (VCD) that deals with CD arising from molecular vibrational transitions.[4, 5] Vibrational Raman optical activity (VROA), also evolving since early 1970s and arising from molecular vibrational transitions, is a distinctly different phenomenon dealing with differential scattering of right and left circularly polarized light.[6, 7] VCD and VROA are collectively referred to as vibrational optical activity (VOA).

The conventional vibrational absorption (VA), or infrared (IR), spectra are generally obtained using unpolarized IR light and measuring the absorbance of the sample as a function of incident light wavelength (or wavenumber). VCD can be visualized as an extension of VA, obtained using alternating left and right circularly polarized infrared light and measuring the difference in absorbance (see Section 2.1.1). Vibrational Raman spectra are generally obtained using unpolarized, or linearly polarized, visible laser light and measuring the scattered light intensities as a function of wavenumber shift associated with the scattered light. VROA can be visualized, as an extension of vibrational Raman, obtained using alternating right and left circularly polarized incident laser light and measuring the difference in scattered intensities for a given linear scattered polarization (see Section 2.1.2).

The number of accessible molecular vibrational transitions is far greater than the corresponding number of electronic transitions, which endows VOA with increased information content. Moreover, vibrational transitions involving different regions of space in the molecule permit selectivity. This situation is contrary to the chromophoric electronic transitions, that are restricted to the chromophores in ECD measurements. These two differences render VOA enhanced opportunities for molecular structure elucidations.

The determination of molecular structures of natural products is a challenging task. Despite the use of multiple established methods, errors do occur in determining the structures.[8-11] Therefore, it is important not only to develop new methods, but also to apply as many different methods as possible, for arriving at confident structure determinations. NMR is an indispensable tool to ascertain the relative configurations of natural products. However, situations do exist where its application may not be successful and VOA spectroscopy provides a useful alternative. This point will be evident among some of the studies reviewed here. Another technique encountered for characterizing the natural products is conventional ECD spectroscopy. ECD spectra undoubtedly provide powerful means to ascertain the AC of molecules containing two interacting chromophores via the exciton coupling phenomenon. However, it is appropriate to recapitulate

the limitations of this widely used method. (a). ECD spectroscopy cannot be used in the absence of chromophores that absorb in the visible spectral region; (b). If the chromophore is not directly attached to the chiral center of interest, then the resulting ECD signals are often weak and difficult to interpret; (c). ECD spectra are often inadequate for discriminating between diastereomers. VOA spectroscopy can provide a better approach in such cases and this point will also be evident in the studies reviewed here. It should be added that, identifying the limitations of other methods do not make the VOA spectroscopy infallible. As with any new scientific method, certain limitations trail the potential advantages and it is important to be cognizant of these limitations, which are summarized in the final section of this review.

Recently two reviews have been reported on the applications of ECD and ORD to natural products, one by Grauso et al[12] and another by Mandi and Kurtan.[13] The later review has also included some applications of VCD. The current review of applications of VCD and ROA to natural products, covering the years 2015-2019, is timely because a large number of applications have appeared since the last review on this topic by Batista and coworkers.[14]

# 2. Experimental and Theoretical Background

Practicing natural product scientists are likely to find details on three aspects of VOA spectroscopy useful: (a). experimental methods, which include instrumentation for undertaking the experimental measurement of VOA spectra; (b). theoretical predictions of VOA spectra using modern quantum chemical (QC) computation methods; and (c). Analysis of experimental and theoretical spectra to deduce the absolute configurations. Recent review articles, individually covering either VCD or VROA spectroscopy, can be consulted for a more in-depth background information.[15-21]

## 2.1. Experimental methods

The instrumentation for VCD and VROA spectral measurements is based around the conventional IR and Raman spectrometers, respectively, with two major differences: (a). generation of alternating circular polarizations of light; and (b). detection of synchronous difference in absorbance or scattering intensities. While these differences by themselves are not insurmountable, reliable measurements become challenging owing to the fact that the VCD and VROA magnitudes are of the order of one part in $10^4$ to $10^6$. In the early years of development of VOA, the experimental measurements were tedious because, most early researchers had to build their own VCD and VROA instruments. This situation has now changed. Owing to the availability of commercial instruments, spectral measurements have now become routine for both VCD and VROA. Succinct details on instrumentation, sample handling, and suitable solvents for liquid solution phase measurements are given below.

### 2.1.1. Vibrational circular dichroism

VCD spectroscopy had its beginnings in the first experimental measurements in early seventies[4, 5] and has now flourished into a mature field of research, as reflected by dedicated books available on the subject.[2, 22-24]

*2.1.1.1. Instrumentation*. For latest developments in VCD instrumentation, recent articles can be consulted.[25-27] A majority of the VCD measurements are being conducted in the mid-infrared (Mid-IR) region (~2000-900 $cm^{-1}$) because observed VCD bands in this region can be adequately interpreted using theoretical predictions within harmonic approximations. Those in the higher energy hydrogen stretching region (~3500-2500 $cm^{-1}$ region) are usually complicated by the presence of anharmonic effects, while the measurements in the lower energy region (~900-100 $cm^{-1}$)[28] are not yet established. Most of the current Mid-IR VCD measurements are based around Fourier transform infrared (FTIR) spectrometers, while the grating-based dispersion IR spectrometers are limited to individual laboratories, building their own instruments. For VCD measurements, the commercial FTIR instruments have to be modified by inserting a linear polarizer and photoelastic modulator (PEM) in front of the sample. The linearly polarized light exiting the linear polarizer is converted into alternating left and right circular polarizations by the PEM at a high frequency (usually ~ 35 KHz). Since chiral samples exhibit differential absorption for left and right circular polarizations, the signal at the detector oscillates at the same frequency and is processed by a lock-in amplifier. Typical VCD signals are very small (of the order of $10^{-4}$ - $10^{-6}$) compared to the normal IR absorption, and such small signals can be easily overwhelmed by artefacts arising from birefringence in the components in optical train subsequent to PEM. Such artefacts can be minimized by reducing the number of optical components between sample and detector and by scrambling the polarization of light exiting the sample using a second PEM (operating at a slightly different frequency from the first PEM) placed right after the sample (and before the detector).[29] Stokes-Muller matrix analysis provides a deeper insight into the function of dual PEMs.[24] FTIR-VCD instruments with this dual PEM setup[30, 31] are recommended for artefact-minimized VCD measurements.

Most commercial FTIR instruments can be modified as a described above, or an accessory to an existing FTIR instrument can be purchased, for making VCD measurements. The first commercial FTIR-VCD instrument was introduced by BioTools Inc.[32] Some manufacturers of FTIR instruments (Bruker, Jasco and Thermo-Fisher) also supply stand-alone VCD instruments.

It is hoped that the readers will recognize the possibility for artefact VCD signals and not use the commercial instruments as black boxes. The minimal quality control to ensure artefact-free spectra is to measure the spectra for some selected enantiomeric samples as controls and verifying their mirror image quality. Since most natural product samples are not available in both enantiomeric forms, enantiomeric samples related to the desired natural products can serve as controls.

*2.1.1.2. Measurements in Liquid phase*: The solvents suitable for measuring the VCD spectra are those that do not absorb strongly in the IR region of interest. Solvents that permit VCD measurements in a larger chunk of Mid-IR region (2000-900 $cm^{-1}$) are $CCl_4$, $CS_2$, $CHCl_3$, $CDCl_3$, $CH_2Cl_2$, $CD_2Cl_2$, $CD_3CN$, $CD_3OD$, $(CD_3)_2SO$ and THF-$d_8$.

The hydrogen bonding ability of $CD_3OD$ and $(CD_3)_2SO$ solvents should be kept in mind before selecting these solvents. The presence of hydrogen bonding between solvent and solute makes spectral interpretations difficult, because accurately representing hydrogen bonding in theoretical predictions is non-trivial, which renders the analysis of experimental and theoretical spectra difficult.

$H_2O$ represents the least favored solvent for VCD measurements in the Mid-IR region because of strong infrared absorption of $H_2O$ at ~1650 $cm^{-1}$. Very high sample concentrations (of the order of 100 mg/mL) and short path lengths (~ 6 micrometers) are needed for using $H_2O$ as solvent. $D_2O$ solvent can be used in place of $H_2O$, but still the strong absorption of $D_2O$ at ~1200 $cm^{-1}$ limits the spectral region measurable in $D_2O$ solvent.

Liquid samples can be used as such, without dissolving in a solvent, provided the absorbance for vibrational bands of interest, can be kept below 1.0. This can be realized by using different cells with different path lengths, or with a single variable path length cell.

*2.1.1.3. Measurements in gas phase*:[33, 34] The main limitation for the use of gas samples is the low vapor pressure associated with most samples. Gas sample cells for VCD measurements need to be of single-pass type, because reflections in a multi-pass gas cells can cause deterioration of the quality of circularly polarized light with consequential artefacts plaguing the experimental spectra.

*2.1.1.4. Measurements in solid phase*:[35-39] Solid samples have been studied as thin films, mulls or pellets. Thin films are made by dissolving the sample in a suitable solvent and making a film by either drop-cast method or spin coating method. The amorphous films provide better quality artefact free spectra, compared to the micro crystalline films. The mulls are prepared by grinding the sample in nujol mull and pellets are prepared by grinding the sample with KBr powder. In all these cases, precautions are required to ensure that the collected spectra are artefact free. The spectral measurements using the sample holder rotated around the light beam, either manually or in a continuous rotation, are needed to ensure artefact-free spectra.[40] The safest way to ensure artefact-free spectra is to measure the spectra for enantiomeric samples and verifying the mirror image spectra. Most natural product samples are not available in the enantiomeric forms, and therefore verifying the mirror image spectra may not be feasible for natural product samples. In such cases, measurements on some standard samples that are available in enantiomeric form would be needed.

### 2.1.2. Vibrational Raman Optical Activity

VROA spectroscopy had its beginnings in the first experimental measurements in early seventies[6, 7] and has now evolved into a mature field of research as reflected by dedicated books available on the subject.[2, 22, 24, 41]

*2.1.2.1. Instrumentation*. VROA spectra can be measured in different scattering arrangements, namely right angle (90°) scattering, backscattering (180°) and forward (0°) scattering. In each scattering geometry, one can either use linearly polarized incident light and monitor the right and left circular polarizations scattered by the chiral sample or use incident alternating right and left circular polarized laser light and monitor linearly polarized scattered light. An optical design developed by Hug using backscattering (180°) geometry has become the standard for current VROA measurements.[42] In this design, unpolarized visible laser light is shined on to the sample and the scattered right and left circular polarizations scattered by the chiral sample are brought via two separate fiber bundles on to the separate pixels of CCD detector. The sum and difference signals recorded on these pixels provide vibrational Raman and VROA spectra simultaneously.

A commercial instrument supplied by BioTools Inc.[32], is based on this design. As mentioned for VCD measurements, it is important to ensure artefact-free spectra by measuring the spectra for some selected enantiomeric samples as controls and verifying their mirror image quality. Recent articles can be consulted for new developments in VROA instrumentation.[15, 43-45]

*2.1.2.2. Measurements in Liquid phase*: The solvents suitable for measuring the VROA spectra are those that do not have strong vibrational Raman bands. $H_2O$ is an excellent solvent for VROA spectral measurements because of its poor Raman scattering. Liquid samples can be used as such, without dissolving in a solvent. The amount of sample needed for VROA measurements in liquid phase can be as small as a few microliters, because the sample volume need to be just large enough for covering the waist of laser light beam.

*2.1.2.3. Measurements in gas phase*:[46] VROA spectral measurements in vapor phase are possible for only those samples with high vapor pressure.

*2.1.2.4. Measurements in solid phase*: VROA spectral measurements in solid phase are not common due to possible reflection artefacts.

*2.1.2.5. Wavelength of incident laser light*: The Raman scattering intensities are proportional to inverse fourth power of incident laser wavelength while the corresponding VROA intensities are proportional to inverse fifth power of incident laser wavelength. Therefore, shorter wavelength is preferred over longer wavelength for incident laser light. However, if the incident laser wavelength falls near or close to the wavelength of molecular electronic transitions, resonance can take place. In extreme cases, sample burning can occur. With low laser powers, resonance enhanced spectra can be obtained. Resonance enhanced VROA spectroscopy[47, 48] is an evolving field and much knowledge needs to be gained before using this as a practical method. Similarly, surface enhanced VROA[49] is also an evolving field that needs further developments before routine applications can be undertaken.

## 2.2. Theoretical predictions of VOA spectra

Modern QC methods have revolutionized the applications of VCD and VROA spectroscopies because of their ability to reliably predict the spectra for a given chemical structure. For detailed descriptions of QC methods, specialized articles on the subject can be consulted.[50-57] The focus here is to provide a general background needed to adopt QC calculations.

The prediction of VOA spectra for a given sample requires considering multiple pieces of information: (a). possible diastereomers; (b). possible molecular conformers, and their populations, for each diastereomer; (c). vibrational energies (to define the vibrational band positions); (d). vibrational transition moment vectors, for defining the VA and VCD band intensities and vibrational transition polarizability tensors for defining the vibrational Raman and ROA intensities; and (e). line widths (to define the band shapes).

For a given chiral molecule $2^n$ diastereomers are possible, where n represents the number of chiral elements in the molecule. Of these, one-half are enantiomers of the other half. Since enantiomers have mirror image VOA spectra, it is sufficient to undertake calculations for $2^{n-1}$ diastereomers. It

is important to predict VOA spectra for all of the $2^{n-1}$ diastereomers and compare them with the experimental spectra to ascertain if the predicted spectra for only one daistereomer can match the experimental spectrum.

All possible molecular conformers, of each diastereomer to be evaluated, can be determined using one of the many conformation search programs (such as Conflex, Spartan, Macromodel). The vibrational band positions for each conformer are then obtained through a vibrational frequency calculation, which involves determining the force constants (second order derivatives of potential energy with respect to nuclear displacements). This calculation must be undertaken at the minimum of the potential energy curve. In practical terms, this amounts to determining the molecular geometry at the minimum of potential energy curve through a geometry optimization process (an option built into QC programs) for each conformer. The electronic energies at the optimized geometries, or Gibbs energies of the optimized conformers obtained through vibrational frequency calculation, provide estimates of the relative populations of the conformers. Occasionally, one encounters molecules where incorporation of dispersion corrections can make a difference in identifying the energy order for conformations.

VCD spectral intensities for each conformer are determined by two different vibrational transition moment vectors: one is electric dipole transition moment (EDTM) vector and another is magnetic dipole transition moment (MDTM) vector. The calculation of the former has been well established. There are different approaches for the calculation of MDTM: (a). coupled oscillator[2, 58] and generalized coupled oscillator models[59] (b). the magnetic field perturbation approach[60, 61] and (c). nuclear velocity perturbation approach.[62, 63] The dot product of the EDTM vector with itself determines the integrated VA band intensity (or infrared band intensity), while the dot product between EDTM and MDTM vectors determines the integrated VCD band intensity. Although the vibrational frequency and transition moment vector calculations can be undertaken at different levels of theory, it is a common practice to undertake both calculations at the same level of theory (this option, also, built into QC programs). For visual analysis of how nuclear motions influence the electron charge circulation,[64, 65] advanced tools have also been developed for displaying the three dimensional vibrational transition current density maps.[66]

For analyzing the liquid phase VCD spectra, ab initio molecular dynamics (AIMD) simulations, in conjunction with either nuclear velocity perturbation method[67] or Fourier transform of the cross-correlation function of time dependent electric and magnetic dipole moments[68, 69] were used.

VROA spectral intensities are determined by three different vibrational transition polarizabilities. In practical terms, these transition polarizabilities amount to calculating normal coordinate derivatives of electric dipole-electric dipole (EDED), electric dipole-magnetic dipole (EDMD), and electric dipole-electric quadrupole (EDQD) polarizability tensors. While vibrational Raman band intensities are determined solely by the mean and anisotropy of EDED polarizability derivative tensor, VROA band intensities require the calculation of three tensor product invariants. These invariants are: (a). the mean product ($\overline{\alpha}\overline{G}'$) of EDED and EDMD polarizability derivative tensors; (b). anisotropy ($\gamma^2$) of the product of EDED and EDMD polarizability derivative tensors; (c). anisotropy ($\delta^2$) of the product of EDED and EDQD polarizability derivative tensors. A linear

combination of these three invariants, with each invariant multiplied by a scattering geometry dependent coefficient, determines the VROA band intensity.

For non-specialists, it is a common practice to undertake both, vibrational frequency and intensity, calculations at the same level of theory (this option, also, built into QC programs). Although early VOA calculations used the Hartree-Fock theoretical methods, density functional theoretical (DFT) methods have enjoyed much success in recent times. DFT methods involve choosing a combination of a density functional with a basis set. A variety of density functionals and basis sets are built into the QC programs. Larger basis sets demand larger computing time. B3LYP and B3PW91 are the most commonly used density functionals. The smallest basis set suitable for vibrational property calculations is 6-31G*, but with currently available computing processors much larger basis sets such as 6-311++G(2d,2p) or aug-cc-pVDZ are becoming routine.

Because of the extensive computing time demands involved in calculating VROA intensities, some time savings can be realized by using different basis sets for vibrational frequencies and transition polarizabilities.[70] A detailed study on the basis set dependence of vibrational Raman and ROA intensities can be consulted for additional information.[71]

Before undertaking the QC calculations of VOA spectra, one needs to consider the nature of intermolecular interactions that may have influenced the experimental spectra. (a). isolated molecule or vacuum calculations are suitable for interpreting the experimental spectra measured for vapor phase molecules or for liquid solutions involving inert (non-hydrogen bonding and non-interacting) solvents, such as $CS_2$ and $CCl_4$; (b). For liquid solutions made of polar and non-hydrogen bonding solvents, such as $CH_3Cl$ and $CH_2Cl_2$, polarizable continuum model (PCM)[72, 73] or conductor-like screening model (COSMO)[74] can be used to model the electrostatic interaction of a solute molecule with the solvent. (c). For liquid solutions made of hydrogen bonding solvents, such as $H_2O$, $CH_3OH$, $CH_3CN$, and $(CH_3)_2SO$, proper modeling of hydrogen bonding interactions would be needed. These situations can be handled either by including a specified number of explicit solvent molecules hydrogen bonded to the solute molecule, or by modeling a solute molecule in a bath of solvent molecules via molecular dynamics (MD) simulations.[75] The representations of solvent molecules by fluctuating charges, or other means, have been developed for both VCD[76, 77] and VROA[77, 78] calculations.

For interpreting the VROA spectra of neat liquids, AIMD simulation method in conjunction with classical magnetic dipole moments was used to obtain the needed polarizability tensors.[79] Calculations of resonance enhanced VROA spectra require special precautions[80-83] and these applications are not yet routine.

For calculating the VOA spectra of larger molecules, Cartesian tensor transfer[84, 85] and molecules-in-molecules fragmentation[86-88] approaches have been developed.

The conventional methods undertake prediction of vibrational properties for all of the vibrational transitions, even when the experimental VOA measurements are available only for a limited region (VCD in the Mid-IR, VROA in the ~2000-200 $cm^{-1}$ region). There are now methods available to

predict the vibrational properties in selected vibrational frequency range,[89] although this approach is not yet practiced widely.

The predicted VOA spectra can vary depending on the choice of the density functional, as well as the basis set. This type of "method" dependent VOA spectral variations can be subdued by taking weighted average of the VOA spectra obtained from different "methods"[90] and goodness of fit criteria.[91] Such analyses are in the very early stages.

Calculations within harmonic oscillator approximation are generally sufficient for most situations. Anharmonic oscillator calculations,[92, 93] which fall in the purview of specialists, may be undertaken for more rigorous interpretations.

## 2.3. Spectral simulations

The calculated vibrational frequencies and integrated intensities yield the line spectra associated with a given conformer belonging to a chosen diastereomer. When multiple conformers are present, the intensities of each conformer are multiplied with the population of that conformer and population weighted line spectrum is calculated. The populations of conformers are determined from the relative (either electronic or Gibbs) energies obtained during vibrational frequency calculation. The measured experimental spectra contain broad bands, instead of lines. To compare with experimental spectra it is then necessary to convert each spectral line into a simulated band with certain bandwidth. The vibrational band shapes are generally represented by Lorentzian band profiles. Therefore, predicted line spectra are converted into simulated spectra using Lorentzian band profiles. The width associated with spectral lines is chosen in such a way that the simulated band shapes appear similar to those seen in the experimentally observed bands. Two freely available spectral simulation programs, CDSpecTech[94, 95] and SpecDis[96], and one commercial program, VOACompare,[32] can be used for spectral simulations.

## 2.4. Analysis of experimental and predicted VOA spectra

The comparison of predicted spectra for a given diastereomer with experimental spectra can be undertaken in different ways.

*2.4.1.* *Visual comparison analysis*: Here, a given experimental VOA spectrum is either overlaid or stacked above the predicted spectrum and band-to-band comparison is made. The presence of a satisfactory correspondence between experimental and predicted VOA bands, with matching signs, indicates that the AC used for calculations reflects that of the sample used for experimental measurements. On the other hand, if the experimental VOA band signs are opposite to those of predicted VOA bands, then opposite AC is inferred. A reliable calculation should reproduce not only the VOA spectrum, but also the corresponding VA/Raman spectrum. For this reason, the above mentioned analysis for VOA spectrum should accompany the corresponding experimental and predicted VA or Raman spectra. Even though VA or Raman spectral band intensities are all positive, one should make sure that each simulated VA/Raman band corresponds to an experimental band with closely matching intensity. A qualitative visual comparison analysis,

however, need not give unambiguous conclusion and is subject to user bias. For this reason, a quantitative spectral comparison analysis should be preferred.

*2.4.2. Integrated band intensity analysis*:[97, 98] One approach to quantitative comparison between experimental and predicted spectra is to integrate the experimental vibrational bands individually and compare the experimental and predicted integrated intensities. This approach can work for small molecules with a limited number of vibrational bands, but is fraught with difficulties for typical molecules. This is because, condensed phase vibrational spectra are often obtained at low resolution and have overlapping neighboring bands. It would be very difficult to resolve individual experimental vibrational bands, especially when a large number of vibrational bands appear in a small region of interest. As a result, this approach is not popular.

*2.4.3. Similarity Overlap analysis.* In another approach to quantitative comparison, one calculates the similarity overlap between experimental and simulated spectra in the region of interest. Two different similarity overlap functions (Tanimoto similarity index introduced by Shen et al[99] and Carbo similarity index introduced by Bultinck et al[100]) are in current use. These two functions differ only in the way the overlap function is normalized. The similarity overlap functions using Tanimoto index are designated for VA and VCD spectra as *Sim*VA and *Sim*VCD, respectively, and corresponding functions for Raman and ROA spectra as *Sim*Raman and *Sim*ROA, respectively. The ranges for *Sim*VA and *Sim*Raman values are from 0 to +1 and those for *Sim*VCD and *Sim*ROA values are from -1 to +1. The similarity overlap functions using Carbo index are designated as similarity index (SI), which has the same ranges as those for *Sim* functions. Bultinck et al have introduced a new measure, called enantiomeric similarity index (ESI),[100] for VCD spectra. The range for ESI values is from 0 to +1 and a high ESI value indicates that the spectra computed for one of the enantiomers has a better agreement with the experimentally measured spectrum. Using a VCD database for compounds of known ACs, and their ESI values, a confidence level measure was also introduced for the proposed AC assignments.

In the analysis of experimental and simulated VOA spectra, *Sim*VCD/*Sim*ROA value of +1 indicates perfect agreement, suggesting that the AC used for calculations corresponds to that of the sample used for experimental measurements. A *Sim*VCD/*Sim*ROA of -1 indicates opposite AC. In practice, maximum values of +1/-1 are never realized, but one hopes to obtain high similarity overlap values, approaching +1/-1.

The predicted vibrational frequencies are usually shifted from the corresponding experimentally observed vibrational frequencies. For this reason, predicted vibrational frequencies are normally scaled by a constant. Since the optimal scaling factor depends on the theoretical level used, similarity overlap values are evaluated with varying scaling factor to find the scaling factor that yields maximum overlap. A spectral similarity overlap (SSO) plot displays the similarity overlap as a function of the frequency scaling factor.

The analysis of experimental VCD or VROA spectra should always accompany the corresponding VA or Raman spectra, because the quantities that determine the VA/Raman intensities are also a part of those that determine the VOA intensities. The corresponding similarity overlap analysis for VA or Raman spectra (always positive, with a maximum value of +1) indicates the level of

agreement for the associated VA or Raman spectra. Different similarity overlap analysis programs[32, 94-96] are available for this purpose.

*2.4.4. Analysis of experimental and predicted ratio spectra.* In addition to analyzing the VCD and VA spectra individually, one can also evaluate the ratio of VCD to VA. This ratio represents dimensionless vibrational dissymmetry factor (VDF). Similarly, in addition to analyzing the VROA and VA spectra individually, one can also evaluate the ratio of vibrational ROA to Raman. This ratio represents dimensionless vibrational circular intensity difference (CID). Similarity overlap function of VDF, designated as *Sim*VDF, provides much more stringent criterion, than *Sim*VCD alone, for analyzing the experimental and predicted VCD spectra and hence of the AC assignment. In the same vein, similarity overlap function of vibrational CID, designated as *Sim*CID, provides much more stringent criterion, than *Sim*ROA alone, for analyzing the experimental and predicted ROA spectra and hence of the AC assignment. There is one freely available program[94, 95] for the similarity overlap analysis of VDF and/or CID.[101-107]

While a spectral similarity overlap of 1 is the desired goal that is almost never achieved in practice, a realistic goal is to look for a spectral similarity overlap of $\sim 0.4$, or greater,[105] for VCD and VDF in the VCD spectral analysis and for ROA and CID in the ROA spectral analysis. Higher similarity overlap values are generally seen for conventional VA and Raman spectra.

For illustration purposes, the comparisons of experimental and predicted VA, VCD, and VDF spectra in the 1475-925 $cm^{-1}$ region, and Raman, ROA and CID spectra in the 1800-200 $cm^{-1}$ region, are shown, respectively, in Figures 1 and 2. The experimental and predicted spectra overlaid in Figures 1 and 2 provide visual spectral comparison to assess the degree of agreement between them. A quantitative assessment of this agreement can be gained from the SSO plots in Figure 3. In these plots, the maximum *Sim*VA, *Sim*VCD and *Sim*VDF values are, respectively, 0.91, 0.66 and 0.60; the maximum *Sim*Raman, *Sim*ROA and *Sim*CID values are, respectively, 0.66, 0.79, and 0.82.

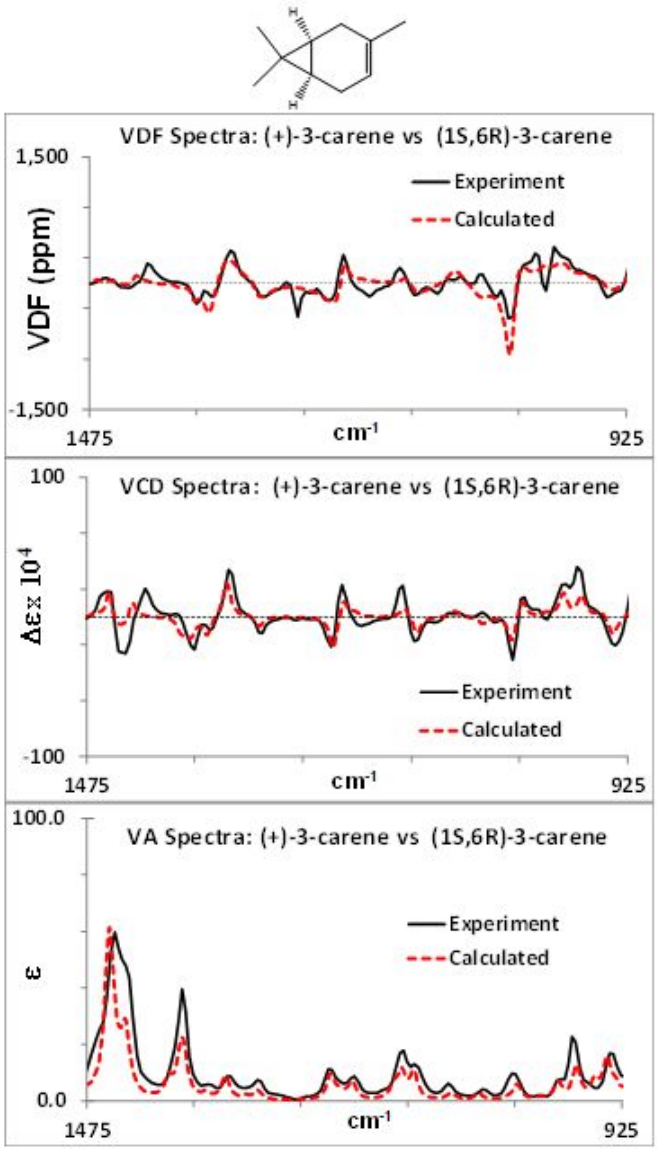


**Figure 1**. Comparison of experimental VA (bottom panel), VCD (middle panel) and VDF spectra in $CCl_4$ solvent with corresponding predicted spectra at B3LYP/aug-cc-pVDZ level. Data replotted with permission from Ref.[105] Copyright (2017) John Wiley and Sons.

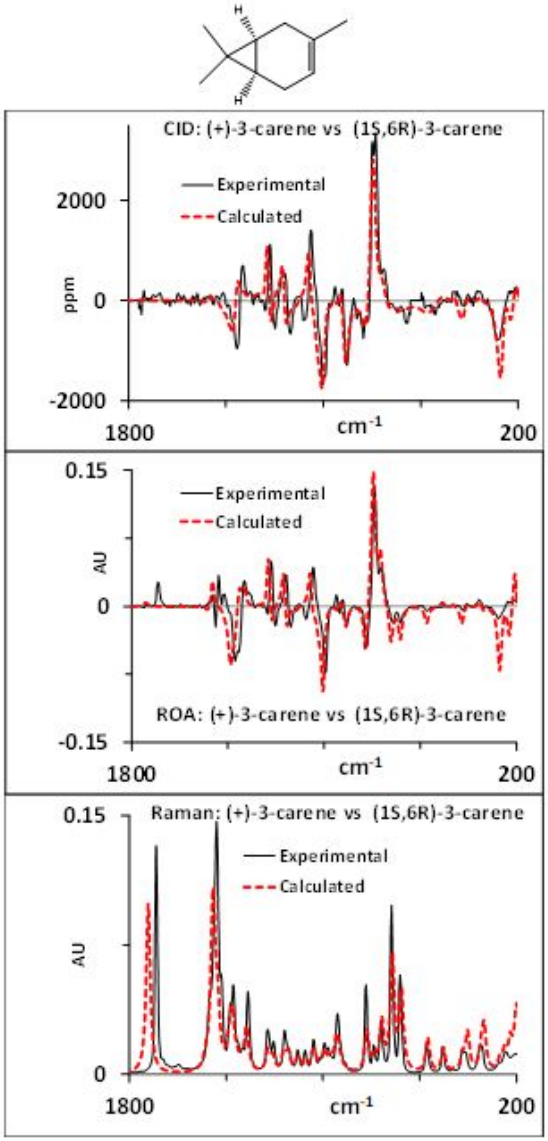


**Figure 2**. Comparison of experimental vibrational Raman (bottom panel), ROA (middle panel) and CID spectra of liquid sample with corresponding predicted spectra at B3LYP/aug-cc-pVDZ level. Data replotted with permission from Ref.[105] Copyright (2017) John Wiley and Sons.

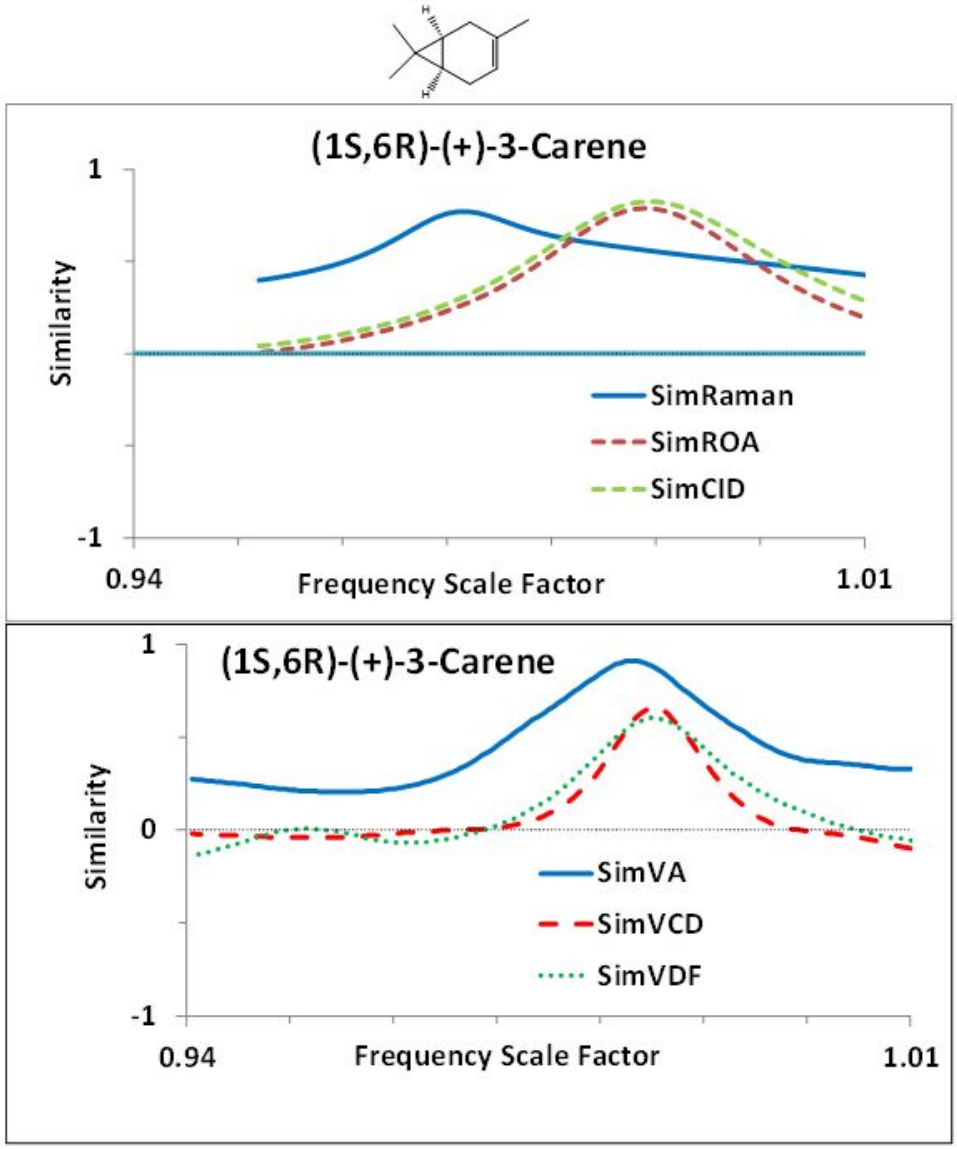


**Figure 3**. Spectral similarity overlap plots for VA, VCD and VDF (Bottom panel) and Raman, ROA and CID (top panel). The maximum *Sim*VA, *Sim*VCD and *Sim*VDF values are, respectively, 0.91, 0.66 and 0.60. The maximum *Sim*Raman, *Sim*ROA and *Sim*CID values are, respectively, 0.66, 0.79, and 0.82. *Sim*VCD and *Sim*VDF profiles appear sharper than those for *Sim*ROA and *Sim*CID, because the latter are obtained from a wider vibrational region (1800-200 $cm^{-1}$), while the former are obtained in a narrower vibrational region (1475-925 $cm^{-1}$). Data replotted with permission from Ref.[105] Copyright (2017) John Wiley and Sons.

Although VCD and VROA spectroscopies originate from fundamentally different phenomena, both techniques probe the same molecular vibrations, but provide independent and complementary structural information. The comparisons of experimental and predicted VCD spectra in Figure 1, and quantitative similarity analysis in Figure 3, provide confirmation that the AC of the sample used for experimental measurements is that used for theoretical predictions. An

independent confirmation of this conclusion is seen from the comparisons of experimental and predicted VROA spectra in Figure 2, and corresponding similarity analysis in Figure 3.

It should be noted that, different researchers follow different formats for spectral presentation. Some publications contain the data corresponding to the bottom two panels of either Figure 1 or 2. For this reason, the format of some of the figures reproduced from literature in the following sections will be different from that shown in Figures 1-3.

# 3. Applications of Vibrational Circular Dichroism

In this section we present a comprehensive list of compounds subjected to VCD investigations during years 2005-2019. It is our hope that the new, as well as established, researchers benefit from such periodic state-of-the-art reviews. Since individual laboratories focus on specific chiral natural products of their own research interest, we find it difficult to classify the reported natural product studies into a limited generalized categories. For this reason, the subtitles in the following sections pertain to compounds (or a group of compounds) in individual investigations.

***Cepharanthine*** (**Scheme 1**, **structure 1**): This compound isolated from *Epigeal Srephaia* roots, has been used for a wide variety of medicinal applications. Based on chiroptical spectroscopic studies it was suggested[108] that previously stated AC of cepharanthine, (+)-(1*R*,10*S*), and also those of some of its analogues, have to be revised. While the experimental specific rotation at sodium D line is +230, the corresponding calculated values for (1*R*,10*S*) at B3LYP/6-311+G(d) level were +25 in gas phase and +60 using PCM representing the solvent. On the other hand, those calculated for (1*R*,10*R*) at B3LYP/6-311+G(d) level were +181 in gas phase and +206 using PCM representing the solvent. The experimental SORs at other wavelengths, namely 365, 405, 436 and 546 nm, also matched poorly with those calculated for (1*R*,10*S*), but matched better with those calculated for (1*R*,10*R*). These observations suggested that the originally assigned (+)-(1*R*,10*S*) has to be reassigned as (+)-(1*R*,10*R*). This assessment was supported by the analysis of experimental ECD, as well as VCD, spectra of (+)-cepharanthine with corresponding calculated spectra for (1*R*,10*S*) and (1*R*,10*R*) configurations. Similar investigations were undertaken for cepharanthine derivatives and it was suggested that the ACs of 13, out of a total of 37, cepharanthine analogues are to be reassigned.

***Anacolosins A-F and Corymbulosins X and Y, Clerodane Diterpenes***: Eight new compounds, Anacolosins A−F (**Scheme 1**, **structures 2-7**) and Corymbulosins X and Y (**Scheme 1**, **structures 8, 9**), and two known compounds, one with unassigned name, **10**, and caseamembrin S, **11**, isolated from the plant *Anacolosa clarkii* Pierre (Olacaceae) displayed cytotoxic activities against pediatric solid tumor cell lines.[109] The relative configurations of these compounds were determined from $^{1}$H NMR coupling constant data, and ROESY experiments. While the ACs of two of these compounds, Anacolosin A and Anacolosin B, were determined from VCD and ECD spectral analyses, those of the rest were derived from ECD spectral analyses. For Anacolosin D, ECD was unable to distinguish between (*R*) and (*S*) configurations at C-2′, so hydrolysis products were analyzed, and found to be consistent with the (*S*) configuration at C-2′. The experimental ECD spectra were analyzed with those predicted at the CAM-B3LYP/SVP level. The experimental VCD spectra were analyzed with those predicted at the B3LYP/6-31+G(d,p) level. Qualitative visual

comparisons were used to assess the match between experimental and predicted ECD and VCD spectra.

***Azaphilone derivatives***: Six new azaphilone derivatives, pleosporalones B and C and pleosporalones E−H and one known analogue pleosporalone D, but with unassigned AC, were derived from fungus *Pleosporales* sp. CF09-1 (**Scheme 1**, **structures 12-18**).[110] The AC at C-7 in pleosporalones B-D was based on the literature assignment, leaving the ACs at chiral centers C-2' and C-3' as unknowns. The relative configuration at these two chiral centers derived from NOESY experiments left two possibilities, (2′*S*,3′*R*) and (2′*R*,3′*S*), for the assignment of AC of pleosporalones B-D. To address this issue, the experimental ECD spectra were measured for pleosporalone D, and corresponding spectra calculated for (2′*S*,3′*R*) and (2′*R*,3′*S*) structures, using B3LYP functional and 6-311++G (2d,p) basis set. The calculated ECD spectra for these two structures were similar and therefore ECD was not useful to resolve the issue. Then the experimental VCD spectra were measured for pleosporalone D at a concentration of 10.0 mg in 120 microL of $CDCl_3$ and the corresponding spectra calculated for (2′*S*,3′*R*) and (2′*R*,3′*S*) structures using B3LYP functional and 6-311+G(d) basis set. On visual comparison, the experimental spectrum was considered to be better reflected by the calculated spectrum for (2′*S*,3′*R*) structure. Based on shared biogenesis, the same assignment was proposed for pleosporalone B and C. Pleosporalones E and F were determined to be epimers based on the NMR data, differing in the AC at C-11. ECD spectra of Pleosporalones E and F were almost identical, indicating that the ECD method had limitations in the assignment of the C-11 absolute configuration. The computed VCD spectra and SORs were also similar for the two epimers, leading to the conclusion that ECD, VCD or SOR are unable to distinguish between the epimers, Pleosporalones E and F. The authors have then used the experimental chemical shift differences and compared them with corresponding chemical shift differences. Based on these chemical shift differences, the configurations of C-11 for Pleosporalones E and F were suggested to be *R* and *S*, respectively. However, the chemical shift differences for epimers G and H could not resolve the AC at C-11 and therefore, the AC at C-11 in Pleosporalones G and H remained unassigned.

***(-)-Crispine A analogue*** (**Scheme 2**, **structure 19**)[107]: (1*R*,10*bR*)-1'-((*R*)-1,2-Dihydroxyethyl)-1-hydroxy-8,9-dimethoxy1,5,6,10b-tetrahydropyrrolo [2,1-a]isoquinolin-3(2H)-one, an analogue of (-)-crispine A, with three stereogenic centers was synthesized from garcinia acid (a natural product isolated from tropical plant native to South Asia), and its absolute configuration (AC) established using the combined information derived from synthetic scheme and x-ray single crystal diffraction data. The AC of **19** could be correctly established using VCD, when the relative configuration is constrained to be that derived from x-ray data, or the ACs of two of the chiral centers are constrained to be those derived from the synthetic scheme. In the absence of this outside information, it was found that VCD spectral analysis alone is not sufficient to determine the AC. However, VDF spectral analysis, supplemented with electronic dissymmetry factor analysis, was able to determine the correct AC.

***Frondosin B:*** (**Scheme 2**, **structure 20**) Chiral natural product molecules are often assumed to be in an enantiomerically pure or enriched form.[111] Such information is often derived from an assessment of experimental specific rotations. However, experimental specific rotations often can have large errors either because of small amounts of samples used, or because of the presence of chiral impurities in the natural product samples. This happened to be the case when total synthesis

of **20** (originally extracted from marine sponge) was undertaken and the presence of a minor impurity (~7%) present in the late step of synthesis changed the sign of observed specific rotation. This sign reversal influenced the literature assignment of AC for this natural product. Experimental VCD and ECD measurements were used to determine the AC of synthesized **20** as **(*R*)**,[112] and this investigations led to the identification of minor impurities that resulted in conflicting assignments of AC in the earlier synthetic efforts.

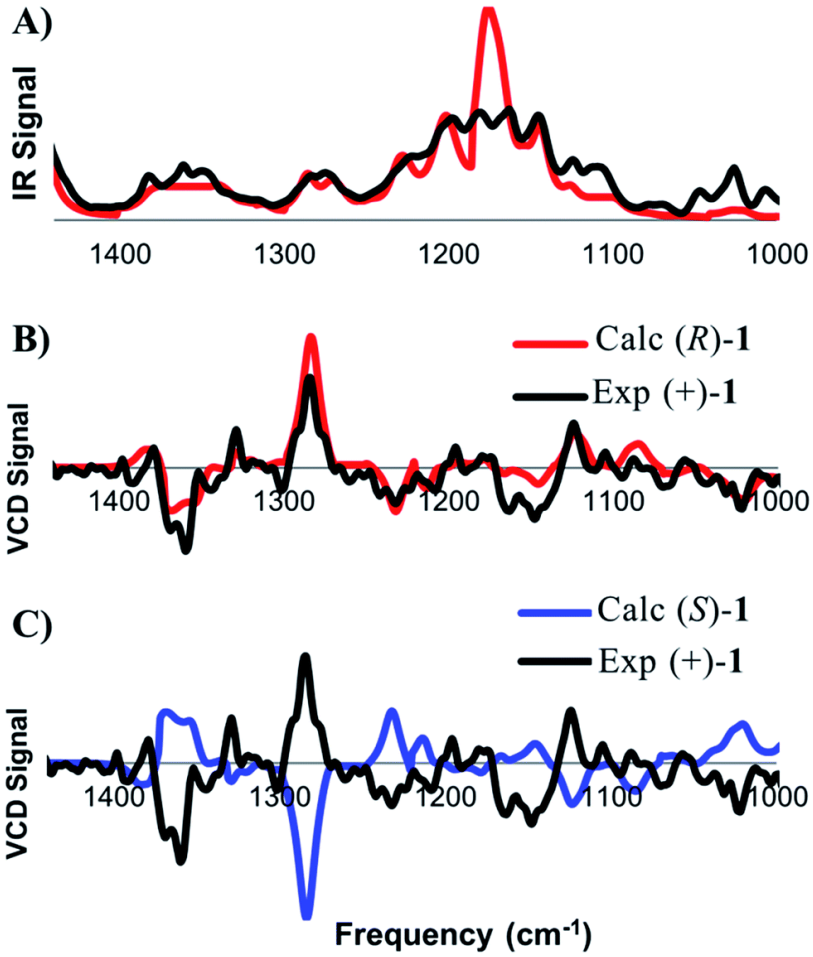


**Figure 4**. Experimental and predicted VCD spectra of **20**. This investigation helped uncover the source for conflicting literature AC assignments made for **20**. Reprinted from Ref[112] with permission from the Royal Society of Chemistry.

***Dibenzoylmethanes***: C-8 substituted dibenzoylmethanes (DBMs), assume a di-keto form, which generates a chiral center at position 8. The AC of the chiral center generated in C-8 substituted DBMs was not known. To address this issue, 2'-methoxy-8-(α-α-dimethylallyl)-[3',4':4",5"]-furan-dibenzoylmethane (**Scheme 2**, **structure 21**) a C-8 substituted DBM was isolated from the plant roots of *Dahlstedtia glaziovii*, and its AC was determined to be (*S*) based on the experimental and calculated VCD spectrum.[113] The presence of two carbonyl groups, flanking the chiral center, leads to the generation of bisignate VCD couplet originating from the two C=O stretching vibrations.[2, 58] The VCD spectra calculated using B3LYP functional and 6-31G(d) basis set for (*S*)

configuration reproduced the experimentally observed positive bisignate couplet (positive VCD at lower wavenumber and negative VCD at higher wavenumber). Based on this agreement, the AC of isolated 2'-methoxy-8-(α-α-dimethylallyl)-[3',4':4",5"]-furan-dibenzoylmethane was concluded to be (*S*).

***Citrinin derivatives***: These are a class of bioactive polyketide compounds isolated from the fungal genera *Penicillium*, *Aspergillus* and *Monascus*. Penicitrinone A (**Scheme 2**, **structure 22**), a citrinin derivative, was obtained from the Bohai Sea fungus *Penicillium janthinellum*.[114] The experimental ECD spectra were measured for the isolated compound and analyzed with calculated ECD spectra using B3LYP functional and 6-311+G(d) basis set. However, this analysis could not discriminate between (2'*R*,3'*S*,3*R*,4*S*) and (2'*S*,3'*R*,3*R*,4*S*) diastereomers. Then the VCD spectra were measured for the isolated compound at a concentration of 12.0 mg in 120 microL of $CDCl_3$ and analyzed quantitatively with calculated VCD spectra using B3LYP functional and 6-311+G(d) basis set. For (2'*R*,3'*S*,3*R*,4*S*) diastereomer, quantitative analysis yielded *Sim*VA: 0.89; *Sim*VCD: 0.46; *Sim*VDF: 0.40, while the corresponding numbers for (2'*S*,3'*R*,3*R*,4*S*) diastereomer were *Sim*VA: 0.85; *Sim*VCD: 0.19; *Sim*VDF: 0.10. A few additional calculations using PCM, as well as different basis sets, were considered not to have improved the agreement between experimental and calculated VCD spectra. Based on this analysis, the absolute configuration of isolated Penicitrinone A was concluded to be (2'*R*,3'*S*,3*R*,4*S*). This assignment was further supported via NMR shift calculation using the mPW1PW91 functional 6-311+G(d,p) basis set.

***Metabolites Isolated from Rutstroemia***: Isolation and identification of three chiral compounds 9-O-methylfusarubin, 5-O-methylnectriafurone and terpestacin, from a diseased *Bromus tectorum* plant, were reported.[115] Terpestacin compound was previously known in the literature. The unknown absolute stereochemistry at C-3 of 9-O-methylfusarubin (**Scheme 2**, **structure 23**) was determined from the analysis of experimental ECD and VCD spectra with the corresponding calculated spectra. ECD calculations using B3LYP functional and def2-TZVP basis set, and VCD calculations using ωB97X-D functional and 6-311+G(d,p) basis set, both with PCM representing the solvent, were used for analyzing the corresponding experimental spectra. VCD similarity indices indicated 0.57 for (*R*) enantiomer and 0.037 for the (*S*) enantiomers by VCD. Therefore, AC of isolated 9-O-methylfusarubin was inferred as (*R*).

***Jonquailine***: (**Scheme 2**, **structure 24**) This alkaloid isolated from *Narcissus jonquilla quail* (an Amaryllidaceae species plant) shows significant activity against several malignant cancer cell types. The AC at C-3, C-4a and C-6a and at the junction of rings B, C and D have been taken from the literature studies. But AC at C-8 remained unknown. To resolve this issue, experimental ECD, ORD and VCD spectral measurements were analyzed with corresponding predicted data, the calculations were undertaken for two diastereomers, (12b*S*,3*S*,4a*S*,6a*R*,8*S*) and (12b*S*,3*S*,4a*S*,6a*R*,8*R*).[116] The ECD spectra were calculated using CAM-B3LYP functional and aug-cc-pVDZ basis set using the geometries optimized at B3LYP functional and TZVP basis set. The computed ECD spectra for the two diastereomers were similar, so ECD could not be used for diastereomer discrimination. Then SOR values calculated using B3LYP functional and aug-cc-pVDZ basis set, at different wavelengths, for the two diastereomers were compared to the corresponding experimental data. The magnitudes of predicted SOR values for (8*R*) configuration are closer to the experimental magnitudes, but that alone does not provide a solid evidence for AC assignment. Then experimental VCD spectra were compared to those predicted for the two

diastereomers using B3LYP functional and 6–311+G(d,p) basis set (Figure 5). Quantitative similarity analysis indicated better agreement of experimental VCD spectrum with that calculated for (8*R)*. Thus, the AC of isolated Jonquailine was determined to be (12b*S*,3*S*,4a*S*,6a*R*,8*R*).

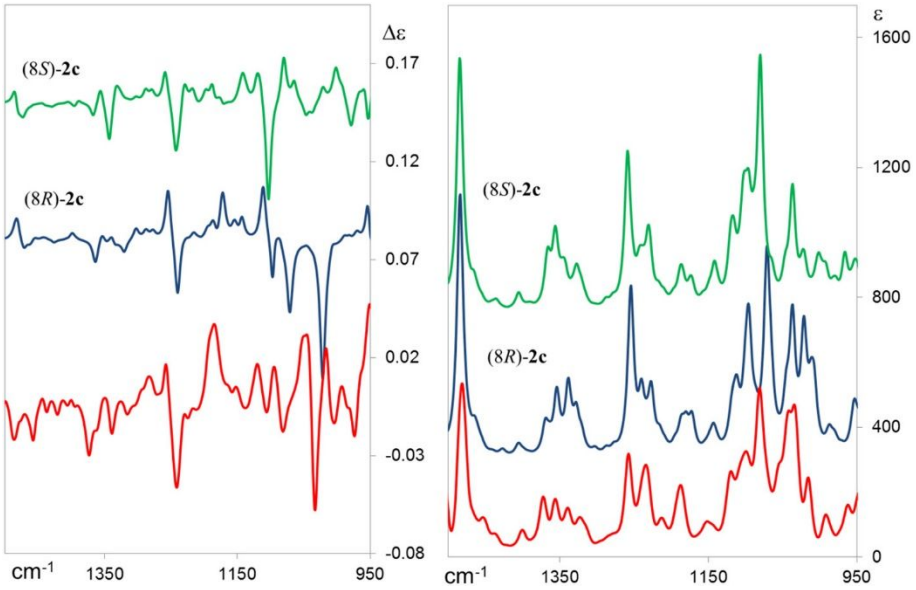


**Figure 5**: Experimental (red trace) and predicted spectra for **24**. While ECD spectra were unable to distinguish between (12b*S*,3*S*,4a*S*,6a*R*,8*S*) and (12b*S*,3*S*,4a*S*,6a*R*,8*R*) diastereomers, VCD spectra were able to assign (12b*S*,3*S*,4a*S*,6a*R*,8*R*) for **24**. Reprinted with permission from Ref.[116] Copyright Elsevier (2018).

***Triterpenoids***: Although two triterpenoids, icetexone and conacytone, (**Scheme 2**, **structures 25, 26**), were isolated four decades ago from *Salvia ballotaeflora* plant, their characterization left several uncertainties. To alleviate this situation, new x-ray crystal structures were obtained for icetexone and conacytone, using Cu Kα radiation, which permitted calculation of Flack and Hooft parameters and establishing ACs.[117] As an independent confirmation of the ACs of icetexone and conacytone, experimental VCD spectra were measured for their acetate derivatives, namely icetexone acetate and conacytone triacetate. The VCD spectra were calculated for these acetate derivatives with the ACs derived from X-ray structures, using B3LYP functional and DGDZVP basis set. Although visual inspection reveals significant differences between experimental and calculated VCD spectra, the agreement was deemed satisfactory to independently confirm the AC.

***Cascarosides***: Five cascarosides (**Scheme 2**, **structure 27**) were extracted from the bark of *Rhamnus purshiana* plant and their ECD and VCD spectra were analyzed for verifying the applicability of empirical rules. ECD spectra were measured at a concentration of 250 μM in methanol and VCD at 69 mM in methanol-$d_4$. ECD and VCD spectra were calculated using B3LYP functional and 6-31G(2d,p) basis set using PCM to represent the solvent.[118] The calculated spectra were found to satisfactorily reproduce the experimental spectra. The use of methanol solvent for experimental measurements allows the possibility for hydrogen bonding between solute and solvent molecules. Even though the PCM does not account for such hydrogen bonding influence, the satisfactory reproduction of experimental spectra was attributed to the dominance of intramolecular H-bonding. This assertion was supported by the predictions resulting from molecular dynamics simulations in methanol solvent.

***Xanthocidin and its derivatives***: Naturally occurring xanthocidin and its six derivatives were identified from the culture of *Streptomyces sp.* bacteria AcE210. 1D and 2D NMR spectroscopy, as well as, HRMS were used to elucidate their planar structures.[119] The experimental VCD spectra were measured for homoxanthocidin B (**Scheme 2**, **structure 28**) in $CDCl_3$ at a concentration of 130 mM. Calculated VCD spectra were obtained using B3LYP functional and 6–311++G(d,p) basis set. Based on visual comparison of experimental and calculated VCD spectra, the absolute configuration at C-8 of homoxanthocidin B was determined to be (*S*).

***Cyclic sotolon, maple furanone and their dimers***: Naturally occurring plant derived sotolon, (*R*)-3-hydroxy-4,5-dimethylfuran-2(5H)-one, and maple furanone, (*R*)-5-ethyl-3-hydroxy-4-methylfuran-2(5H)-one (**Scheme 3**, **structures 29-30**) are used as food additives for wine and maple sugar. Experimental SOR, ECD and VCD measurements were undertaken for these two compounds and analyzed them using corresponding predicted data.[120] The predicted data were obtained with different density functionals (namely B3LYP and MWP1MPW91) and basis sets, (6-31+G(d) and 6-311++G(2d,p)). Both gas phase calculations and PCM, for representing the chloroform solvent, were used. These two compounds differ in the presence of methyl group in the former and ethyl group in the latter at C-5. It was concluded that the former exists as dimer, while the latter exists as monomer, in chloroform solution.

***Griseorhodins A and C*** (**Scheme 3, structures 31-32**): These compounds were isolated from leaf-cutter ants *Acromyrmex rugosus rugosus*. The AC of Griseorhodin A was previously determined by ECD spectral calculations as (6*S*,6a*S*,7*S*,8*S*). In this work, VCD spectral analysis was used to investigate the ACs of Griseorhodins A and C.[121] The visual comparison of experimental and predicted IR and VCD spectra led to assignment of the absolute configurations of Griseorhodins A and C as (6*S*,6a*R*,7*S*,8*S*) and (6*R*,6a*R*,7*S*,8*R*), respectively. The calculated spectra were obtained using B3LYP functional, 6-31G(d) basis set and PCM for representing the DMSO solvent. A correction was communicated later[122] that changed the AC of Griseorhodin A to (6*S*,6a*S*,7*S*,8*S*) and of Griseorhodin C to (6*R*,6a*S*,7*S*,8*R*).

***Diterpenoids from Jatropha dioica***: Jatropholones A and B, jatrophatrione, and citlalitrione (**Scheme 3**, **structures 33-36**) were isolated from the plant roots of *Jatropha dioica* Sessé. The acetate derivatives of Jatropholones A and B, jatrophatrione, and citlalitrione were subjected to VCD spectra analysis.[123] For VCD calculations on acetate derivative of Jatropholone A, the relative configuration derived from literature X-ray structure was used, and spectral predictions were obtained using B3LYP functional and DGDZVP basis set. Based on quantitative similarity analysis of experimental and calculated VCD spectra, the acetate derivative of Jatropholones A was inferred to be of (*M*,2*S*,9*S*,11*R*) configuration. Analogous quantitative similarity analysis of experimental and calculated VCD spectra of the acetate derivative of Jatropholone B, (*M*,2*R*,9*S*,11*R*) structure was assigned for Jatropholone B. This information was independently confirmed using the X-ray structure of acetate derivative of Jatropholone B, obtained with Cu Kα radiation, and associated Flack and Hooft parameters. Jatropholone A and B differ only in the configuration at C-2. Based on the similarities and differences in the experimental VCD spectra of Jatropholone A and B, it was suggested that VCD is able to differentiate between a pair of epimeric compounds in the presence of an inherently dissymmetric chromophore. VCD spectral analysis was undertaken for jatrophatrione, and citlalitrione, using the same protocol as was used for

Jatropholone A and B. Based on quantitative similarity analysis, jatrophatrione was suggested to have (2*R*,9*R*,13*S*,15*S*) configuration and the same AC was correctly assumed in the literature. Based on analogous analysis, (2*R*,3*S*,4*R*,9*R*,13*S*,15*S*) configuration was suggested for citlalitrione, and was independently confirmed using X-ray crystal structure of citlalitrione and associated Flack and Hooft parameters. Jatrophatrione, **35**, citlalitrione, **36**, riolozatrione and 6-epi-riolozatrione, (**Scheme 3, structures 37-38**), were isolated from the roots of *Jatropha dioica*. While jatrophatrione and citlalitrione were isolated and studied previously,[123] Riolozatrione, 6-epi-riolozatrione were not. It was found that riolozatrione could be generated from 6-epi-riolozatrione and not vice versa, the latter was considered more likely to serve as a reactive biosynthetic precursor of riolozatrione. The relative configurations of these two compounds were established from NOE correlations and their ACs determined from VCD investigations.[124] The experimental VCD spectra were obtained for $CDCl_3$ solutions at ~5 mg/150 microL. The quantitative comparison of VCD spectrum, predicted using B3LYP functional and DGDZVP basis set, for riolozatrione with (2*S*, 6*S*, 7*S*, 9*S*, 11*R*, 12*S*) configuration was considered to satisfactorily reproduce the experimental VCD spectrum. Similar VCD spectral analysis lead to the conclusion of (2*S*, 6*R*, 7*S*, 9*S*, 11*R*, 12*S*) configuration for 6-epi-riolozatrione, (2*R*, 9*R*, 13*S*, 15*S*) configuration for jatrophatrione, and (2*R*,3*S*,4*R*,9*R*,13*S*,15*S*) configuration for citlalitrione. These ACs were further confirmed using X-ray crystal structures obtained for riolozatrione, 6-epi-riolozatrione and citlalitrione.

***Caffeic acid ester derivatives***: Three different caffeic acid ester derivatives (**Scheme 3**, **structures 39-41**) were isolated from the leaves of *T. diversifolia.* One, (2*S*,3*S*)-4-O-Caffeoyl-2-C-methyl-D-erythronic acid, is a new compound and the other two, (2*S*,3*S*)-3-O-Caffeoyl-2-(2-propyl)-2-hydroxybutanedioic acid and (2*S*,3*S*)-3-O-Caffeoyl-2-((*S*)-2-butyl)-2-hydroxybutanedioicacid, are previously known compounds. The ACs of these compounds were suggested based on experimental and calculated $^{13}C$ NMR chemical shifts, ECD and VCD spectroscopies.[125] VCD calculations were undertaken using B3LYP functional and 6-31G(d) basis set with PCM representing the methanol solvent. ECD calculations were undertaken using CAM-B3LYP functional, TZVP basis set and PCM representing methanol solvent. $^{13}C$ NMR shielding constants were calculated using mPW1PW91 functional and 6-31G basis set. VCD spectra were recorded for $CD_3OD$ solutions at concentrations of 10 mg/170 microL for 4-O-Caffeoyl-2-C-methyl-D-erythronic acid, 5 mg/130 microL for the other two compounds. ECD spectra were recorded for 0.2 mg/mL solutions. <u>(2*S*,3*S*)-4-O-Caffeoyl-2-C-methyl-D-erythronic acid</u>: The relative configuration of this compound was determined from HRESIMS data obtained for this compound and also that for a lactone derivative, which led to two possibilities for its AC: (2*S*,3*S*) or its enantiomer. Conformational search was conducted for (2*S*,3*S*) diastereomer. Based on visual comparison of experimental and calculated VCD spectra, the AC of this compound was determined to be (+)-(2*S*,3*S*). This conclusion was supported by the comparison of experimental and calculated ECD spectra. It was mentioned that the VCD spectra calculated for OH-deuterated and undeuterated molecules yielded spectra with near mirror image features (except carbonyl region) and combined analysis of both calculations was needed for the AC assignment. However, such difficulty was not noticed for the following two compounds. <u>3-O-Caffeoyl-2-(2-propyl)-2-hydroxybutanedioic Acid</u>: Since relative configuration could not be readily established from NMR experimental data, conformational search was conducted for (2*S*,3*S*)- and (2*R*,3*S*)-diastereomers. Based on visual comparison of experimental and calculated VCD spectra, the AC of this compound was suggested to be (+)-(2*S*,3*S*) and corroborated by the comparison of experimental and

calculated ECD spectra. 3-O-Caffeoyl-2-((*S*)-2-butyl)-2-hydroxy butanedioicacid: Since relative configuration could not be determined confidently from NMR data, four diastereomers, (2*S*,3*R*,20*S*)-, (2*R*,3*S*,20*S*)-,(2*R*,3*R*,20*S*)- and (2*S*,3*S*,20*S*) were investigated. The observed and calculated $^{13}C$ NMR chemical shifts were considered close for (2*R*,3*R*,2'*S*)- and (2*S*,3*S*,2'*S*) diastereomers. The visual comparison between experimental and the calculated VCD spectra lead to the (+)-(2*S*,3*S*,2'*S*) assignment, which was supported by the comparison of experimental and calculated ECD spectra.

***Serrulatane-type diterpenoids***: Four serrulatane-type diterpenoids (**Scheme 4**, **structures 42-45**) three of which are new compounds, euplexaurenes A–C, and one known compound, anthogorgiene P, were isolated from gorgonian samples of *Euplexaura sp*. (a sea fan) collected in the South China Sea. The relative configuration of the 5,3,6-tricyclic unit in euplexaurene A was deduced by NOESY experiments. The absolute configuration at C-8 was assigned as (*S*) based on Mosher's method using MTPA esters. Thus, the configuration of tricyclic nucleus of euplexaurene A was determined to be (1*S*,4*R*,5*R*,8*S*,9*R*,10*S*). The NMR data, and HMBC cross peaks, suggested that the α, β-unsaturated ketone group in anthogorgiene P was hydrogenated in euplexaurene A. Based on NOESY cross peaks, euplexaurene B is determined to be the 8-epi-isomer of euplexaurene A. The planar structure of euplexaurene C was assigned as a 22,23-dehydro analogue of anthogorgiene P and based on ECD data, both are determined to have the same AC, (1*S*,4*R*,5*R*,9*R*,10*S*). Then the AC at position C-11 remained to be determined. To resolve this issue, conformational searches for two diastereomers of anthogorgiene P, (1*S*,4*R*,5*R*,9*R*,10*S*,11*S*) and (1*S*,4*R*,5*R*,9*R*,10*S*,11*R*), were undertaken and VCD spectra predicted using B3LYP functional and 6-311+G(d) basis set.[126] Then the predicted VCD spectra were compared to the experimental spectra measured in $CDCl_3$ solution. Based on visual comparison of the experimental and predicted VCD spectra, the AC at C-11 in anthogorgiene P was determined to be *S*.

***Aloesaponol III 8-Methyl Ether***: The AC of (-)-1-oxo-4,9-dihydroxy-8-methoxy-6-methyl-1,2,3,4-tetrahydroanthracene, or aloesaponol III 8-methyl ether (**Scheme 4**, **structure 46**) extracted from the plant roots of *Eremurus persicus* (Jaub & Spach) Boiss, was determined to be (*R*), based on the visual comparison of experimental and calculated VCD and ECD spectra.[127] VCD spectra were measured for 0.056 M solutions in $CDCl_3$ and ECD for 0.002 M to 0.004 M in $CHCl_3$ and $CH_3CN$. Predicted spectra were obtained using B3LYP functional and TZVP basis set with PCM representing the solvent.

***Antiprotozoal Acyclic Diterpene***: Bifurcatriol (**Scheme 4**, **structure 47**), 3,7,11,15-tetramethylhexadeca-2,10,14-triene-1,7,13-triol, a new linear diterpene with two stereogenic centers, isolated from the Irish brown alga *Bifurcaria bifurcate*. The relative stereochemistry of bifurcatriol was determined using NOESY experiments in conjunction with $^{1}H$ and $^{13}C$ NMR chemical shifts and coupling constants. Its absolute configuration was suggested from the experimental and predicted VCD spectra.[128] VCD spectra were measured at a concentration of 4.7 mg in 60 microL of benzene-$d_6$. Predicted VCD spectra were obtained for two diastereomers, (7*S*,13*S*) and (7*R*,13*S*), using B3LYP functional and 6-311++G(2d,p) basis set with PCM representing benzene solvent. Based on visual spectral analysis, AC was determined to be (7*S*,13*S*). This conclusion was supported by the comparison of calculated NMR chemical shifts with corresponding experimental data, and using DP4 probability criterion.

***Secondary metabolites of phytotoxin producing fungi***: Diplobifuranylones A−C, diplofuranone A, (4*S*,5*S*)-sapinofuranone B and sapinofuranone C (**Scheme 4**, **structures 48-53**), are the secondary metabolites of phytotoxin producing fungi, *D. corticola*. The AC of sapinofuranone C was determined in the literature by X-ray analysis combined with the advanced Mosher's method. The AC of sapinofuranone B was also deduced in the literature as (4*S*,5*S*) from stereoselective total synthesis. It was hypothesized that sapinofuranones are common biosynthetic precursors of both diplofuranones and diplobifuranylones. The authors of this work attempted to independently assign the AC of diplobifuranylones A−C, diplofuranone A, sapinofuranone B, and sapinofuranone C, using combined experimental and predicted spectral analysis of ECD and VCD and ORD.[129] VCD experimental spectra were obtained for $CDCl_3$ solution (at ~0.2 M), ECD for $CH_3CN$ solutions (at ~0.01 M) and ORD for $CHCl_3$ solutions (at ~ 0.2 g/100 mL). B3LYP functional and TZVP basis set was used for VCD, CAM-B3LYP functional and TZVP basis set for ECD and CAM-B3LYP functional and 6-311++G(d,p) basis set for ORD predictions. Quantitative similarity analysis of calculated experimental VCD spectra suggested (2*S*,2′*S*,5′*S*,6′*S*) configuration for Diplobifuranylones A, (2*S*,2′*R*,5′*S*,6′*R*) for Diplobifuranylones B and (2*S*,2′*S*,5′*R*,6′*R*) for Diplobifuranylones C. However, the calculated sign of ORD did not match the observed ORD sign for Diplobifuranylones B. For diplofuranone A, sapinofuranone B and sapinofuranone C, the ECD data turned out to be at odds with any of the two possible AC assignments. These observations point to the ambiguities that can sometimes result from using chiroptical methods.

Diplopyrone, **53**, a fungal phytotoxic metabolite, was isolated from culture filtrates of *Diplodia mutila* (Fr.) apud Mont., and this natural product was characterized as having two rings connected via cis junction with H4a and H8a on the same side, and opposite to H6, and with (*S*) configuration at C9.[130] Later, ECD and SOR calculations were undertaken for 9(*S*),6(*R*),4a(*S*),8a(*S*) and 9(*S*),6(*S*),4a(*R*),8a(*R*) diastereomers and the predicted data for former diastereomer were found to be in agreement with the corresponding experimental data.[131] Total synthesis of 9(*S*),6(*R*),4a(*S*),8a(*S*) diastereomer was achieved more recently[132] which permitted the comparison of spectroscopic data for synthetic and natural compounds. The $[\alpha]_D$ values, as well ECD spectral features, for the synthetic and natural compounds were similar. However, significant differences were noted for $^1H$ and $^{13}C$ NMR data of synthetic and natural compounds, suggesting a need for the revision of the AC for natural diplopyrone. To resolve this discrepancy, experimental VCD spectra were measured for natural diplopyrone (Figure 6) and predicted VCD, ECD and SOR data obtained for four diastereomers: 9(*S*),6(*R*),4a(*S*),8a(*S*); 9(*S*),6(*S*),4a(*S*),8a(*S*); 9(*R*),6(*R*),4a(*S*),8a(*S*); 9(*R*),6(S),4a(*S*),8a(*S*).[133] The VCD calculations undertaken here were of highest quality that included anharmonicity as well vibronic and rovibrational couplings, double hybrid functionals and dispersion corrections. The quantitative similarity analysis indicated that experimental VCD spectra are better matched by those predicted for 9(*R*),6(*S*),4a(*S*),8a(*S*) diastereomer, thereby revising the earlier assigned ACs at C9 and C6. The predicted ECD spectra did not reveal enough discrimination among the diastereomers to favor one over the other. The investigations on diplopyrone highlight the importance of emphasizing on unbiased investigations and of VCD spectral analyses to verify the conclusions derived from NMR, ECD and/or SOR data.

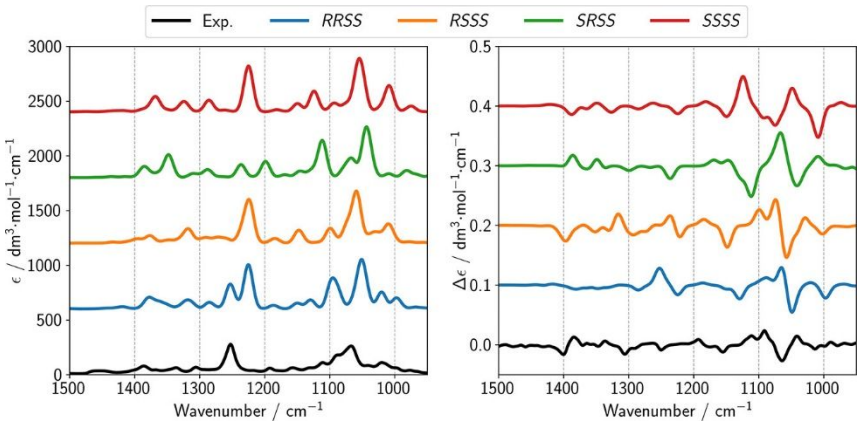


**Figure 6**: Experimental and predicted VA (left panel) and VCD (right panel) spectra for diastereomeric structures of **53**. The predicted VCD spectra revised the earlier assigned ACs at C9 and C6, established 9(*R*),6(*S*),4a(*S*),8a(*S*) configuration for **53**, thereby eliminating the uncertainties resulting from ECD, ORD and NMR analyses. Reprinted with permission from Ref.[133]. Copyright (2019) American Chemical Society.

***Dioxomorpholines and Derivatives***: Two new dioxomorpholines, 9-deoxy-PF1233 B and 9-deoxy-PF1233 A, three new derivatives, seco-PF1233 B carboxylic acid, 9-deoxy-seco-PF1233 B carboxylic acid and 4,9-dideoxy-seco-PF1233 B carboxylic acid and the known compound, PF1233 B, were isolated from a marine-facultative *Aspergillus sp.* MEXU 27854 Their structures were established by 1D and 2D NMR and HRESIMS data analysis. The relative configurations were deduced from NOE correlations. The absolute configurations of 9-deoxy-PF1233 B and 9-deoxy-PF1233 A, (**Scheme 5**, **structures 54, 55**) were elucidated as (2*S*,4*S*,12*R*,2′*S*) by quantitative comparison of experimental and predicted VCD spectra.[134] The experimental VCD spectra were obtained for $CDCl_3$ solutions at ~4-10 mg/150 microL. Predicted spectra were obtained using B3PW91 functional and DGDZVP basis set.

***Isopimarane-type diterpenoid***: A new isopimarane-type diterpenoid, Callicapene M3, was isolated from the *Callicarpa macrophylla* Vahl, and its planar structure was established using $^{1}H$ NMR, $^{13}C$ NMR and HMBC spectra. The relative configuration was determined from NOESY correlations and the AC from a visual comparison of experimental ECD and VCD spectra with corresponding theoretical spectra.[135] The experimental VCD spectra were obtained for $CDCl_3$ solution. The predicted VCD spectra were obtained using B3LYP functional and 6-311++G (2d, p) basis set, while ECD spectra were obtained using CAM-B3LYP functional and TZVP basis set. The structure of Callicapene M3 was identified as (4*S*, 5*S*, 9*S*, 10*S*, 13*S*, 14*S*)-14a-hydroxy-7,15-isopimaradien-18-oic acid (**Scheme 5**, **structure 56**).

***Trichothecenes***: Two trichothecenes, trichodermin and trichoderminol (**Scheme 5**, **structures 57-58**) were isolated from *T. albolutescens* culture medium. The structures of these compounds were determined by MS and NMR experiments, and relative configurations from NOESY data. The absolute configurations were determined, based on visual comparison of experimental and calculated VCD spectra, as 2*R*,4*R*,5*S*,6*R*,11*R*,12*S*.[136] Predicted VCD spectra were obtained using B3LYP functional and 6-31+G(d,p) basis set.

***Fungal Metabolites***: The readers are encouraged to consult the review on ECD, OR, and VCD applications for fungal metabolites, reported by Superchi and coworkers.[20] In this review, the reader can find VCD studies on (a). dioxolanone-type secondary metabolites isolated from the culture filtrates of the fungus *Guignardia bidwellii* (found in grape black rot) (b). fungal phytotoxin oxalicumone C, isolated in the marine-derived fungus *Penicillium oxalicum,* (c) fungal phytotoxins phyllostin and scytolide, produced by *Phyllosticta cirsii* (found in diseased Cirsium arvense leaves) (d). oxysporone, isolated from a strain of *Diplodia Africana* (found in fruit trees in South Africa and Holm Oak in Italy ) and (e). fungal phytotoxin seiricardine A, produced by *Seiridium* fungi (associated with the canker disease of Italian cypress).

***Ocimene monoterpenoids***: The essential oils of domesticated specimens of *Artemisia absinthium*, were the source for naturally occurring ocimenes, 2,6-dimethyl-2,3-epoxyocta-5,7-diene and 2,6-dimethylocta-5,7-dien-2,3-diol. The latter was not subjected to VCD studies due to possible intermolecular associations that may make the interpretation of VCD more difficult. Instead, experimental and predicted VCD spectra of 2,6-dimethyl-2,3-epoxyocta-5,7-diene, and monoacetate and acetonide derived from 2,6-dimethylocta-5,7-dien-2,3-diol, (**Scheme 5**, **structures 59-61**) were undertaken. Their ACs were determined from the quantitative comparison of experimental and predicted VCD spectra,.[137] The experimental VCD spectra were measured in $CDCl_3$ solutions at ~10 mg/150 microL. Predicted VCD spectra were obtained using B3LYP functional and the DGDZVP basis set. Based on these results, the ACs of the four isolated compounds were determined to be: (−)-(3*S*,5*Z*)-2,6-dimethyl-2,3-epoxyocta-5,7-diene, (−)-(3*S*,5*Z*)-2,6-dimethylocta-5,7-dien-2,3-diol, (−)-(5*S*)-2,2,4,4-tetramethyl-5-[(2*Z*)-3-methylpenta-2,4-dien-1-yl]-1,3-dioxolane and (+)-(3*S*,5*Z*)-2,6-dimethylocta-5,7-dien-2-ol-3-yl acetate.

***Fusiccocadiene***: Fusicocca-2,10(14)-diene (**Scheme 5**, **structure 62**) was isolated from a fermentation of *Saccharomyces cerevisiae* CEN.PK2-1c [pRS313-*upc2.1*, pRS315-*thmgr*, pVV214-*abfs*]. The AC of fusicocca-2,10(14)-diene, was previously deduced via total synthesis, or indirectly from crystal structures of fusicoccin A. In this work, the authors have confirmed the relative stereochemistry of fusicocca-2,10(14)-diene by comparison of experimental and predicted $^{13}C$ NMR chemical shifts for four diastereomers. The connectivity information obtained from 2D–NMR spectroscopy in the assignment of the experimental to the calculated $^{13}C$ NMR shifts, and DP4 probability measure, were used to identify one diastereomer, or its enantiomer, as the most likely candidate. Then the AC was determined as (6*S*,7*S*,11*R*) from a qualitative comparison of the experimental and predicted VCD spectra.[138] Experimental VCD spectra were measured for 0.18 M solution in chloroform-$d_1$. Predicted VCD spectra were obtained using B3LYP functional and the 6–311+G(2d,p) basis set with PCM representing the chloroform solvent.

***Chiral compounds from Bubonium graveolens essential oil***: Three chiral compounds, cis-chrysanthenyl acetate, oxocyclonerolidol, and cis-acetyloxychrysanthenyl acetate, (**Scheme 5**, **structures 63-65**) were isolated from essential oils of leaves and flowers from *Bubonium Graveolens,* using preparative HPLC. The ACs of these compounds were determined from a comparison of experimental and predicted VCD spectra.[139] Experimental VCD spectra were measured for $CCl_4$ solutions at ~11-24 g $L^{-1}$. Predicted VCD spectra were obtained using B3LYP functional and 6-31G(d,p) basis set with PCM representing the solvent. The AC of cis-chrysanthenyl acetate was previously known. This AC was confirmed in this work using VCD

spectral analyses. Theoretical VCD spectra were obtained for one enantiomer of cis-chrysanthenyl acetate and one enantiomer of trans-chrysanthenyl acetate. Qualitative visual comparison analyses led to the determination of AC of (−)-cis-chrysanthenyl acetate as (1*S*,5*R*,6*S*)-(−)-2,7,7-trimethylbicyclo[3.1.1]hept-2-en-6-yl acetate. Predicted VCD spectra of oxocyclonerolidol were obtained for four diastereomers and via visual comparison of the experimental and predicted VCD spectra, the AC was determined as (2*R*,6*R*)-(+)-oxocyclonerolidol. For cis-acetyloxychrysanthenyl acetate, cis relationship between the 6-methyl group and the 2-methyl group was established using NOESY experiments, leaving two possibilities for the AC. Predicted VCD spectra were obtained for four diastereomers and based on the above mentioned restrictions and qualitative comparison of experimental and predicted VCD spectra, the AC was assigned as (1*S*,5*R*,6*R*,7*S*)-(−)-7-(acetyloxy)-2,6-dimethylbicyclo[3.1.1]hept-2-en-6-yl]methyl acetate. From an analysis of the VCD spectra obtained for essential oils separately found in the leaves and flowers, it was concluded that oxycyclonerolidol is the main chiral compound in the leaves, while cis-chrysanthenyl acetate is the main chiral constituent of flowers, together with variable amounts of cis-acetyloxychrysanthenyl acetate, depending on the sample origin.

***Chiral compounds from the Talaromyces aculeatus***: Two new chiral compounds, (1'*S*,5'*S*,6'*S*)-5',6'-dihydroxy-2',6'-dimethyl-3'-(2"-oxopentyl)cyclohex-2'-en-1'-yl 2,4-dihydroxy-6-methylbenzoate, and (*S*)-1-(3,5-dihydroxy-4-methylphenyl)-4-hydroxypentan-2-one, (**Scheme 5**, **structures 66-67**) were obtained from the fungus of *Talaromyces aculeatus* and their planar structures established using HMBC and HMQC spectra. To determine the AC of 5',6'-dihydroxy-2',6'-dimethyl-3'-(2"-oxopentyl)cyclohex-2'-en-1'-yl 2,4-dihydroxy-6-methylbenzoate, it was converted to acetonide and its experimental and predicted VCD spectra were analyzed.[140] Calculations were undertaken for (1'*S*,5'*S*,6'*S*) and (1'*R*,5'*S*,6'*S*) diastereomers. Based on the SOR values, +140.0 for (1'*S*,5'*S*,6'*S*), and +52.7 for (1'*R*,5'*S*,6'*S*), predicted using B3LYP functional and the 6-311++G(2d,p) basis set, and their comparison to the experimental SOR value of +258, (1'*S*,5'*S*,6'*S*) was considered to be the correct choice. The predicted ECD spectra, using B3LYP functional and the 6-311++G(2d,p) basis set, for (1'*S*,5'*S*,6'*S*) and (1'*R*,5'*S*,6'*S*) diastereomers were similar, and matched the experimental ECD spectrum, so ECD was found to be not suitable for suggesting the AC. The predicted VCD spectra, using B3LYP functional and 6-311+G(d) basis set, for (1'*S*,5'*S*,6'*S*) and (1'*R*,5'*S*,6'*S*) diastereomers also did not match the experimental spectrum very well. Nevertheless, selected experimental VCD bands were found to have better match with those predicted for (1'*S*,5'*S*,6'*S*) diastereomer. With these assumptions, the AC of 5',6'-dihydroxy-2',6'-dimethyl-3'-(2"-oxopentyl)cyclohex-2'-en-1'-yl 2,4-dihydroxy-6-methylbenzoate was assigned as (1'*S*,5'*S*,6'*S*). For 1-(3,5-dihydroxy-4-methylphenyl)-4-hydroxypentan-2-one, the observed SOR was +25, while that calculated for (*S*) configuration was +176.7. Based on the agreement between the signs of SOR, the AC of 1-(3,5-dihydroxy-4-methylphenyl)-4-hydroxypentan-2-one was assigned as (*S*).

***Plakinidone***: The planar structure of plakinidone was originally mis-assigned and some questions remained persisting. To alleviate this situation, the authors have isolated plakinidone (**Scheme 5, structure 68**) and obtained two stable derivatives, one with the OH group converted to $OCH_3$, and the second one a p-methoxy phenyl ketone devoid of the five membered lactone ring (**Scheme 6**, **structures 69, 70**) that are impervious to air-oxidation and used ECD and VCD spectral analysis to assign the AC.[141] Experimental VCD spectra were obtained for 0.14 M solution in $CH_3CN$.

Experimental ECD spectra were measured for $1.7x10^{-4}$ M) solution in $CH_3CN$. Predicted spectra were obtained using B3LYP functional and the aug-cc-pVDZ basis set using PCM for representing the $CH_3CN$ solvent. The ECD experimental bands were considered to be better reflected by the simulated spectrum of the (11*S*,17*R*)-epimer. The confidence level for the agreement between the experimental VCD spectrum in the 1400–1000 $cm^{-1}$ region and that predicted for (11*S*,17*R*)-epimer, was found to be 71%. Based on these observations the AC of natural plankinidone (**Scheme 5**, **structure 68**) was assigned as (11*S*,17*R*).

***Stegane lignans*** (**Scheme 6**, **structures 71-73**): Natural (-)-(8*R*,8'*R*)-5'-desmethoxyyatein (found in *Bursera* Species) was subjected to oxidative cyclization to yield (+)-(*M*,8*R*,8'*R*)-5'-desmethoxyisostegane, **71** and a byproduct, (+)-(*M*,8*R*,8'*R*)-3,4-dihydroxy-3',4'-dimethoxyisosteganolide, generated by cleavage of the methylenedioxy group. Thermal atropisomerization of **71** yielded (-)-(*P*,8*R*,8'*R*)-5'-desmethoxystegane, **72**. (-)-(*P*,7*R*,8*R*,8'*R*)-5'-desmethoxysteganol, was synthesized from **72**. (-)-(*P*,7*R*,8*R*,8'*R*)-5'-desmethoxysteganacin **73** was obtained by acetylation, and (-)-(*P*,8*R*,8'*R*)-5'-desmethoxysteganone by oxidation, of (-)-(*P*,7*R*,8*R*,8'*R*)-5'-desmethoxysteganol. The novel steganes found were characterized by extensive NMR studies. Compounds **71-73** were subjected to VCD spectral analysis and their ACs validated via quantitative comparison of their experimental VCD spectra with those predicted using B3LYP functional and DGDZVP basis set.[142] Experimental VCD spectra were obtained at ~ 4-7 mg in 150 microL $CDCl_3$ solvent. Compounds **71** and **72** are pseudo-enantiomers, with opposite axial chirality, but the same central chirality. The opposite axial chirality is evidenced in the oppositely signed VCD bands arising from the aromatic transitions between 1550 and 1400 $cm^{-1}$. Based on the results from conformational analysis and NMR data it was stated that while a single conformation dominates for **71** and **73**, equilibrium between two conformations is present for **72**. Crystal structure of **72** revealed that the preferred conformation in the solid state has a close similarity to the most stable conformation that emerged from geometry optimizations and subsequently used for VCD analysis.

***Sphingosine***: Experimental VCD spectra of D-*erythro* sphingosine, L-*erythro* sphingosine, D-*threo* sphingosine and L-*threo* sphingosine (**Scheme 6**, **structures 74-77**) were presented at a concentration of 0.20 M in $CD_3OD$. Based on the observed differences among the four stereoisomers, it was suggested that VCD can be a useful tool for the stereochemical analysis of synthesized sphingosine.[143] It was found that reaction of sphingosine with glutaraldehyde yields rigid tricyclic derivatives (**Scheme 6**, **structures 78-81**) that dissolve in non-hydrogen bonding solvent $CHCl_3$ and yield enhanced VCD signals. Based on the visual comparison (Figure 7), the experimental and predicted VCD spectra for a model compound (**Scheme 6**, **structure 82)**, that did not have the side chain, were found to be in good agreement. As a result, it was suggested that VCD would be a powerful tool for the analysis of sphinganine and phytosphingosine.

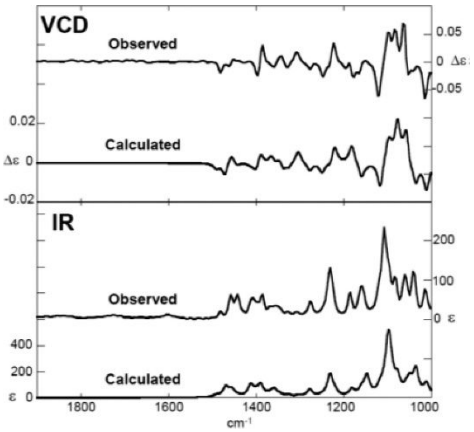


**Figure 7**: Experimental and predicted IR and VCD spectra for **82**, demonstrating that VCD can be used for assigning the absolute configurations of synthesized sphingosines. Reprinted with permission from Ref.[143]. Copyright (2016) American Chemical Society.

***Isocorilagin***: Ellagitannin corilagin (**Scheme 7**, **structure 83**), is a phytochemical marker in *Phyllanthus* species. The alpha-anomer of corilagin isolated from *Pelargonium reniforme* was named isocorilagin (**Scheme 7**, **structure 84**). Apparently, the NMR of corilagin compound was always analysed in DMSO-$d_6$, while that of isolcorilagin in $CD_3OD$. As a consequence, there was a confusion as to the separate existence of corilagin and isocorilagin, and it was not realized that corilagin could have adopted different conformations in different solvents. Batista and coworkers undertook a detailed combined analysis of NMR, ECD and VCD spectroscopies in different solvents, in conjunction with MD simulations and theoretical ECD and VCD spectral predictions.[144] The experimental VCD spectra were obtained at a concentration of 3.8 mg in 150 microL of either methanol-$d_4$ or DMSO-$d_6$ solvent. ECD spectra were obtained at a concentration of 0.2 mg $mL^{-1}$. VCD calculations were undertaken using B3LYP functional, 6-31G(d) basis set and PCM for representing the solvent. ECD calculations were performed using CAM-B3LYP functional, TZVP basis set and PCM for representing the solvent. First, the NMR spectra in $CD_3OD$ and DMSO-$d_6$ solvents gave indication of a conformational change in going from methanol to DMSO solvents. Then MD simulations, and subsequent geometry optimizations, were undertaken to identify the lowest energy conformers of alpha- and beta-anomers. Once the lowest-energy conformers for each configuration were identified, ECD and VCD spectra were calculated and compared to the experimental spectra. It was found that experimental VCD spectra in $CD_3OD$ were reproduced by the predicted spectra for both alpha- and beta-anomers. But experimental ECD spectra were better reproduced by those calculated for beta-anomer with the glucose core in the $^1C_4$ conformation. On the other hand, the experimental VCD spectra obtained in DMSO-$d_6$ solvent were considered to be satisfactorily reproduced by those predicted for two conformations, $B_{1,4}$ and $^oS_5$, of the β-glucose core. Based on these results it was concluded that the beta-glucose core of corilagin adopts an inverted $^1C_4$ conformation in methanol, and $B_{1,4}$ and $^oS_5$ conformations in DMSO. In both cases, the hexahydroxydiphenoyl moiety was found to be in (*aR*) configuration.

***Sesquiterpenoids***: Three new sesquiterpenoids, vetiverianines A, B and C, (**Scheme 7**, **structures 85-87**), and a known eudesmane sesquiterpenoid, (+)-1*β*,4*β*,6*α*-trihydroxyeudesmane, were isolated from the roots of *V. zizanioides*. The structures of these compounds were analyzed using NMR and confirmed using X-ray crystallography; the relative configurations were determined from NOESY or NOE correlations and/or X-ray crystallography. The ACs were determined from

a qualitative comparison of the experimental and calculated VCD spectra.[145] The experimental VCD spectra were measured at a concentration of ~4-6 mg in 150 microL of $CDCl_3$. Theoretical VCD spectra were obtained using B3PW91 functional and DGDZVP2 basis set. The AC of **85** was determined to be (4*S*,5*S*,6*S*,7*S*,10*S*); The chemical name of **86** was given as (4*R*,5*S*,7*R*)-7,11-epoxy-*α*-vetivone; and that of **87** as (4*R*,5*S*,7*R*,11*R*)-2-deoxo-7,11-epoxy-13-hydroxy-*α*-vetivone.

***Menthene Derivatives*** (**Scheme 7, structures 88-100**): (−)-(3*S*,4*R*,5*R*,6*S*)-3,5,6-trihydroxy-1-menthene 3-*O*-*β*-D-glucopyranoside, **88**, and (−)-(3*S*,4*S*,6*R*)-3,6-dihydroxy-1-menthene 3-*O*-*β*-D-glucopyranoside, **90** were extracted from the aerial parts of *Ageratina glabrata*. Characterization of these compounds was achieved via products, **89, 91-100**, generated from acid hydrolysis, peracetylation, and/or acetonide derivatization. For (+)-(1*S*,4*S*,5*R*,6*R*)-5-Acetyloxy-1,6-dihydroxy-2-menthene 1,6-acetonide, **95,** and (+)-(1*S*,4*S*,6*R*)-1,6-Dihydroxy-2-menthene 1,6-acetonide, **100,** the experimental VCD spectra were measured at a concentration of 4 and 10 mg, respectively, in 150 μL $CDCl_3$ solvent and their predicted VCD spectra were obtained using B3LYP functional and DGDZVP basis set. The quantitative comparison of experimental and predicted VCD spectra led to the determination of absolute configurations of **95** and **100**.[146] The X-ray structure of (+)-(3*S*,4*S*,6*R*)-3,6-dihydroxy-1-menthene, **97,** established its AC. The ACs of remaining compounds were deduced from the ACs of **95**, **97** and **100**. These results resulted in the reassignment of the literature AC of **97** isolated from *Brickellia rosmarinifolia*, *Mikania saltensis*, *Ligularia muliensis*, *L. sagitta*, and *Lindera strychnifolia*, as well as of (+)-(1*R*,4*S*,6*R*)-1,6-dihydroxy-2-menthene, **98,** isolated from *Cacalia tangutica*.

***Matrine- and Artemisinin-Type Herbal Products***: Three matrin-type alkaloids, matrine, oxymatrine, sophoridine, (**Scheme 8**, **structures 101-103**), can be extracted from the dry root of *Sophora flavescens*, and their crystal structures are known. The crystal structures of dihydroartemisinin and artemisinin (**Scheme 8**, **structures 104, 105**) are also known. The ACs of these compounds were not in question, but VCD studies were undertaken with the aim to identify the spectroscopic features that might be able to differentiate the potential stereoisomers and to investigate the solvent effects by deploying two different solvents, $CDCl_3$ and DMSO-$d_6$.[147] The H atom in $CHCl_3$ is expected to be more acidic (than that in $CH_4$), and can form weak hydrogen bond to oxygen atom in C=O group. As a consequence, in $CDCl_3$ solvent, 1:1 solute-solvent complex is expected for matrine and sophoridine, while oxymatrine can form 1:2 solute-solvent complex due to the presence of a N→O dative bond as well. Accordingly, it was found that the spectra predicted for solute-solvent complexes, embedded in solvent dielectric continuum using PCM, better matched the experimental spectra (Figure 8). Since the DMSO solvent, on the contrary, does not have a proton donor, solute-solvent complex was not necessary to obtain theoretical predictions for **101-103** in DMSO-$d_6$. The presence of O-H group in **104** on the other hand favors H-bonding between this group and =O of DMSO solvent. Accordingly, substantial improvement in the agreement between theory and experiment was noted for **104** in DMSO-$d_6$, when predicted spectra were obtained for 1:1 dihydroartemisinin:DMSO-$d_6$ complex, embedded in solvent dielectric continuum using PCM. This study emphasized the importance of including the explicit solvent molecules in obtaining the predicted spectra, when hydrogen bonding interactions are present between solute and solvent molecules.

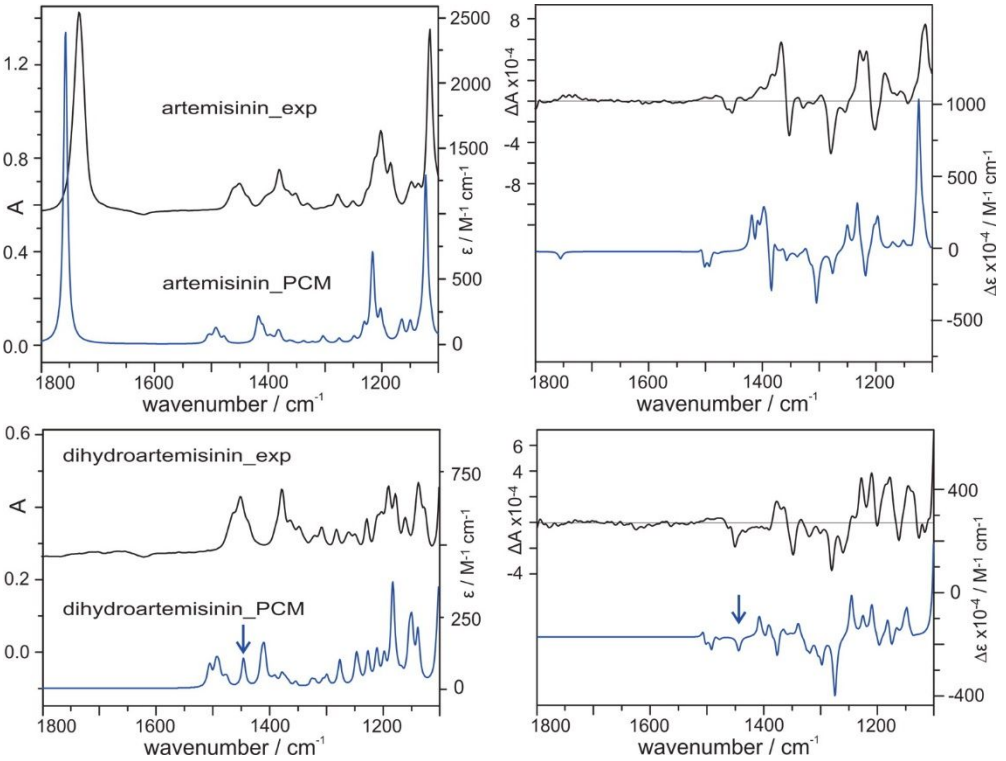


**Figure 8**: Experimental and predicted VCD spectra for dihydroartemisinin **104**, and artemisinin **105**, demonstrating the application of VCD for configuration assignment. Reprinted with permission from Ref.[147]. Copyright (2016) American Chemical Society.

***Agathisflavone*** (**Scheme 8**, **structure 106**): This compound is a dimeric flavonoid, isolated in optically active form for the first time from *Schinus terebinthifolius* Raddi (Anacardiaceae), known as Aroeira or the Brazilian pepper tree. Only a few examples of dimeric flavonoids possessing an axis of chirality as the sole stereogenic element are known to be optically active. The experimental VCD and VDF spectra in methanol-$d_4$, analyzed with corresponding QC predictions using B3LYP functional and 6-311++G(2d,2p) basis set and the numerical measures of similarity between experimental and calculated spectra, permitted the AC assignment for (−)-agathisflavone as (*aS*).[101] This conclusion was also supported by analogous analyses of ECD spectral data and ORD curves, measured in $CH_3OH$ at a concentration of 1.38 mg/mL. VCD spectra were measured in $CD_3OD$ at a concentration of 32 mg/mL.

***Limonene***: In this work the authors used limonene, (**Scheme 8**, **structure 107)** as a test case for verifying if the absolute configuration can be determined correctly using experimental VCD (and also ORD and ECD) when analyzed with corresponding predicted spectral data.[148] It was emphasized that it is important to determine the conformer populations using experimental NMR chemical shifts.

***Farinosin***: The known structure of Farinosin, (**Scheme 8**, **structure 108**), and its relative stereochemistry were reevaluated using modern methods. **108** was isolated from air-dried leaves of *Encelia fariginosa* A. Gray var. *farinosa* A. Gray (Asteraceae). The $^1$H NMR spectrum of **108** was completely assigned and $^{13}$C NMR spectrum was measured and assigned for the first time. Its structure was determined from single crystal x-ray diffraction data using Cu Kα monochromatic

radiation. Alhough the small value for Hooft parameter could be used to suggest the AC, it was deemed necessary to confirm independently using VCD spectral analysis.[149] Conformational search using B3PW91 functional and the DGDZVP basis set, indicated a single low energy conformer, which is same as that found in crystal structure. The VCD spectrum predicted for the AC derived from X-ray data was found to match the experimental VCD spectrum, obtained at a concentration of 6.0 mg in 150 microL $CDCl_3$ solvent. The quantitative similarity overlaps between experimental and predicted VCD spectra was considered satisfactory for relying on the assigned AC.

***Artemisia herba-alba essential oils***: Essential oils (EOs) obtained from the aerial parts of *Artemisia herba-alba* (AHA), a species belonging to the Asteraceae family, contain (-)-*alpha*-thujone, (+)-*beta*-thujone and (+)-camphor, (**Scheme 8**, **structures 109-111**). Interestingly, the presence of (+) or (-)-camphor and the relative proportions of these components depend on the natural source. Roussel and coworkers have measured the experimental VCD spectra of pure samples, **109-111** and compared them with those predicted for the known ACs.[150] For **109** and **110,** the predicted VCD spectra were found to reproduce the respective experimental spectra, while for **111** that was done previously in the literature. Then the experimental VCD spectra were measured for four different EOs and were analyzed with the experimental VCD spectra of pure components. Using least square estimation (LSE) the percent composition of pure components in each of the four EOs were determined and these compositions were found to agree with those derived from gas chromatography. The spectra reconstructed using the determined compositions were found to agree with the experimental VCD spectra measured for EOs, as reflected by the Pearson coefficients.

***(-)-flustramine B*** (**Scheme 8**, **structure 112**): This compound was isolated from the bryozoan *Flustra foliacea* and its AC was known from chemical correlations. Joseph –Nathan and coworkers have opted to determine the AC of this natural product using VCD. For this purpose, the ACs of diastereomers of a series of 6-bromooxindolylacetylphenyloxazolidinones were suggested, based on the bisignate VCD couplets that originate from interaction between C2 and C9 amide carbonyl groups.[151] The conclusions were supported by NMR and X-ray crystallographic data. For assigning the AC of **112**, the enantiomers of 2-(6-bromo-1,3-bis(3-methylbut-2-enyl)-2-oxoindolin-3-yl)acetic acids, (**Scheme 13**, **structure 113**), prepared from the diastereomers of bromo-1,3-bis(3-methylbut-2-enyl)-2-oxoindolin-3-yl)acetyl)-4-phenyloxazolidin-2-one, (**Scheme 8**, **structure 114**), were converted to amides, (**Scheme 8**, **structure 115**), and their ACs determined from X-ray diffractions measurements. A clockwise twist between C2=O and C9=O was also used independently to deduce the AC from its VCD spectrum. As the synthesis of natural product **112**, was carried out from the amides mentioned above, the AC of **112** was deduced from that of **115**.

***Esquelane derivatives***: Esquelane derivatives are found as the main components of *Adesmia boronioides* essential oil. The ACs of esquel-7-en-9-one, acetylphenol and cacalol acetate, (**Scheme 9**, **structures 116-118**), were investigated to clarify some uncertainties in the literature.[152] The experimental VCD spectra were measured for **116-118** (at a concentration of 6.0 mg/ 150 microL in $CDCl_3$), and compared with the corresponding spectra predicted using B3LYP functional and DGDZVP basis set. Based on the quantitative comparison of these spectra, the AC of **116** was found to be (1*S*,4*R*,5*R*) and of **117** to be (4*R*). These assignments are opposite to those previously reported. The AC of **118** however, was same as that known previously.

***Inuloxin A*** (**Scheme 9**, **structure 119**): This compound was isolated from the organic extract of *Inula viscosa* plant and its relative stereochemistry was deduced to be (4*E*,7*R**,8*R**,10*S**).[153] VCD spectra were recorded in $CDCl_3$ solvent at a concentration of 32.4 mg/60 microL and 32.4 mg/220 microL. Predicted VCD spectra using B3LYP functional, TZVP basis set and PCM representing $CDCl_3$ solvent did not agree with the experimental spectra satisfactorily. Therefore, VCD analysis was considered unsuitable for an independent AC assignment for **119**. However, based on the experimental and predicted ECD and ORD curves, using CAM-B3LYP functional, aug-cc-pVDZ basis set and PCM for representing the $CH_3CN$ solvent, the AC of **119** was suggested to be (+)-(7*R*,8*R*,10*S*). Seiricardine A, (**Scheme 9**, **structure 120**), was isolated from the culture filtrates of *Seiridium cardinal* and its relative stereochemistry was deduced to be: (1*S**,2*R**,3a*S**,4*S**,5*R**,7a*S**). VCD, ECD and ORD methods were considered to be inadequate for assigning the AC of **120**, due to the associated weak signals. For this reason, **120** was converted to 2-O-p-bromobenzoate ester, (**Scheme 9**, **structure 121**) and its ECD, ORD and VCD spectra were analyzed. Here again, it was noted that the AC assignment of **121** cannot be made independently by the VCD method, while ECD and ORD analyses indicated the AC to be (-)-(1*S*,2*R*,3a*S*,4*S*,5*R*,7a*S*). These are unusual cases where VCD spectra could not provide definitive AC information.

***13-beta-hydroxyazorellane***, (**Scheme 9**, **structure 122**): Isolated from *Laretia acaulis*, medicinal plant from Andes, this compound was subjected to VCD analysis for deducing the previously known AC.[154] Experimental VCD spectra were measured for 9.1 mg/150 microL solution in $CDCl_3$. Predicted spectra were obtained using B3LYP hybrid functional and the DGDZVP basis set. The quantitative similarity between experimental and predicted VCD spectra was considered reliable enough to suggest that its AC is same as that of azorellanol, whose AC was known from x-ray single crystal diffraction data of its 7-p-bromobenzoate derivative.

***Rhizopine***: The AC of natural rhizopine was deduced by means of analytical and semi-preparative supercritical fluid chromatography (SFC) and VCD spectroscopy.[155] For this purpose, a natural rhizopine sample was isolated and a racemic synthetic rhizopine was prepared and both samples were derivatized into the peracetyl derivatives. The SFC chromatograms of the peracetylated synthetic racemate resolved the two enantiomers and their correlation to the peracetylated natural extract identified enantiomer of natural sample. For VCD studies, a solution containing 2.0 mg of fraction 2 of synthesized peracetylated sample in ~100 microL of $CDCl_3$ was used and predicted spectra were obtained using B3LYP functional, B3PW91 functional, cc-pVTZ basis set and PCM for representing the solvent. A good quantitative agreement is found between the theoretically calculated spectrum for **123** (**Scheme 9**) and the experimental spectrum for fraction 2. Thus, the AC of fraction 2 is assigned as (1*R*,2*R*,3*S*,4*R*,5*R*,6*S*)-4-acetamido-6-methoxycyclohexane-1,2,3,5-tetrayl tetraacetate. Since chromatographic peak of peracetylated natural rhizopine corresponded to fraction 1 of synthesized peracetylated sample, the AC of peracetylated natural rhizopine corresponded to (1*S*,2*S*,3*R*,4*S*,5*S*,6*R*)-4-acetamido-6-methoxycyclohexane-1,2,3,5-tetrayl tetraacetate. Therefore, the AC of natural rhizopine corresponded to (1*R*,2*S*,3*R*,4*R*,5*S*,6*R*)-4-amino-6- methoxycyclohexane-1,2,3,5-tetraol, (**Scheme 9**, **structure 124**).

***Brevianamide B***: The stereochemical assignments for brevianamide A and B were known in the literature, originally isolated from *Penicillium brevicompactum* mould. The naturally occurring

(+)-brevianamide B is enantiomorph of the synthetic product (**Scheme 9**, **structure 125**). Bultinck and coworkers have undertaken[156] experimental and predicted ECD spectral investigation for brevianamides A and B. While the predicted ECD spectra for brevianamide A compared well with corresponding experimental ECD spectra, it was not the case for brevianamide B. The experimental and predicted ECD spectra did not confirm the presence of dimers of brevianamide B in solution, at the concentrations used. This difficulty led the authors to measure and predict VCD spectra for (-)-brevianamide B. Experimental VCD spectra were obtained at a concentration of 1.2 mg in 0.135 mL of TFE-$d_3$. Due to the low amount of available sample, the VCD spectrum was limited to the carbonyl region (Figure 9). The positive VCD bisignate couplet (positive band at lower wavenumber and negative band at higher wavenumber) observed in the carbonyl stretching region could be reproduced by the predicted spectra using MN12L functional, 6-311++G(d,p) basis set and PCM for representing the solvent. The authors mentioned that VCD is a more reliable method than ECD for the deducing the ACs of compounds investigated in this work.

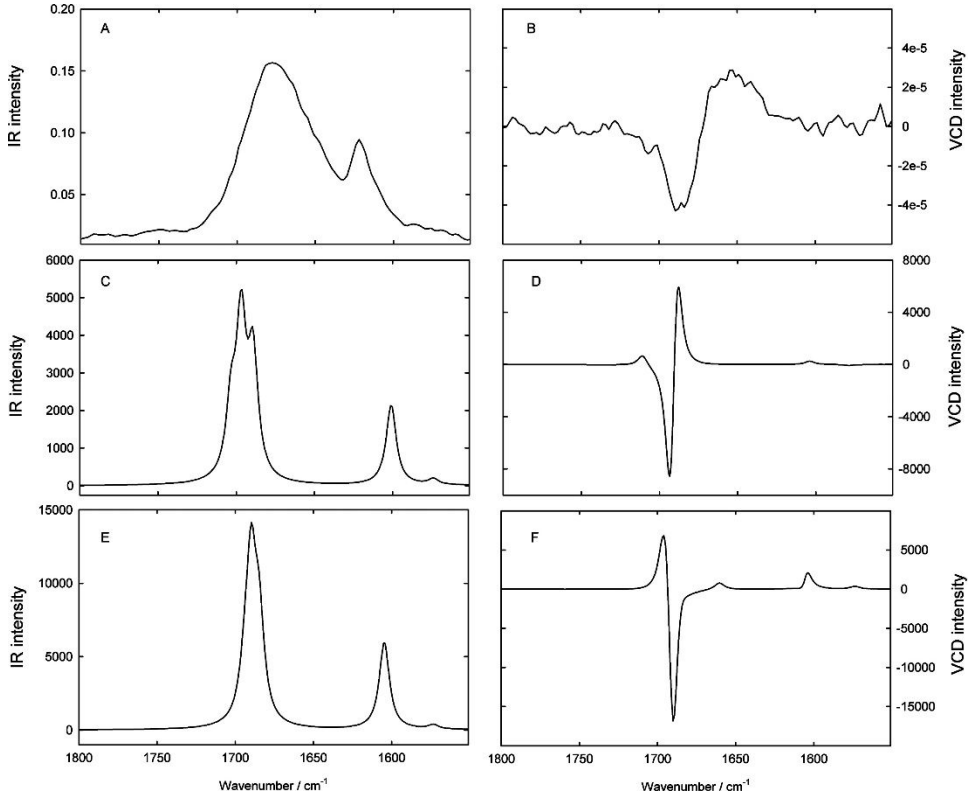


**Figure 9**: VA and VCD spectra for **125**. Panels A and B are experimental spectra; Panels C and D are spectra predicted for the monomeric structure; E and F are for dimeric structure. VCD was concluded to be a more reliable method than ECD for the deducing the ACs of compounds investigated. Reprinted with permission from Ref.[156] Copyright (2015) American Chemical Society.

***Phloroglucinol Derivatives***: 3-[{5,7-dihydroxy-2,2-dimethyl-8-(2-methylbutanoyl)-2H-chromen-6-ylmethyl]-6-ethyl-4-hydroxy-5-methyl-2H-pyran-2-one, (**Scheme 9**, **structure 126**), was isolated from *A. satureioides* plant and its experimental VCD spectra were measured at a

concentration of 12.1 mg in 150 microL $CDCl_3$ solvent.[157] Predicted VCD spectra for this molecule with (*S*) configuration were obtained using B3LYP functional and DGDZVP basis set. Qualitative visual comparison of the experimental and predicted VCD spectra was used to assign (*S*) configuration for the isolated compound.

***ent-Kaurene Glycosides***: Isolation from *Ageratina cylindrica* plant, and structural characterizations of *ent*-kaurenoic acid glycoside derivatives, (**Scheme 9**, **structure 127**) using $^{1}H$ and $^{13}C$ NMR, and COSY, HSQC, ROESY, and HMBC correlations, were reported.[158] Due to the uncertainty of some NOE effects, the AC at C-15 of *ent*-kaurenoic acid glycoside derivatives remained to be independently determined. For this purpose, two model compounds, methyl xylopate, (**Scheme 9**, **structure 128**) and its epimer, 15-Acetoxykaurenoic acid methyl ester, (**Scheme 9**, **structure 129**), were synthesized and subjected to VCD spectral analyses. The experimental VCD spectra were obtained at a concentration of 7.0 mg of **128** (Figure 10) and 9.4 mg of **129** each in 150 microL $CDCl_3$. The predicted VCD spectra were obtained using B3PW91 functional and DGDZVP basis set for two low energy conformers of each of these two molecules. The quantitative similarity analysis of experimental and predicted VCD spectra led to the assignment of AC at C-15, in **128** and **129**, which was also supported by NOE correlation in **128**.

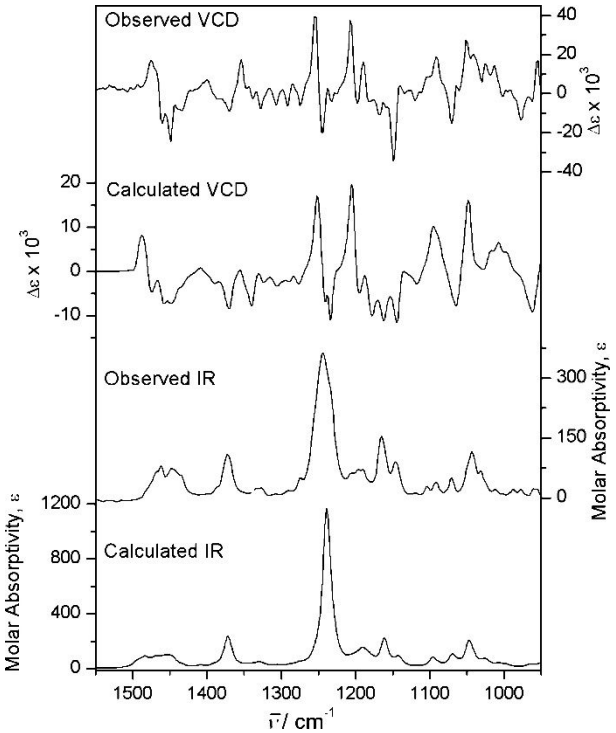


**Figure 10**: The experimental and predicted VCD spectra confirming the assignment of AC at C-15, in **128**. Reprinted with permission from Ref.[158] Copyright (2015) American Chemical Society.

***Centratherin***: The relative configuration of Centratherin, (**Scheme 10**, **structure 130**), was known in the literature, but its AC was not. **130** was extracted from *Eremanthus crotonoides* plant, and its structure and relative configuration were deduced from NMR chemical shifts. To determine the AC of **130**, VCD spectra were measured[103] at a concentration of 23 mg/mL in $CD_3CN$ solvent and predicted VCD spectra were obtained for 16 low-energy conformers of (6*R*,7*R*,8*S*,10*R*,2′*Z*) configuration using B3LYP functional and aug-cc-pVDZ basis set. Quantitative similarity analysis

between experimental and predicted VCD (as well as VDF) spectra suggested the AC of centratherin to be (6*R*,7*R*,8*S*,10*R*,2′*Z*). This conclusion was also supported with simultaneous analysis of experimental and predicted ECD and ORD data.

***beta-artemether***: Artemether is a methyl ether derivative of artemisinin (found in *Artemisia annua* plant), and the *beta*-isomer, *beta*-artemether (**Scheme 10**, **structure 131**), is known to possess the antimalarial activity. While the AC of *beta*-artemether is already known in the literature from its x-ray crystal structure, the authors undertook this study to verify if the AC of **131** could be determined from VCD spectral analyses.[159] The experimental VCD spectrum was compared with that predicted using B3LYP as well as B3WP91 functionals and 6-311+G(2d, p) basis set. It was concluded that there is a substantial agreement between experimental and predicted VCD spectra.

***Tobacco alkaloids***: (−)-*S*-anabasine, (**Scheme 10**, **structure 132**), is one of the minorities piperidinic nicotinoids in tobacco leaves. The VCD spectra of **132** were measured for neat liquid as well as for $CCl_4$ solution (1-2 M).[160] Predicted VCD spectra were obtained using B3PW91 functional and aug-cc-pVTZ basis set. The spectra obtained for neat liquid and $CCl_4$ solutions were found to be similar. The predicted spectra, obtained from two conformations as a 2:1 population mixture, visually matched the experimental spectra.

***α,β-Unsaturated Germacranolide***: The x-ray structure of 6-epi-Desacetyllaurenobiolide, (**Scheme 10**, **structure 133**), isolated from *Montanoa grandiflora* and more recently from *Laurus nobilis* plants. was reported in the literature, but its AC was assumed. To determine the AC of **133**, its x-ray structure with the evaluation of the Flack and Hooft parameters was used. Also, the experimental VCD spectra were measured and compared to the corresponding predicted VCD spectra.[161] The AC determined from a quantitative similarity comparison of experimental and predicted VCD spectra was found to be, (6*S*,7*S*,8*S*), consistent with that determined from x-ray data. In addition, the acetylated derivative, 6-epi-laurenobiolide, (**Scheme 10**, **structure 134**), and its reduced diastereomers, (**Scheme 10**, **structure 135-136**) were also studied by VCD, along with x-ray crystal structure of **136**. The experimental VCD spectra were measured for 6.0 mg of **133**, 5.5 mg of **134**, 6.1 mg of **135**, and 5.5 mg of **136** in 150 microL $CDCl_3$. The predicted VCD spectra were obtained as the population weighted averages of three conformer spectra in each case, using B3LYP functional and DGDZVP basis set.

***Nicotine***: The conformational landscape of (-)-*S*-nicotine, (**Scheme 10**, **structure 137**), a constituent of tobacco plants, in both the gas phase and solution state was investigated.[162] B3LYP and B3PW91 functionals in conjunction with the 6-311++G** and aug-cc-pVTZ basis sets and PCM for representing the solvent were used for assessing the conformations. Two conformations were considered to be populated in the gas phase and in solution. Experimental VCD spectra of **137** have been measured for neat liquid and in solution ($CCl_4$ or DMSO, 0.5 to 2M), and analyzed with corresponding predicted VCD spectra. Based on qualitative visual spectral analysis, the conformational population distribution of the sample was concluded to be relatively independent of the medium.

***Cotinine***: (-)-*S*-cotinine, (**Scheme 10**, **structure 138**), is one of the minor alkaloid tobacco constituents, and is the major peripheral oxidative metabolite of (-)-*S*-nicotine in several animal species. The conformational landscape, the rotational isomerism barrier and solution-state

conformational energy profile of **138** have been investigated utilizing experimental and predicted VCD spectra.[163] The experimental VCD spectra were measured for samples prepared as nujol mulls and in $CCl_4$ solution (0.5 to 2 M). Conformational analysis and predicted VCD spectra were obtained using B3LYP and B3PW91 functionals in conjunction with the 6-311++G** and aug-cc-pVTZ basis sets. To better match the experimental VCD spectra, predicted spectra for four different conformations were considered essential.

***Linear diterpenes from the brown alga Bifurcaria bifurcata***: Elegandiol and bifurcane (**Scheme 10**, **structures 139-140**) are two linear diterpenes, isolated from *Bifurcaria bifurcate* (brown algae seaweeds). The AC at C-13 of these compounds was assigned as (*S*) using VCD spectral analysis.[164] The experimental VCD spectra were measured in $CDCl_3$ at a concentration of 0.65M. Predicted spectra were obtained for 20 lowest energy conformers using B3LYP functional and 6-311++G(2d,p) basis set. The predicted VCD spectra were considered to be in a very good agreement with experimental spectra. It was found that the predicted VCD spectra are determined by the C9–C15 fragment and the contributions from different conformations of C1–C8 fragment averaged out.

***Flavor Compounds***: Patchouli (*Pogostemon cablin*.) is an herbal plant originating from India. Patchoulol, (**Scheme 10**, **structure 141**), was purified from natural patchouli oil. Experimental VCD spectra of **141** were measured in $CCl_4$ at a concentration of 0.30 M.[165] Predicted VCD spectra were obtained as the population weighted average of three conformer spectra, using B3LYP functional and 6-311G(d,p) basis set. Based on the comparison of experimental and predicted VCD spectra, the previously reported absolute stereochemistry of **141**, was confirmed using VCD spectral analyses as (1*R*,3*R*,6*S*,7*S*,8*S*). The application of VCD method was extended to some odor-active furanones that are prone to racemize due to keto-enol tautomerism.

# 4. Applications of vibrational Raman Optical Activity

As in Section 3, we present here a comprehensive list of compounds subjected to VROA investigations during 2005-2019. Also, for the reasons mentioned in Section 3, it is not possible to group the compounds into generalized categories, and therefore, the subtitles in the following sections pertain to compounds (or a group of compounds) in individual investigations.

***Resveratrol***: 3,5,4′-trihydroxystillbene, known as resveratrol, a stilbenoid phytoalexin produced in many food plants, can exit as *E*- and *Z*-isomers (**Scheme 11, structures 142, 143**) and is thought to have multiple health benefits,. The *E*-isomer is prevalent in solution, but *Z*-isomer can be stabilized when appropriate external interacting environment is provided. A co-crystal structure of the resveratrol-bound human tyrosyl-tRNA synthetase indicated a binding-dependent conformational change that facilitated the *Z*-isomer. The steric hindrance between the rings, connected by the stilbene bond, causes the *Z*-isomer to adopt either *P* or *M* helical atropisomer, as dictated by surrounding interacting environment. Similarly, *E*-isomer can also exhibit *P* and *M* atropisomers, as dictated by surrounding interacting environment. This helical chirality can lead to chiroptical signatures that may be used to identify the nature of helicity induced in the bound resveratrol. To explore the nature of anticipated chiroptical signatures, theoretical predictions of ROA and VCD spectra were obtained[166] for the atropisomers using B3LYP functional and 6-

311++G** basis set. The *Z* form was predicted to have significantly more intense VCD signals than the *E* form. Similarly, the ROA spectrum of the *Z* form is predicted to have both positive and negative signals, but the *E* form is predicted to have negligibly small signals. For *P* atropisomer of *Z*-resveratrol, the ROA spectrum is dominated by bands at 1644 and 979 $cm^{-1}$, while the VCD spectrum is dominated by bands at 1600 and 1165 $cm^{-1}$. These bands are suggested to be signatures for detecting the binding of *Z*-resveratrol to the tyrosyl-tRNA synthetase, in *P* atropisomer form.

***Ladderanoic Acids***: Anaerobic ammonium oxidation (anammox) to convert ammonia back to $N_2$ is mediated by bacteria in the *Planctomycetes phylum*. Anammox bacteria are used extensively in wastewater treatment plants to remove ammonium ion from effluent. The anammox pathway includes an intracytoplasmic vesicle called the anammoxosome. The phospholipid membrane of the anammoxosome contains fatty acids and analogous alcohols with multiple concatenated cyclobutane rings known as ladderanes. The two major ladderane components of the anammoxosome are [5]-ladderanoic acid containing five linearly fused cyclobutane rings, and [3]-ladderanoic acid (**Scheme 11, structures 144, 145**) containing three cyclobutane rings fused to a cyclohexane ring. These two acids contain a long alkyl side chain with seven carbon atoms terminated with a carboxylic group. The absolute configurations of these naturally occurring acids were determined[167] using ROA spectroscopy as (-)-(*R*)-5-ladderanoic acid and (+)-(*R*)-3-ladderanoic acid. The experimental ROA spectra of (-)-5-ladderanoic acid and (+)-3-ladderanoic acids were found to match well with Boltzmann weighted predicted spectra, using B3LYP functional and 6-311++G(2d,2p) basis set, for the conformers of these acids with (*R*)-configuration. These assigned ACs were further confirmed via the analysis of respective ORD data and also by obtaining respective single crystal x-ray structures.

***Taxol Precursor***: Paclitaxel, also known as Taxol (found in the bark of *Taxus brevifolia* tree), is widely used as a natural anticancer agent. Chemical modification of a natural taxoid, baccatin III, has been pursued for the commercial production of paclitaxel. Baccatin III functionalized by 1-*t*-butyloxycarbonyl-3-triethylsilyloxy-4-phenyl-2-azetidinone, can lead to four stereoisomers (resulting from two chiral centers), of which the desired one is (3*R*,4*S*) (**Scheme 11, structures 146**). Two enantiomeric samples, A and B, with unknown configurations were obtained for ROA spectroscopy analysis.[168] Since A and B are enantiomeric samples, their experimental ROA spectra are mirror images of each other. The experimental ROA spectra of sample B matched well with the Boltzmann weighted predicted spectra of conformers with (3*R*,4*S*) configuration, while those predicted for (3*S*,4*S*) did not (Figure 11). Predicted spectra were obtained with B3LYP functional and 6-311++G** basis set. Based on these experimental and predicted results, it was concluded that sample B belongs to (3*R*,4*S*) configuration and sample A to (3*S*,4*R*) configuration. ROA spectroscopy was, therefore, concluded to reliably discriminate between the different diastereoisomers of a taxol precursor.

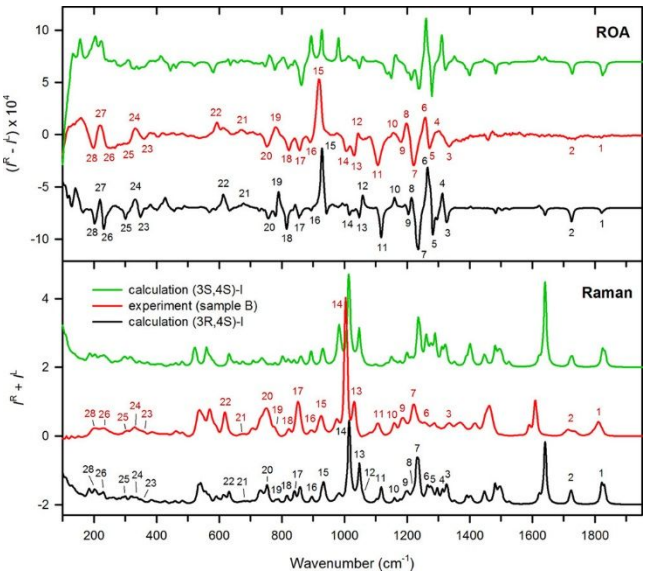


**Figure 11**: Raman and ROA spectra of sample B (red traces) compared to the predicted spectra for (3*S*,4*S*) and (3*R*,4*S*) diastereomers. ROA spectroscopy was concluded to reliably discriminate between the different diastereoisomers of a taxol precursor. Reprinted with permission from Ref.[168] Copyright (2017) American Chemical Society.

***Cocaine Hydrochloride***: Cocaine is a tropane alkaloid found in the leaves of *Erythroxylum coca*. Among the four diastereomers, known as cocaine, pseudococaine, allococaine and allopseudococaine, the most potent is pseudococaine or the "natural" cocaine. Cocaine contains heterocyclic six-membered tropane ring which can exist in either chair or boat conformation. In addition, the N-methyl group can be present in axial or equatorial orientation. The equatorial conformation is the most preferred form due to the possibility for hydrogen bond between $NH^+$ and C=O of $COOCH_3$ group. For the equatorial conformation, four different energetically favored orientations between $COOCH_3$ and benzoyloxy groups are possible, although only two of them dominate the relative populations. The experimental VCD and ROA (along with ECD) spectra and their relation to the conformation of the cocaine ion, as HCl salt, were investigated (**Scheme 11, structures 147**).[169] VCD spectra were measured in $D_2O$ solvent in the 1800–1250 $cm^{-1}$ region, while ROA spectra were measured in the 200 -1800 $cm^{-1}$ region both in $H_2O$ and $D_2O$ solvents. The concentrations used were 100 g $L^{-1}$, which are thousand times larger than those needed for recording ECD spectra. Theoretical VCD and ROA spectra were obtained using B3PW91 functional and 6-311++G** basis set employing PCM for representing the solvent. The predicted spectra were found to agree reasonably well with corresponding experimental spectra. The favored geometries, which reproduced the experimental spectra, indicated that the solution structure of cocaine cation contains, mostly, two conformers differing in the rotation of the benzoyl oxy group and this structure is different from that in crystal. The poor performance of ECD, in terms of agreement between calculations and experiments reported in this work was suggested to be due to slight differences in the geometries used.[170]

***Flavone C-diglycoside***: The anomeric configuration of flavonoid glycosides is usually inferred from NMR coupling constants, but can be prone to errors. The lack of UV-Vis chromophores

within the glycosidic portion of the molecules limits the applicability of ECD spectroscopy for determining anomeric configuration. The application of experimental and calculated Raman/ROA data for the stereochemical characterization of the flavone C-diglycoside isoswertisin-4'-methyl-ether-2"α-L-rhamnoside (**Scheme 11, structures 148**), which was isolated from the aerial parts of *Peperomia obtusifolia* plant, was reported (Figure 12).[171] The predicted ROA spectra depended heavily on the correct description of the conformational ensemble in solution. Conventional molecular mechanics (MM) conformational search and geometry optimization, without explicit water molecules, was found to be inadequate to reproduce the experimental ROA spectra. MD simulations employing solvent molecules, followed by a hybrid QM/MM method were found to be necessary to describe the correct conformations and the absolute configuration of the glycosidic link.

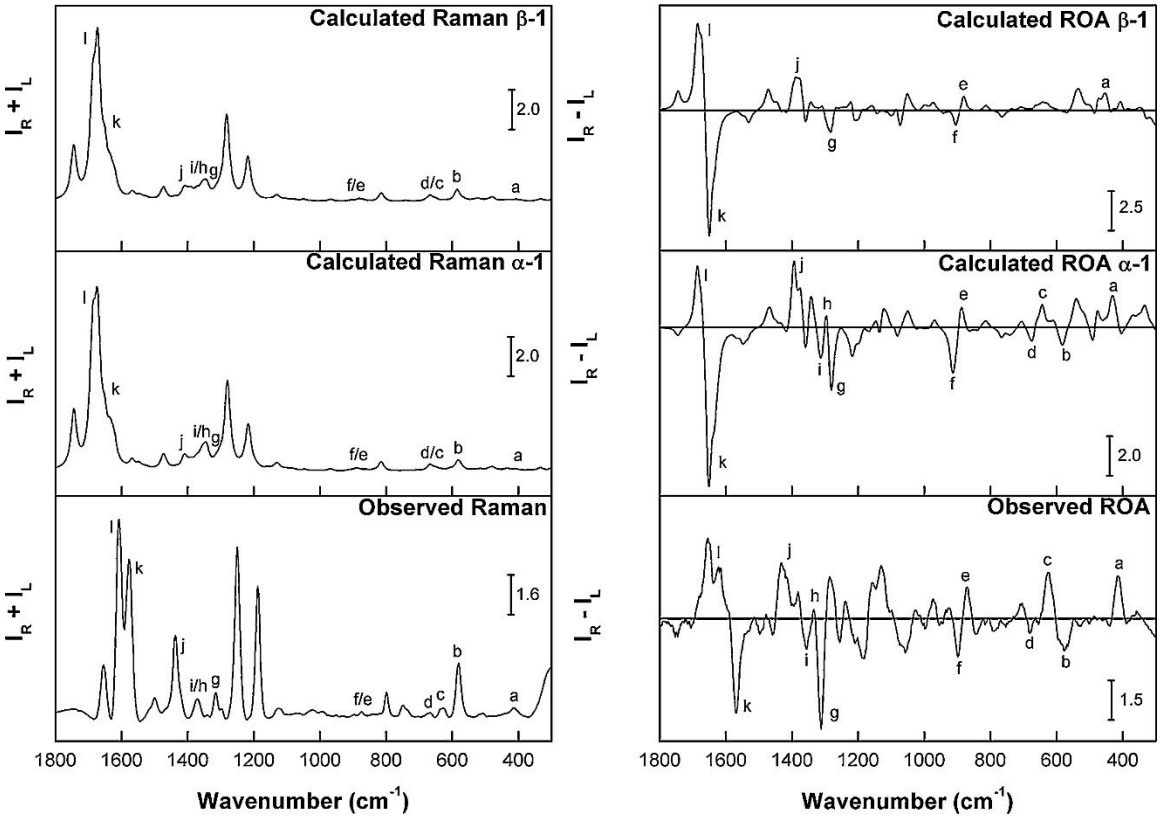


**Figure 12**: Experimental and predicted Raman and ROA spectra of **148**. The configuration for the L-Rha-(1→2)-β-D-glucose linkage in **148** was confirmed to be α, overcoming the uncertainties in the analyses of NMR coupling constants and ECD spectra. Reprinted with permission from Ref.[171] Copyright (2016) Elsevier.

***Zeaxanthin***: Carotenoids are pigments synthesized by plants, algae, and photosynthetic bacteria. Zeaxanthin, or *β,β*-carotene-3,3'-diol, (**Scheme 11, structures 149**), a hydroxylated carotenoid, protects human retina against photo-oxidative damage. ROA spectral studies revealed[48] that while Zeaxanthin monomer and its H-aggregates do not exhibit significant ROA signals, the J1 aggregates of Zeaxanthin exhibit resonance enhanced ROA signals. The reason for this phenomenon is that J aggregates have electronic absorption (at ~510 nm) and associated ECD (at

515 nm), close to the excitation wavelength (532 nm) used for ROA measurements. The monomer and H-aggregates, on the other hand, have electronic absorption and associated ECD bands far removed from the excitation wavelength. Resonance enhanced ROA phenomenon does allow measurements at much lower concentrations. Aggregation induced resonance enhance ROA has been reported also for astaxanthin and lutein derivatives.

***Bicyclic terpenes***: Terpenes, produced by a variety of plants, particularly conifers, have many practical applications. ROA spectra of five different bicyclic terpenes, α-pinene, fenchone, bornyl acetate, 2-carene and 3-carene, **(Scheme 12, structures 150-154**), were investigated. The absolute configurations of these compounds are already known, so the aim here is to assess the predictive capabilities of the existing theoretical methods to reproduce the corresponding experimental ROA spectra. A successful reproduction of experimental ROA spectra gives confidence that an unknown stereo structure can be determined from analyzing its experimental ROA spectrum with corresponding theoretical prediction. A detailed analysis indicated that similarity overlap analysis provides numerical measures of agreement between experimental and predicted spectra and is a useful supplement to the visual spectral comparisons. The absolute magnitudes in experimental and QC predicted VROA properties can be analyzed by using dimensionless CID spectra. To establish a protocol for assigning ACs using VROA spectroscopy, it was suggested[104, 172] that simultaneous similarity overlap analyses of Raman, ROA, and CID spectra are needed, in place of restricting the analysis to just ROA spectra alone.

***Misidentified natural products***: The chemical structures of several natural products were initially mis-assigned in the literature and subsequently corrected later on. To assess if such mis-assignments can be avoided through the use of VCD and ROA spectroscopies, VCD and ROA spectra were calculated for both incorrect and correct structures and compared to the corresponding experimental spectra.[105] This comparison indicated that similarity overlap analyses provides a pathway to identify the incorrect chemical structures. Then the magnitudes of similarity overlap needed to discriminate between incorrect and correct structures was assessed using the experimental and calculated spectra for α-pinene, fenchone, bornyl acetate, **(Scheme 12**, **structures 150-152**), 2-carene and 3-carene (**Scheme 12, structures 153, 154**). Using this information as a guideline, the similarity overlaps between the spectra predicted for incorrect and correct chemical structures of seven natural products, namely, elatenyne (derived from alga), aquatolide (plant derived), annuionone A (plant derived), caespitenone (plant derived), palominol (coral derived), sporol (fungal plant pathogen) and klaivanolide (plant derived) were analysed. Based on this information it was concluded that if the experimental VCD and ROA spectra for these compounds were available, the original mis-assignments could have been avoided.

***Diterpenoids***: The ethanolic extract of the flowers of *Hymenaea stigonocarpa* revealed the presence of a new compound, (+)-(4*R*,5*S*,8*R*,9*S*)-18-hydroxy-ent-halima-1(10),13-(*E*)-dien-15-oic acid, (**Scheme 12, structures 155**) and five additional known substances. This new compound was characterized using NMR ($^{1}$H, $^{13}$C, COSY, HSQC, HMBC, and NOESY) and MS analyses.[173] In particular, NOESY correlations allowed determining the relative orientations of the substituents at chiral centers, resulting in two possibilities for the AC as (4*R*,5*S*,8*R*,9*S*) or its enantiomer. Based on the comparison of Raman and ROA spectra of the experimental spectra of this new compound

with those calculated for (4*R*,5*S*,8*R*,9*S*) structure using B3LYP functional, TZVP basis set and PCM for representing the DMSO solvent, the AC of new compound was assigned as (4*R*,5*S*,8*R*,9*S*). The experimental and Raman and ROA spectra of another known compound, (+)-(5*S*,8*S*,9*R*,10*S*)-labd-13-en-8β-ol-15-oic acid (**Scheme 12, structures 156**) were also found to be reproduced by those calculated in the same manner for the known configuration.

***Ribifolin***: A new cyclic octapeptide ribifolin (**Scheme 12**, **structure 157**) was isolated from *Jatropha ribifolia* plant and characterized using $^{1}H$, $^{13}C$, TOCSY, NOESY, HSQC, HMBC NMR spectra, and MS/MS analyses. MD simulations and NMR data indicated that the backbone structure of this cyclic peptide has a twisted ring shape. The additional sample material of this cyclic peptide, needed for ROA measurements, was synthesized using solid-phase peptide synthesis.[174] The experimental ROA spectra were measured for synthesized sample at a concentration of 40 mg $mL^{-1}$ in 50:50 $H_2O{-}CH_3CN$ solvent mixture. The comparison of experimental ROA spectra to those predicted for cyclic octapeptide with all L-amino acids, using B3LYP functional, 6-311+G(d) basis set and PCM for representing the water solvent, was found to provide good agreement in the 1000-1400 $cm^{-1}$ region. Based on this ROA spectroscopic agreement, and the similarities in optical rotation and NMR of synthesized and natural octapeptide samples, the stereochemistry of natural sample was assigned. Since a single conformer was found to provide 90% of Boltzmann population, the structure of this conformer was used to suggest that, the natural cyclic octapeptide, in partially aqueous solution, adopts a backbone structure with two γ-turns.

***Cinchona alkaloids***: The bark of the Cinchona tree serves as the source for several cinchona alkaloids, which have proven antimalarial properties. Some of the chiral compounds in the class of cinchona alkaloids are quinine (QN), quinidine (QND), cinchonine (CN), and cinchonidine (CND) (**Scheme 12**, **structures 158-161**).While normal Raman spectra of these compounds in solution exhibit similar patterns and cannot be used for differentiation between the derivatives or pseudoenantiomers, corresponding ROA spectra can be quite different enabling differentiation between them.[175] This point was demonstrated by measuring experimental ROA spectra of QN, QND, CN and CND in aqueous solutions. Furthermore, the vibrational origins of observed ROA bands were identified using predicted spectra using B3LYP functional and aug-cc-pVDZ basis set with water solvent represented by PCM. The sequence of double protonation of QN as a function of pH was also monitored using experimental Raman and ROA spectra as a function of pH. These spectra revealed that mono and di-protonated species can also be differentiated using Raman and ROA spectra. The comparison of experimental and predicted Raman and ROA spectra of $(QN\text{-}H)^{+}$ and $(QN\text{-}2H)^{2+}$ was also undertaken (Figure 13).

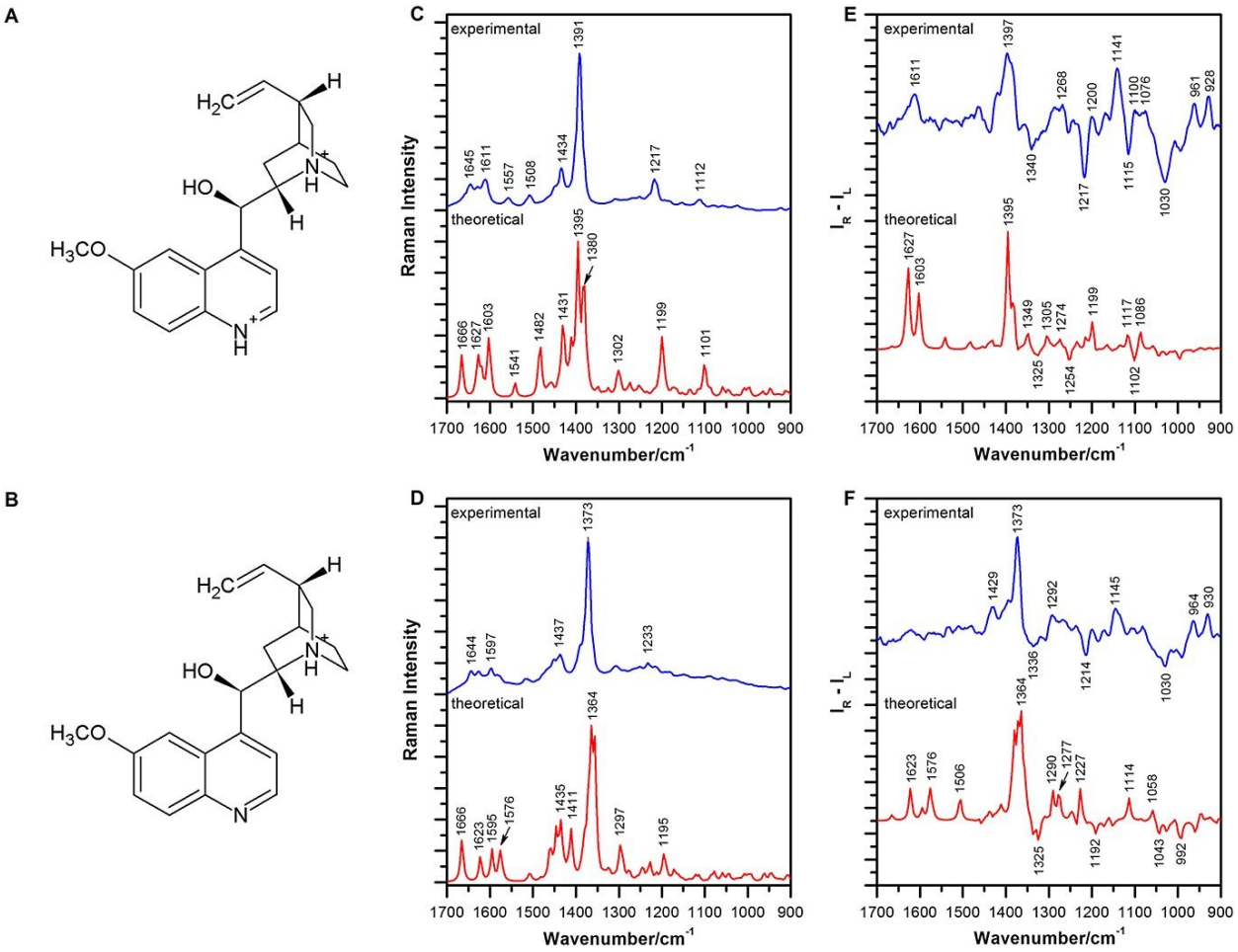


**Figure 13**: Experimental and predicted Raman and ROA spectra for $(QN\text{-}2H)^{2+}$ (A) and $(QN\text{-}H)^{+}$ (B) and demonstrating that mono and di-protonated species can be differentiated using ROA spectroscopy. Reprinted with permission from Ref.[175] Copyright (2015) John Wiley and Sons.

***Homoisoflavanone***: Dry leaves of *Polygonum ferrugineum (Polygonaceae)* are the source for a homoisoflavanone, 5,7-dihydroxy-6-methoxy-3-(9-hydroxy-phenylmethyl)-chroman-4-one (**Scheme 12**, **structures 162**). $[\alpha]_D$ values of this compound were reported to be +62 (c 0.1, $CH_3OH$)), -13.5 (c 0.2; $CH_2Cl_2$), and +44 (c 0.05, $CHCl_3$). Varying signs of specific rotation in different solvents were considered to make it difficult to predict the AC from SOR studies.[176] For this reason, ECD, VCD and ROA were used as alternate methods for determining the AC of isolated homoisoflavanone. Experimental ECD spectra were measured at a concentration of 39.5 μM in methanol, while VCD spectra were measured at a concentration of 4.0 mg in 110 microL of DMSO-$d_6$ and ROA spectra were measured at a concentration of 30 mg/mL in methanol. ECD calculations were carried out using B3PW91 functional and TZVP basis set, while VCD spectral predictions were obtained using B3PW91 functional and 6-31+G(d,p) basis set and ROA spectral predictions were obtained using B3LYP functional and TZVP basis set. All calculations represented the solvent using PCM. The conformers within 1.4 kcal $mol^{-1}$ energy range, corresponding to 95% of the total Boltzmann distribution, were selected for ECD, VCD, and ROA spectral calculations. It was found that ECD was not sensitive enough to the absolute configuration

of the chiral center at C-9, because calculations for both (3*R*,9*R*) and (3*R*,9*S*) yielded very similar spectra. The comparison of experimental VCD spectra in DMSO-$d_6$ with those predicted for (3*R*,9*R*) structure using PCM for representing the DMSO solvent are considered to be satisfactory for assigning the AC of isolated homoisoflavanone to be (3*R*,9*R*). The same conclusion was reached from a comparison of the experimental ROA spectra in methanol (Figure 14) with those predicted with solvent represented by PCM. Based on these combined studies, it was found that the use of more than one chiroptical spectroscopic method can be advantageous and that VCD and ROA methods can be more powerful methods for assigning the AC of natural products.

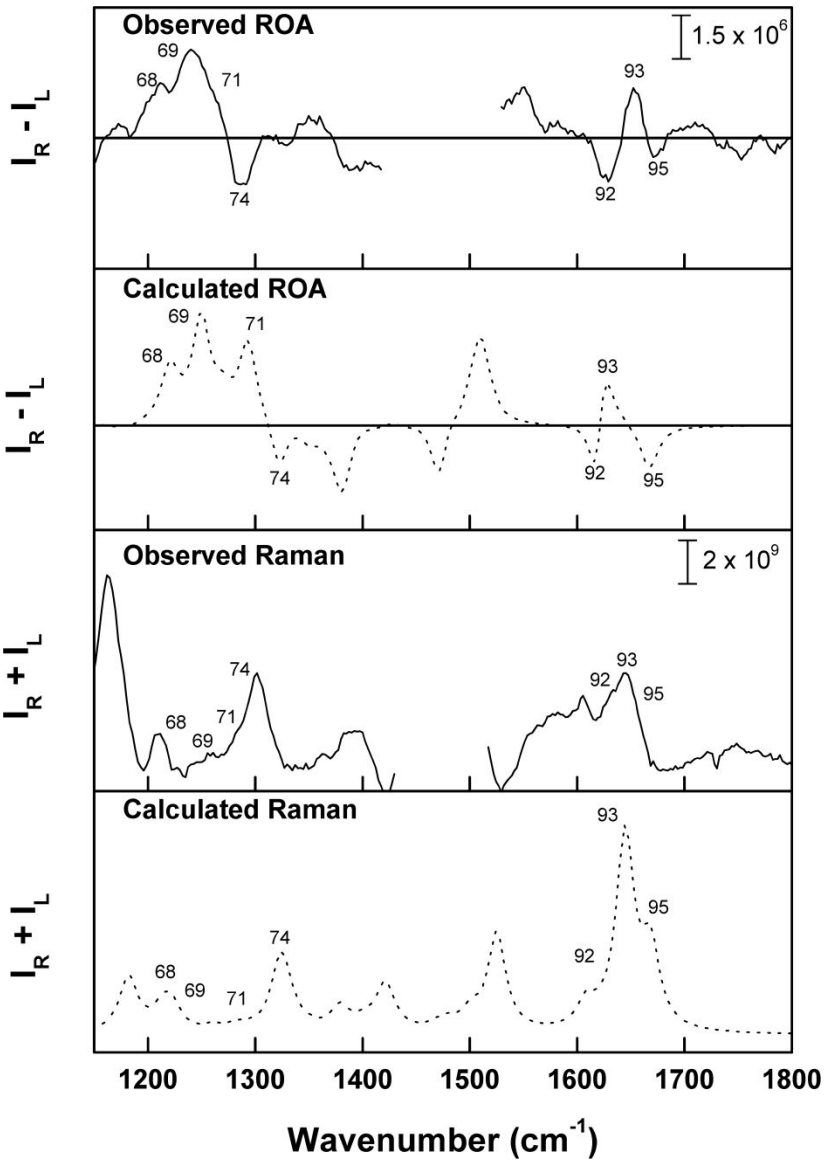


**Figure 14**: Experimental and predicted Raman and ROA spectra of **162**. While ECD was not sensitive enough to the absolute configuration of the chiral center at C-9, ROA spectra confirmed (3*R*,9*R*) configuration of **162**. Reprinted with permission from Ref.[176] Copyright (2015) Elsevier.

# 5. Prospects and Limitations

This review has surveyed more than 150 natural products whose ACs were either determined, or confirmed, using VOA spectroscopy during the years 2015-2019. In the analysis of some of these natural products, the limitations of ECD spectral analyses were encountered for: Anacolosin D,[109] Pleosporalone D,[110] Penicitrinone A,[114] Jonquailine,[116] Griseorhodins A and C,[121] Diplopyrone,[133] (1'S,5'S,6'S)-5',6'-dihydroxy-2',6'-dimethyl-3'-(2"-oxopentyl)cyclohex-2'-en-1'-yl 2,4-dihydroxy-6-methylbenzoate,[140] and (S)-1-(3,5-dihydroxy-4-methylphenyl)-4-hydroxypentan-2-one,[140] Brevianamide B,[156] flavone C-diglycoside,[171] and homoisoflavanone.[176] Similarly, the limitations in the applications of NMR were encountered in the analysis of some other natural products, such as 3-O-Caffeoyl-2-(2-propyl)-2-hydroxybutanedioic acid,[125] 3-O-Caffeoyl-2-((S)-2-butyl)-2-hydroxy butanedioic acid,[125] Diplopyrone,[133], Isocorilagin,[144] and ent-Kaurene Glycosides[158], and flavone C-diglycoside.

It should be noted that VOA spectroscopy is not infallible and certain limitations trail the potential advantages. As already mentioned, the advantages of VOA spectroscopy arises from universal nature, and large number, of molecular vibrational transitions. However, there are some practical limitations. (1). Compounds that can be dissolved only in aqueous media may not be amenable to VCD studies, but may be studied using VROA. (2). Compounds that absorb in the visible spectra region may not be amenable to VROA studies, but may be studied using VCD. (3). The AC determination from VOA spectroscopy relies on matching the experimental spectrum with QC predicted spectra for diastereomers (where applicable). As a result, computational demands become the bottleneck in the analysis of experimental spectra. (4). Almost all of the applications of VOA spectroscopy reported to date are limited to cases where the stereochemistry needed to be determined was for only one, two or at the most three, chiral elements. In some applications, relative stereochemistry was known and the question addressed was that of the correct enantiomer. For natural products possessing more than three chiral elements, which represent a majority situation, additional studies (such as NMR, synthetic schemes etc) had to be used to pre-establish the relative stereochemistry, or the AC of all, but one, two, or at the most three, of the chiral elements. As determining relative configurations or ACs at certain centers using sophisticated NMR methods is quite common, this point is not a serious limitation in natural product research. But it is useful for the young researchers to be aware of this point. (4). From a purely fundamental viewpoint, however, if it is necessary to determine the ACs of multiple stereocenters, it is possible that predicted VOA spectra for more than one diastereomer can exhibit acceptable agreement with the experimental spectra. In such cases, VOA spectroscopy might not be able to provide a unique solution. (5). The implied assumption in VOA spectral analysis is that the chemical structure (i.e atomic composition and atom connectivity) of the compound being investigated is known and correct. In the case of mis-assigned chemical structures, it will be prudent to undertake VOA spectral analysis for all assigned chemical structures to ascertain the chemical structure that best reproduces the experimental spectra.[105] (6). In the spectral analyses involving the comparison of the experimental and simulated spectra, there are multiple variables. Importantly, most diastereomers are endowed with a multitude of conformers. The relative energies, and hence the populations of these conformers, usually determined from the QC calculations, have uncertainties of unknown nature. A simulated VOA spectrum for a given diastereomer is obtained by weighting each conformer with a population determined using the energies obtained from QC calculations. In this context, two points should be kept in mind: (a). If the populations of conformers used in the

simulated spectra are incorrect, then the assigned configuration may be wrong even in the presence of a good agreement between the simulated and experimental spectra; (b). It is not possible to know a priori whether the populations of conformers used are correct or not. Therefore, the agreement between population weighted spectrum for a given diastereomer and the observed experimental spectrum does not ensure that the populations of conformers used in the simulated spectra are indeed correct. The conformer populations deduced from QC calculations are subject to independent experimental verification (7). Collective use of VCD, ECD and ORD can sometimes yield contradictory conclusions (especially for molecules with high degree of conformational freedom[129]) or no definitive conclusion (as for Pleosporalones E and F[110]) regarding AC; (8). The comparison of predicted VCD spectra with experimental spectra sometimes may not provide unambiguous conclusion for determining the AC (as for inuloxin A and Seiricardine A),[153] the reasons for which are not yet clear.

Within the constraints mentioned above, VOA spectroscopy provides a powerful means of deriving absolute configuration information for chiral natural products. The experimental spectral measurements are made routine by the availability of commercial instruments, although one should be wary of spectral artefacts and put in place the necessary quality control safeguards. Although the sample amounts required for VOA spectral measurements are in the milligram range, the samples used for VOA measurements can be safely recovered for subsequent use in other measurements. Therefore, one does not have to be concerned about losing rare and precious samples during these measurements. The availability of both commercial and freeware programs for QC predictions of VOA spectral properties renders the calculation of VOA spectra also routine. Larger molecules with up to 100 atoms can be handled for QC predictions with currently available computers, but constantly evolving progress in computer technology offers a bright future for handling even larger size molecules. The combination of experimental and computational developments achieved to date are making it possible to practice VOA spectroscopy as routinely as conventional IR and Raman spectroscopy are being practiced.

# 6. Conflicts of interest

None

# 7. Acknowledgments

Financial support from National Science Foundation (CHE1464874) is gratefully acknowledged.

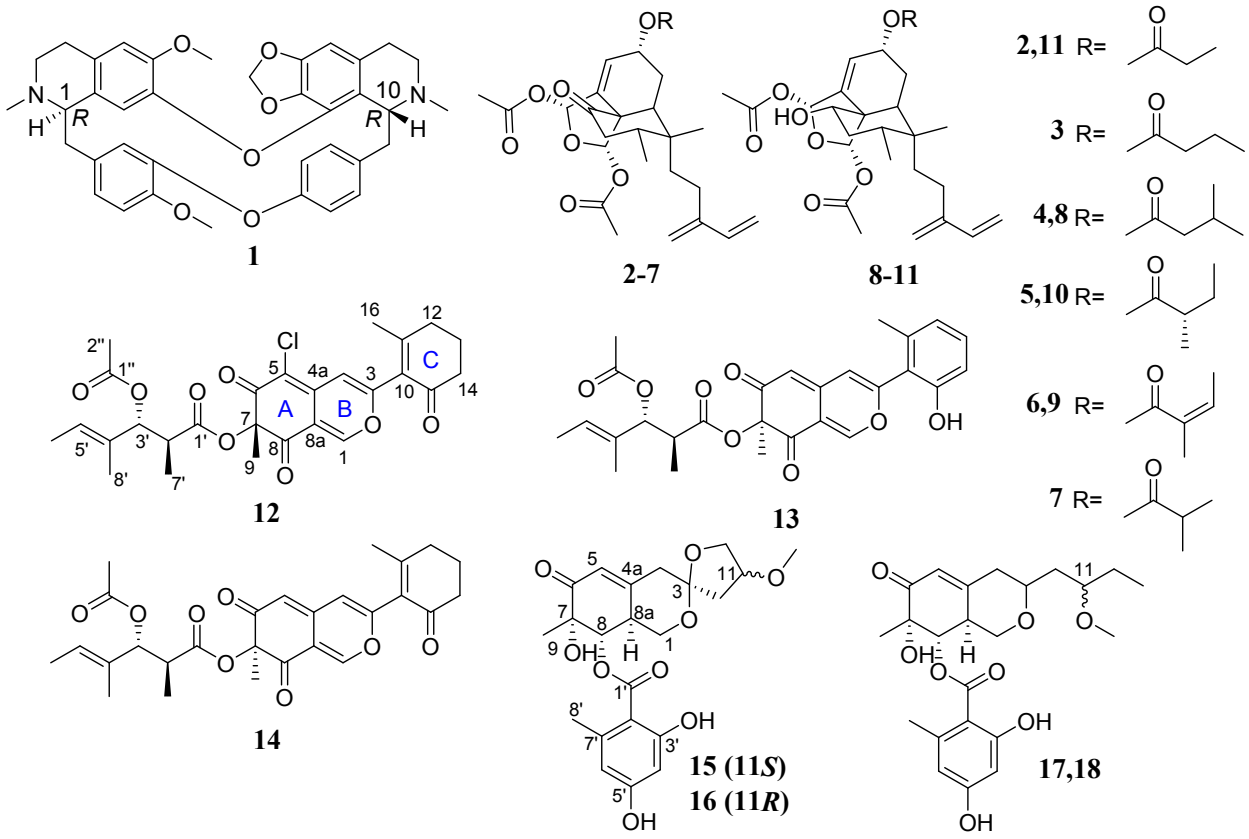


**Scheme 1**

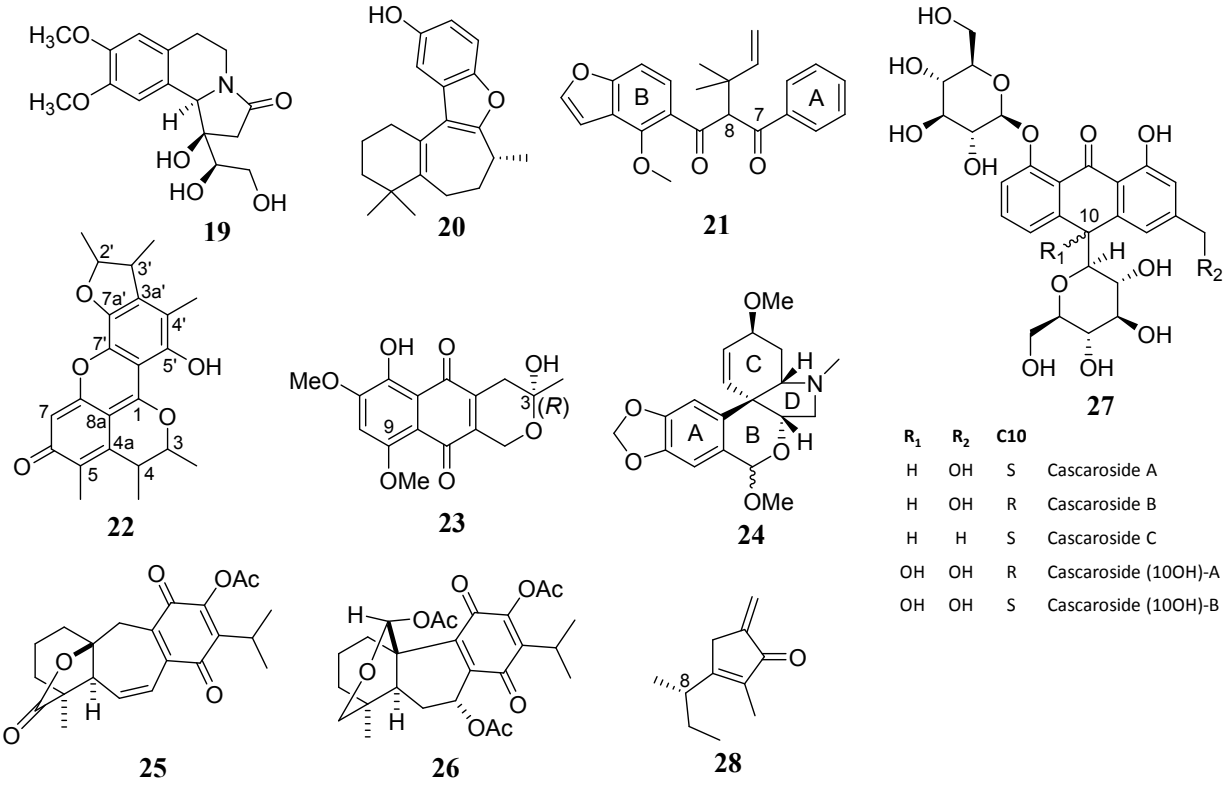


**Scheme 2**

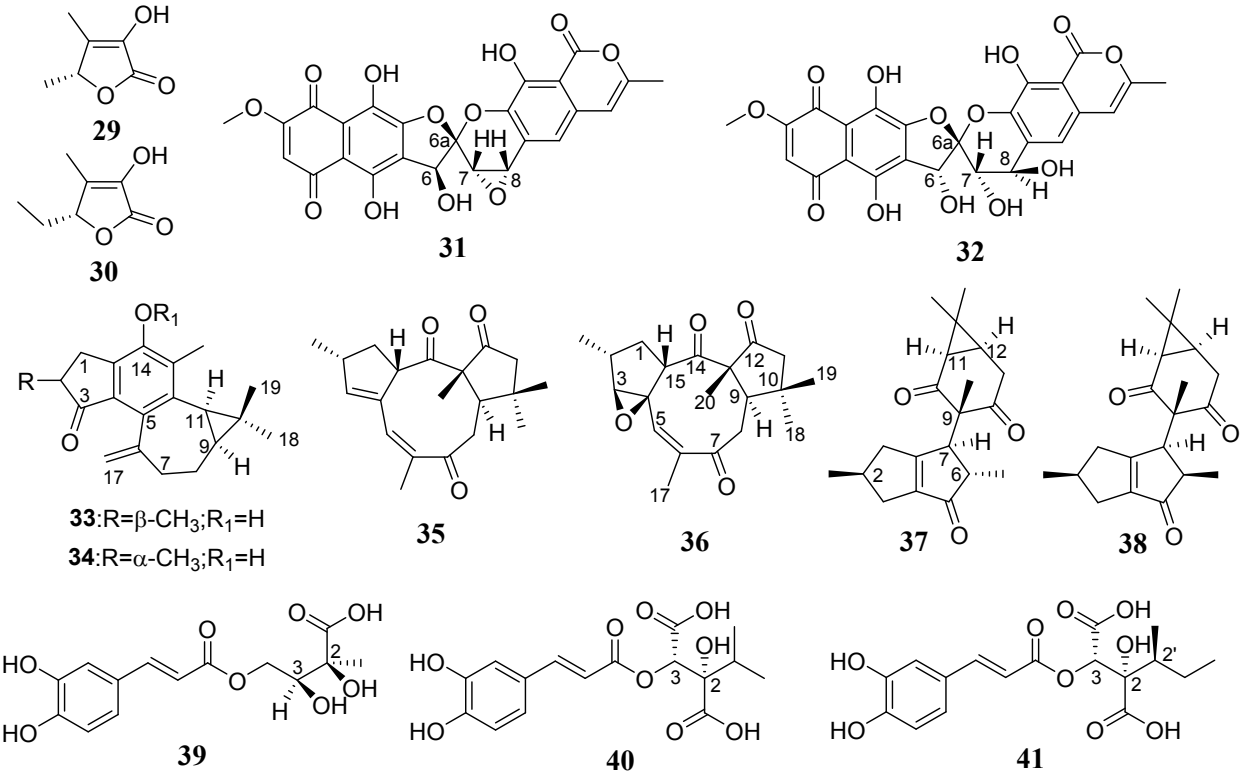


**Scheme 3**

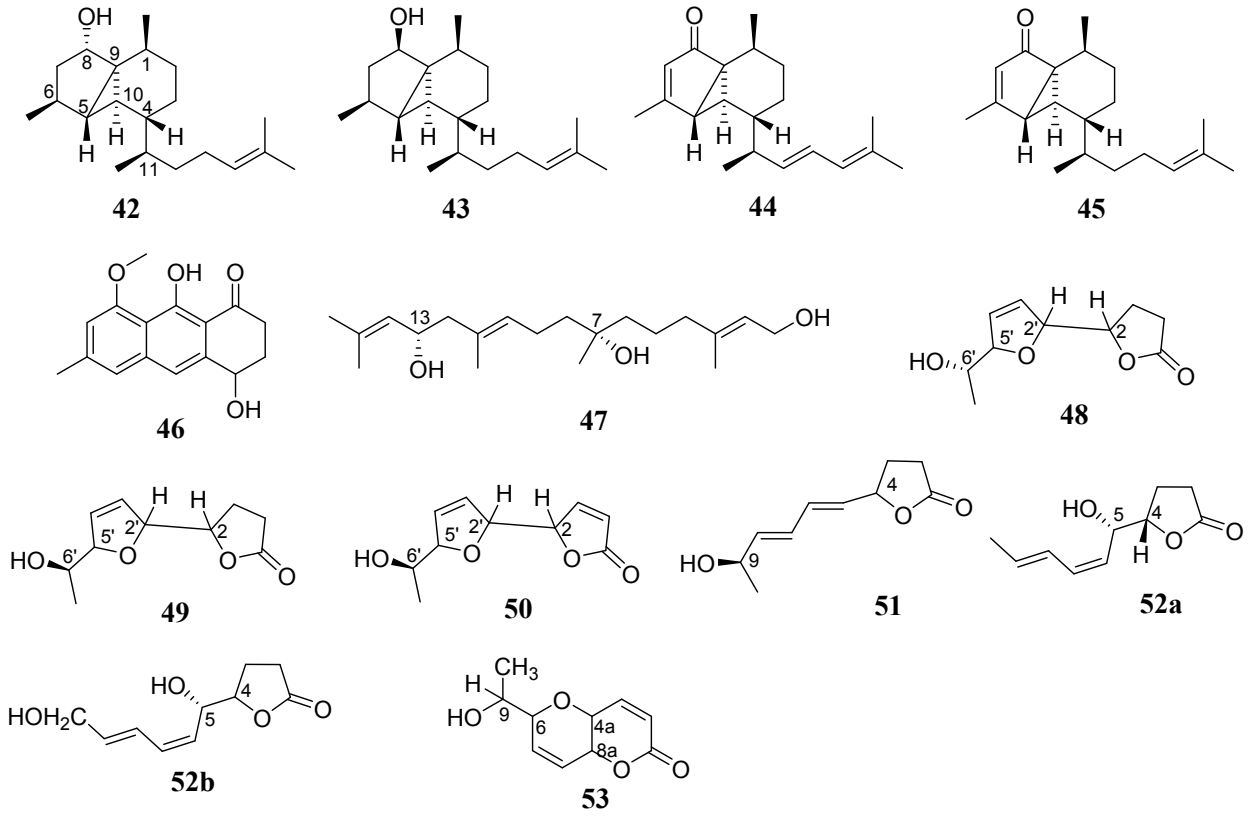


**Scheme 4**

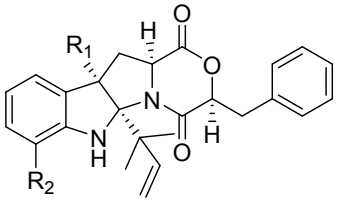

**54**:$R_1$=OH; $R_2$=H
**55**:$R_1$=$OCOCH_3$; $R_2$=H

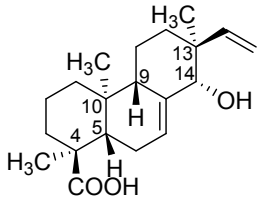

**56**

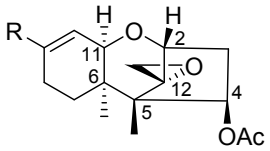

**57**:R=$CH_3$
**58**:R=$CH_2OH$

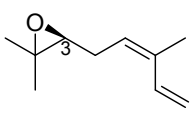

**59**

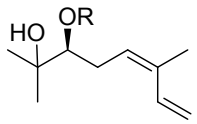

**60**:R=H
**62**:R=Ac

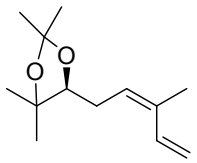

**61**

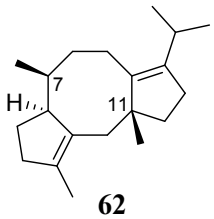

**62**

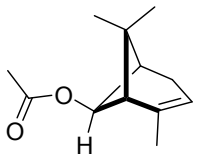

**63**

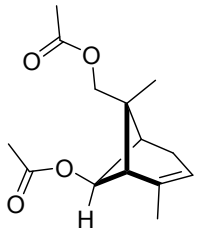

**64**

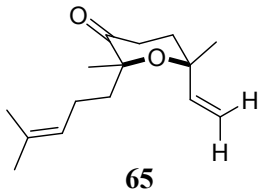

**65**

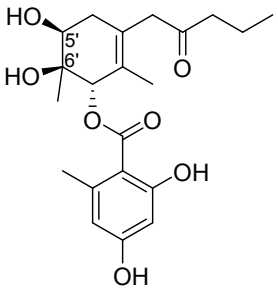

**66**

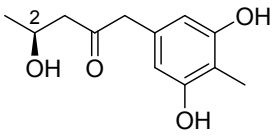

**67**

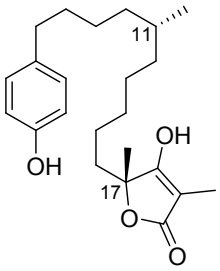

**68**

**Scheme 5**

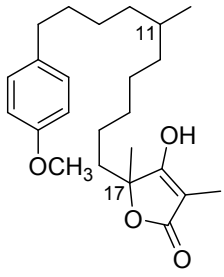


**69**

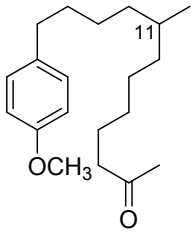


**70**

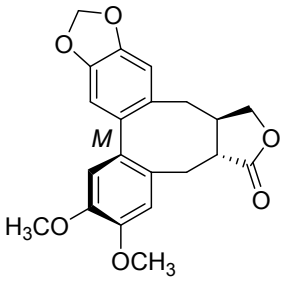


**71**

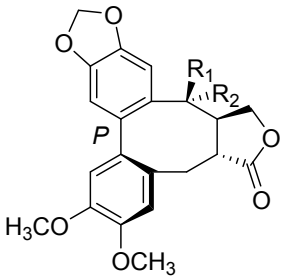


**72**:$R_1$=$R_2$=H
**73**:$R_1$=H;$R_2$=OAc

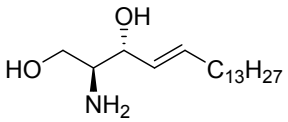


**74**

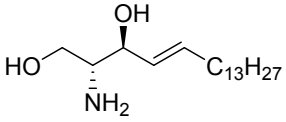


**75**

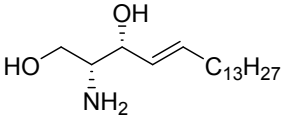


**76**

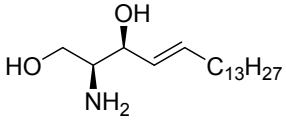


**77**

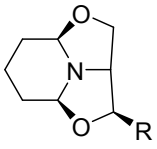


**78**

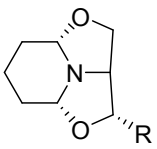


**79**

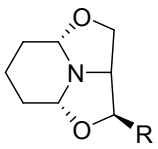


**80**

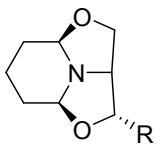


**81**

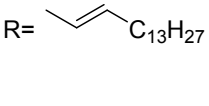


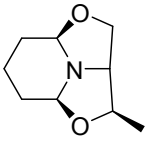


**82**

**Scheme 6**

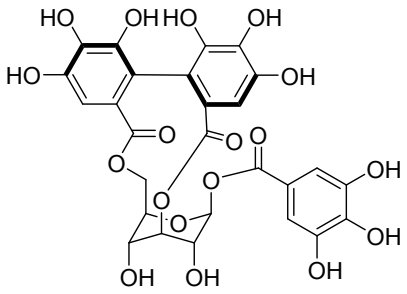

**83**

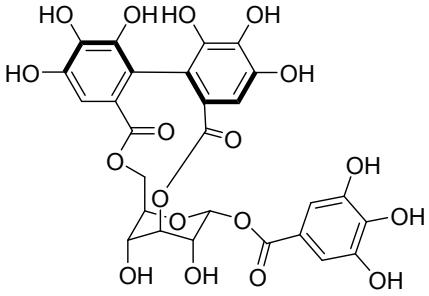

**84**

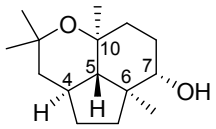

**85**

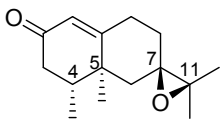

**86**

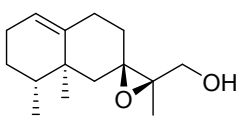

**87**

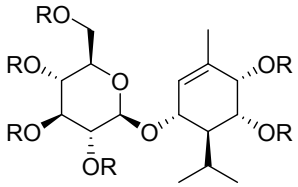

**88**:R=H
**89**:R=Ac

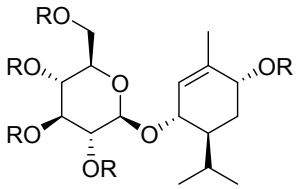

**90**:R=H
**91**:R=Ac

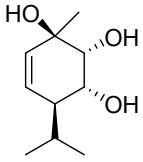

**92**

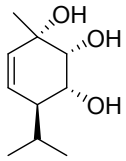

**93**

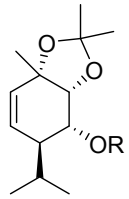

**94**:R=H
**95**:R=Ac

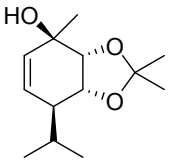

**96**

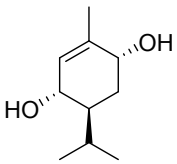

**97**

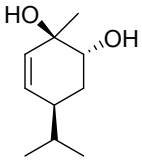

**98**

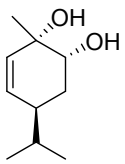

**99**

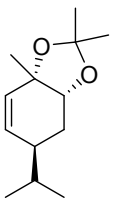

**100**

**Scheme 7**

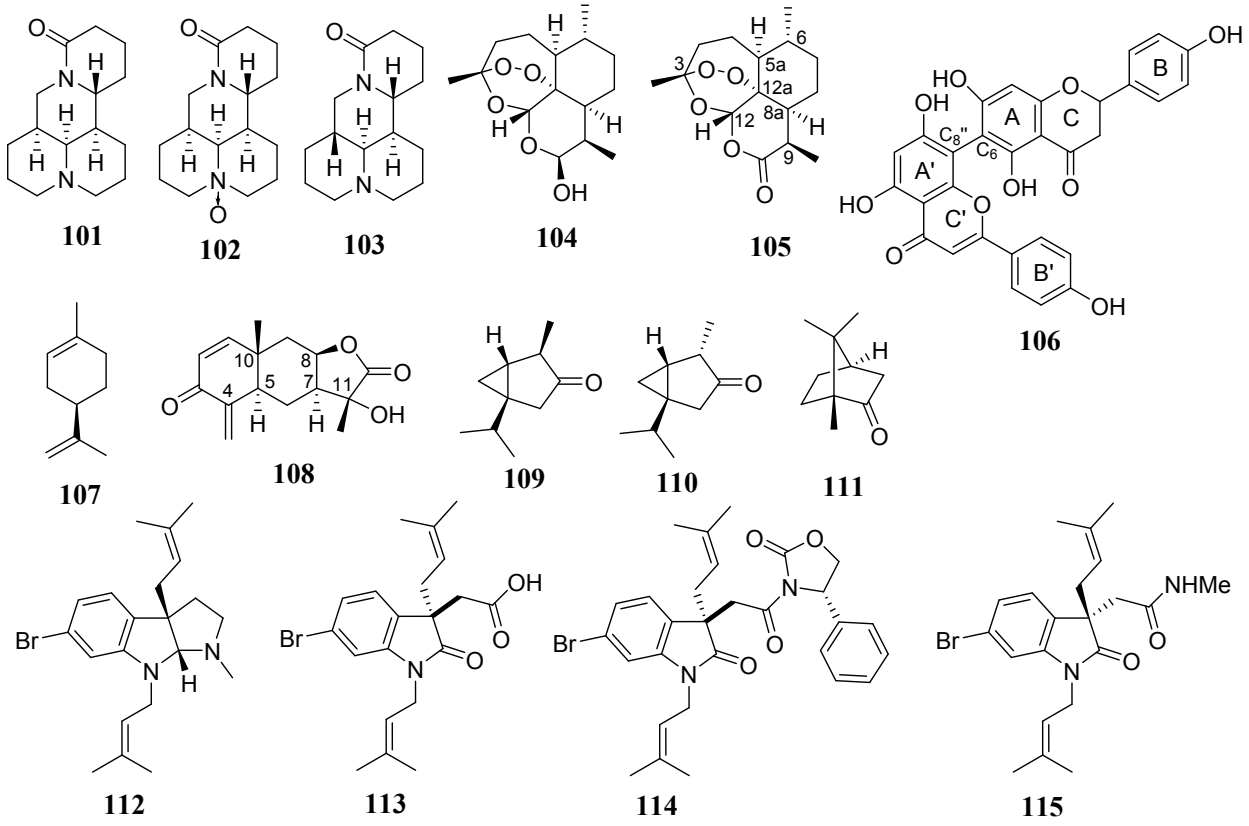


**Scheme 8**

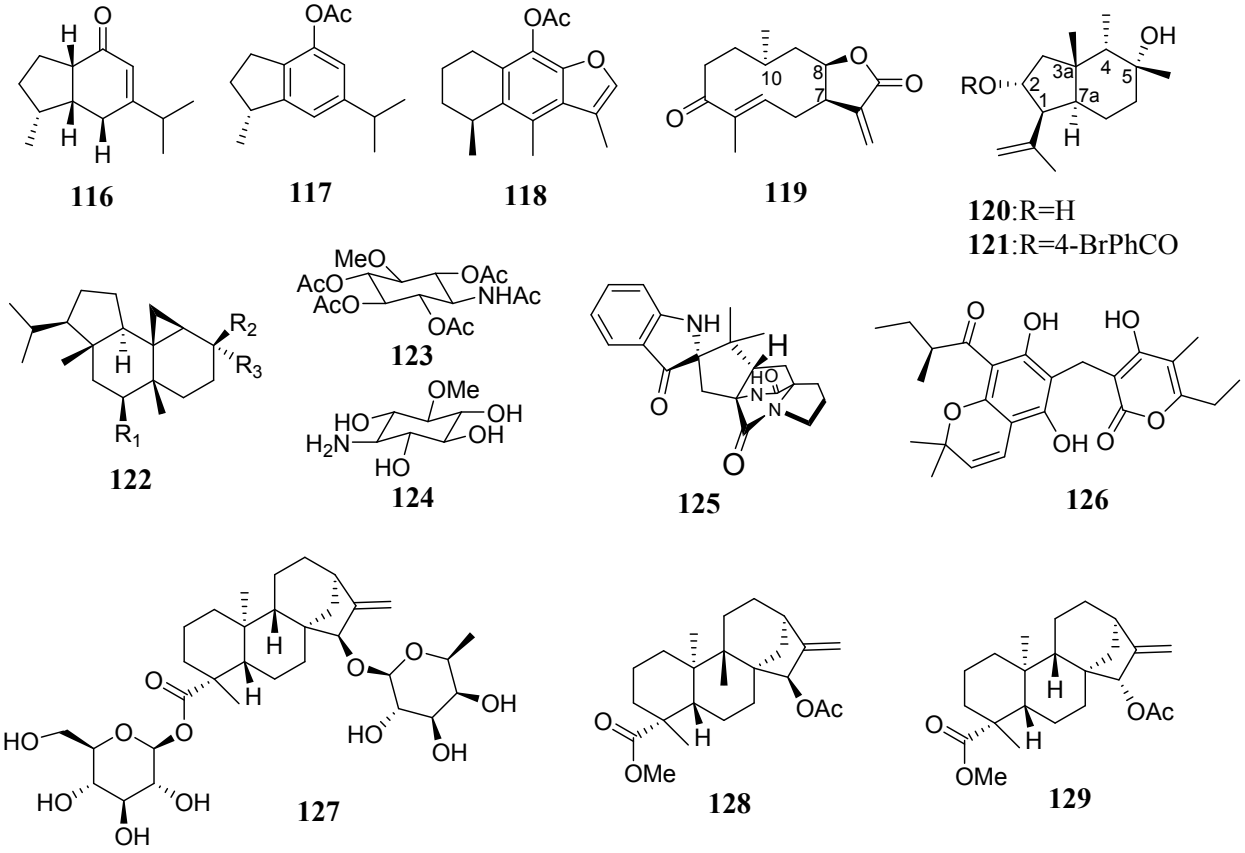
116
117
118
119
120:R=H
121:R=4-BrPhCO
122
123
124
125
126
127
128
129

**Scheme 9**

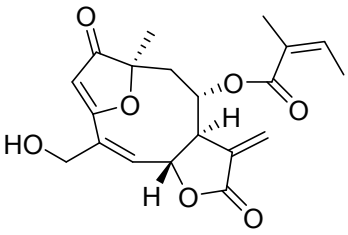

**130**

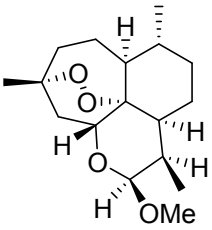

**131**

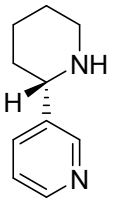

**132**

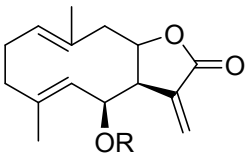

**133**:R=H
**134**:R=Ac

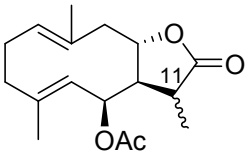

**135**:α-Me(11*R*)
**136**:β-Me(11*S*)

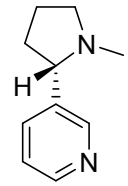

**137**

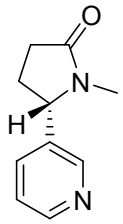

**138**

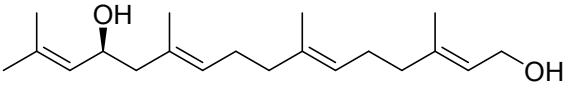

**139**

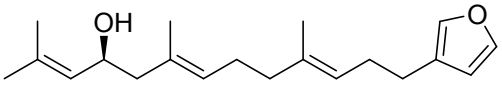

**140**

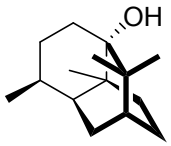

**141**

**Scheme 10**

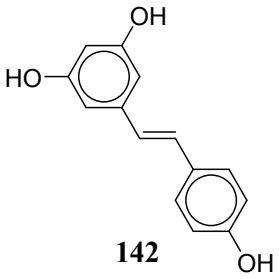


**142**

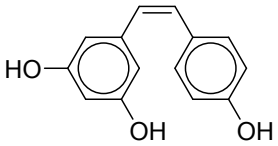


**143**

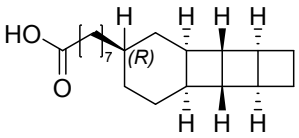


**144**

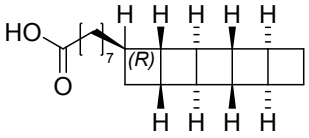


**145**

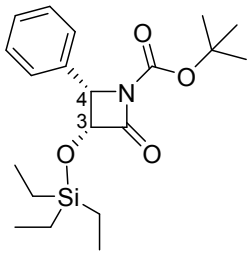


**146**

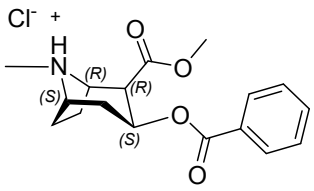


**147**

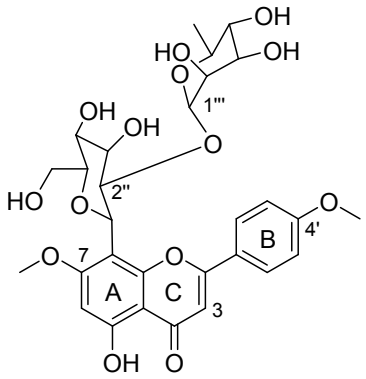


**148**

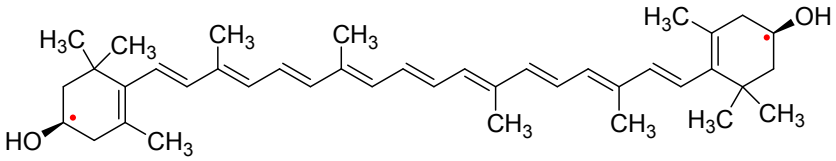


**149**

**Scheme 11**

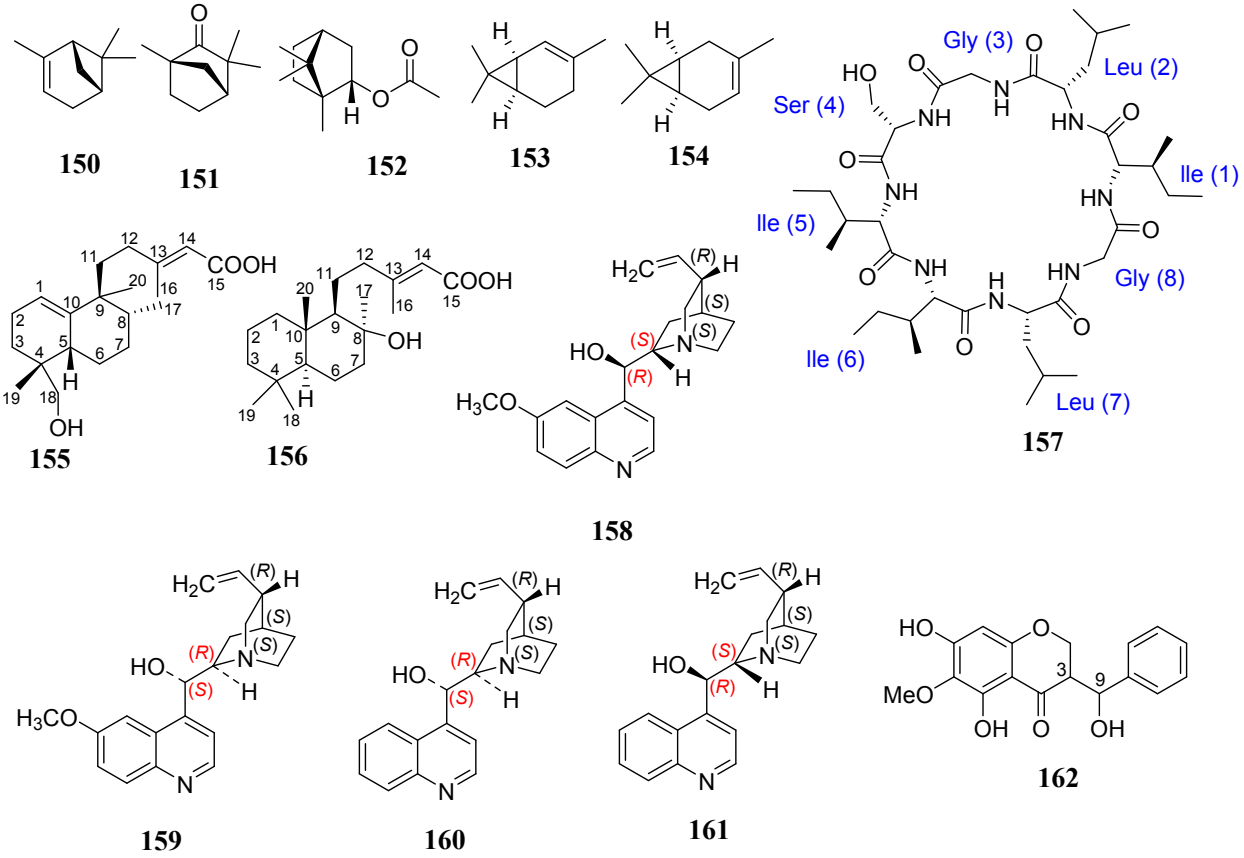
150
151
152
153
154
155
156
157
158
159
160
161
162
Gly (3)
Leu (2)
Ser (4)
Ile (1)
Ile (5)
Gly (8)
Ile (6)
Leu (7)

**Scheme 12**

# 8. Notes and References


1. N. Berova, P. L. Polavarapu, K. Nakamishi and R. W. Woody, eds., *Comprehensive Chiroptical Spectroscopy*, Wiley, 2012.
2. P. L. Polavarapu, *Chiroptical Spectroscopy: Fundamentals and Applications*, CRC Press LLC, 2016.
3. P. L. Polavarapu, *The Journal of Physical Chemistry A*, 2005, **109**, 7013-7023.
4. G. Holzwarth, E. C. Hsu, H. S. Mosher, T. R. Faulkner and A. Moscowitz, *Journal of the American Chemical Society*, 1974, **96**, 251-252.
5. L. A. Nafie, J. C. Cheng and P. J. Stephens, *J. Am. Chem. Soc.*, 1975, **97**, 3842-3843.
6. L. D. Barron, M. P. Bogaard and A. D. Buckingham, *Journal of the American Chemical Society*, 1973, **95**, 603-605.
7. W. Hug, S. Kint, G. F. Bailey and J. R. Scherer, *Journal of the American Chemical Society*, 1975, **97**, 5589-5590.
8. A. G. Kutateladze, E. H. Krenske and C. M. Williams, *Angewandte Chemie International Edition*, 2019, **58**, 7107-7112.
9. K. C. Nicolaou and S. A. Snyder, *Angewandte Chemie International Edition*, 2005, **44**, 1012-1044.
10. M. E. Maier, *Natural Product Reports*, 2009, **26**, 1105-1124.
11. T. L. Suyama, W. H. Gerwick and K. L. McPhail, *Bioorganic & Medicinal Chemistry*, 2011, **19**, 6675-6701.
12. L. Grauso, R. Teta, G. Esposito, M. Menna and A. Mangoni, *Natural Product Reports*, 2019, **36**, 1005-1030.
13. A. Mándi and T. Kurtán, *Natural Product Reports*, 2019, **36**, 889-918.
14. J. M. Batista Jr, E. W. Blanch and V. d. S. Bolzani, *Natural Product Reports*, 2015, **32**, 1280-1302.
15. L. D. Barron, *Biomedical Spectroscopy and Imaging*, 2015, **4**, 223-253.
16. Y. Hamada, in *Introduction to Experimental Infrared Spectroscopy: Fundamentals and Practical Methods*, ed. M. Tasumi, John Wiley and Sons 2014, pp. 321-334.
17. P. Dai, N. Jiang and R.-X. Tan, *Journal of Asian Natural Products Research*, 2016, **18**, 72-91.
18. E. Burgueño-Tapia and P. Joseph-Nathan, *Nat Prod Commun*, 2017, **12**, 641-651.
19. D. Kurouski, *Analytica chimica acta*, 2017, **990**, 54-66.
20. S. Superchi, P. Scafato, M. Gorecki and G. Pescitelli, *Current Medicinal Chemistry*, 2018, **25**, 287-320.
21. S. T. Mutter, F. Zielinski, P. L. A. Popelier and E. W. Blanch, *Analyst*, 2015, DOI: 10.1039/c4an02357a.
22. P. L. Polavarapu, *Vibrational Spectra: Principles and Applications With Emphasis on Optical Activity*, Elsevier, 1998.
23. P. J. Stephens, F. Devlin and J. R. Cheeseman, *VCD Spectroscopy for Organic Chemists*, CRC Press, 2012.
24. L. A. Nafie, *Vibrational Optical Activity: Principles and Applications*, John Wiley and Sons, New York, 2011.
25. X. Lu, H. Li, J. W. Nafie, T. Pazderka, M. Pazderková, R. K. Dukor and L. A. Nafie, *Applied Spectroscopy*, 2017, **71**, 1117-1126.

26. T. A. Keiderling, *Molecules*, 2018, **23**, 2404.
27. T. A. Keiderling and A. Lakhani, *Chirality*, 2018, **30**, 238-253.
28. P. L. Polavarapu and Z. Deng, *Appl. Spectrosc.*, 1996, **50**, 686-692.
29. J. C. Cheng, L. A. Nafie and P. J. Stephens, *J. Opt. Soc. Am.*, 1975, **65**, 1031-1035.
30. L. A. Nafie, *Appl. Spectrosc.*, 2000, **54**, 1634-1645.
31. P. L. Polavarapu and G. Shanmugam, *Chirality*, 2011, **23**, 801-807.
32. BioTools, http://btools.com/products.html, (accessed 1/1/2020, 2020).
33. S. J. Cianciosi, K. M. Spencer, T. B. Freedman, L. A. Nafie and J. E. Baldwin, *Journal of the American Chemical Society*, 1989, **111**, 1913-1915.
34. P. L. Polavarapu, *Chemical Physics Letters*, 1989, **161**, 485-490.
35. M. Diem, E. Photos, H. Khouri and L. A. Nafie, *Journal of the American Chemical Society*, 1979, **101**, 6829-6837.
36. A. G. Petrovic, P. K. Bose and P. L. Polavarapu, *Carbohydrate Research*, 2004, **339**, 2713-2720.
37. G. Shanmugam and P. L. Polavarapu, *Applied Spectroscopy*, 2005, **59**, 673-681.
38. P. Zhang and P. L. Polavarapu, *Applied Spectroscopy*, 2006, **60**, 378-385.
39. I. Kawamura and H. Sato, *Analytical Biochemistry*, 2019, **580**, 14-20.
40. C. Merten, T. Kowalik and A. Hartwig, *Applied Spectroscopy*, 2008, **62**, 901-905.
41. L. D. Barron, *Molecular light scattering and optical activity*, Cambridge University Press, Cambridge, Second edn., 2004.
42. W. Hug and G. Hangartner, *Journal of Raman Spectroscopy*, 1999, **30**, 841-852.
43. J. Kapitán, L. D. Barron and L. Hecht, *Journal of Raman Spectroscopy*, 2015, **46**, 392-399.
44. Y. Zhang, P. Wang, G. Jia, F. Cheng, Z. Feng and C. Li, *Applied Spectroscopy*, 2017, **71**, 2211-2217.
45. F. C. Basilio, P. T. Campana, E. M. Therézio, N. M. Barbosa Neto, F. Serein-Spirau, R. A. Silva, O. N. Oliveira and A. Marletta, *The Journal of Physical Chemistry C*, 2016, **120**, 25101-25109.
46. J. Šebestík and P. Bouř, *The Journal of Physical Chemistry Letters*, 2011, **2**, 498-502.
47. R. Sgammato, W. Herrebout and C. Johannessen, *Journal of Raman Spectroscopy*, 2019, **50**, 1905-1913.
48. M. Dudek, G. Zajac, A. Kaczor and M. Baranska, *Journal of Raman Spectroscopy*, 2017, **48**, 673-679.
49. S. Abdali and E. W. Blanch, *Chemical Society Reviews*, 2008, **37**, 980-992.
50. M. Pecul, *Chirality*, 2009, **21**, E98-E104.
51. K. Ruud and A. J. Thorvaldsen, *Chirality*, 2009, **21**, E54-E67.
52. V. Parchaňský, J. Kapitán and P. Bouř, *RSC Advances*, 2014, **4**, 57125-57136.
53. M. Srebro-Hooper and J. Autschbach, *Annual Review of Physical Chemistry*, 2017, **68**, 399-420.
54. S. Luber, *Journal of Chemical Theory and Computation*, 2017, **13**, 1254-1262.
55. C. Puzzarini, J. Bloino, N. Tasinato and V. Barone, *Chemical Reviews*, 2019, **119**.
56. V. Barone and C. Puzzarini, in *Molecular Spectroscopy: A Quantum Chemistry Approach*, ed. Y. W. Ozaki, Janusz Marek; Popp, Jürgen John Wiley & Sons, New York, 2019, vol. 1, pp. 1-42.

57. M. Pecul and J. Sadlej, in *Molecular Spectroscopy: A Quantum Chemistry Approach*, eds. Y. Ozaki, M. J. Wójcik and J. Popp, John Wiley & Sons, New York, 2019, vol. 1, pp. 171-198.
58. G. Holzwarth and I. Chabay, *The Journal of Chemical Physics*, 1972, **57**, 1632-1635.
59. V. P. Nicu, *Physical Chemistry Chemical Physics*, 2016, **18**, 21202-21212.
60. P. J. Stephens, *Journal of Physical Chemistry*, 1985, **89**, 748-752.
61. A. D. Buckingham, P. W. Fowler and P. A. Galwas, *Chemical Physics*, 1987, **112**, 1-14.
62. A. Scherrer, R. Vuilleumier and D. Sebastiani, *Journal of Chemical Theory and Computation*, 2013, **9**, 5305-5312.
63. A. Scherrer, F. Agostini, D. Sebastiani, E. K. U. Gross and R. Vuilleumier, *The Journal of Chemical Physics*, 2015, **143**, 074106.
64. L. A. Nafie, *The Journal of Physical Chemistry A*, 1997, **101**, 7826-7833.
65. T. B. Freedman, M.-L. Shih, E. Lee and L. A. Nafie, *Journal of the American Chemical Society*, 1997, **119**, 10620-10626.
66. M. Fusè, F. Egidi and J. Bloino, *Physical Chemistry Chemical Physics*, 2019, **21**, 4224-4239.
67. A. Scherrer, R. Vuilleumier and D. Sebastiani, *The Journal of Chemical Physics*, 2016, **145**, 084101.
68. M. Thomas and B. Kirchner, *The Journal of Physical Chemistry Letters*, 2016, **7**, 509-513.
69. S. Abbate, G. Longhi, K. Kwon and A. Moscowitz, *The Journal of Chemical Physics*, 1998, **108**, 50-62.
70. G. Zuber and W. Hug, *The Journal of Physical Chemistry A*, 2004, **108**, 2108-2118.
71. J. R. Cheeseman and M. J. Frisch, *Journal of Chemical Theory and Computation*, 2011, **7**, 3323-3334.
72. G. Scalmani and M. J. Frisch, *The Journal of Chemical Physics*, 2010, **132**, 114110.
73. J. Tomasi, B. Mennucci and R. Cammi, *Chemical Reviews*, 2005, **105**, 2999-3094.
74. A. Klamt and G. Schuurmann, *Journal of the Chemical Society, Perkin Transactions 2*, 1993, DOI: 10.1039/p29930000799, 799-805.
75. A. S. Perera, J. Thomas, M. R. Poopari and Y. Xu, *Front Chem*, 2016, **4**, 9-9.
76. T. Giovannini, M. Olszòwka and C. Cappelli, *Journal of Chemical Theory and Computation*, 2016, **12**, 5483-5492.
77. T. Giovannini, G. Del Frate, P. Lafiosca and C. Cappelli, *Physical Chemistry Chemical Physics*, 2018, **20**, 9181-9197.
78. T. Giovannini, M. Olszówka, F. Egidi, J. R. Cheeseman, G. Scalmani and C. Cappelli, *Journal of Chemical Theory and Computation*, 2017, **13**, 4421-4435.
79. M. Brehm and M. Thomas, *The Journal of Physical Chemistry Letters*, 2017, **8**, 3409-3414.
80. L. N. Vidal, F. Egidi, V. Barone and C. Cappelli, *The Journal of Chemical Physics*, 2015, **142**, 174101.
81. L. N. Vidal, T. Giovannini and C. Cappelli, *The Journal of Physical Chemistry Letters*, 2016, **7**, 3585-3590.
82. A. Baiardi, J. Bloino and V. Barone, *Journal of Chemical Theory and Computation*, 2018, **14**, 6370-6390.
83. J. Mattiat and S. Luber, *The Journal of Chemical Physics*, 2019, **151**, 234110.

84. P. Bouř, J. Sopková, L. Bednárová, P. Maloň and T. A. Keiderling, *Journal of Computational Chemistry*, 1997, **18**, 646-659.
85. N. S. Bieler, M. P. Haag, C. R. Jacob and M. Reiher, *Journal of Chemical Theory and Computation*, 2011, **7**, 1867-1881.
86. K. V. J. Jose and K. Raghavachari, *J Chemical Theory and Computation*, 2016, **12**, 585-594.
87. K. V. Jovan Jose, D. Beckett and K. Raghavachari, *J Chemical Theory and Computation*, 2015, **11**, 4238-4247.
88. K. V. J. Jose and K. Raghavachari, *Chirality*, 2016, **28**, 755-768.
89. T. Q. Teodoro, M. A. J. Koenis, S. E. Galembeck, V. P. Nicu, W. J. Buma and L. Visscher, *The Journal of Physical Chemistry Letters*, 2018, **9**, 6878-6882.
90. G. Monaco, F. Aquino, R. Zanasi, W. Herrebout, P. Bultinck and A. Massa, *Physical Chemistry Chemical Physics*, 2017, **19**, 28028-28036.
91. G. Monaco, G. Procida, A. Di Mola, W. Herrebout and A. Massa, *Chemical Physics Letters*, 2020, **739**, 137000.
92. J. Bloino and V. Barone, *The Journal of Chemical Physics*, 2012, **136**, 124108.
93. J. Bloino, M. Biczysko and V. Barone, *The Journal of Physical Chemistry A*, 2015, **119**, 11862-11874.
94. C. L. Covington and P. L. Polavarapu, *Journal*, 2/23/2016.
95. C. L. Covington and P. L. Polavarapu, *Chirality*, 2017, **29**, 178-192.
96. T. Bruhn, A. Schaumlöffel, Y. Hemberger and G. Bringmann, *Chirality*, 2013, **25**, 243-249.
97. J. He, A. Petrovich and P. L. Polavarapu, *The Journal of Physical Chemistry A*, 2004, **108**, 1671-1680.
98. F. J. Devlin and P. J. Stephens, *Journal of the American Chemical Society*, 1999, **121**, 7413-7414.
99. J. Shen, C. Zhu, S. Reiling and R. Vaz, *Spectrochimica Acta Part A: Molecular and Biomolecular Spectroscopy*, 2010, **76**, 418-422.
100. E. Debie, E. De Gussem, R. K. Dukor, W. Herrebout, L. A. Nafie and P. Bultinck, *ChemPhysChem*, 2011, **12**, 1542-1549.
101. C. L. Covington, F. M. S. Junior, J. H. S. Silva, R. M. Kuster, M. B. de Amorim and P. L. Polavarapu, *Journal of Natural Products*, 2016, **79**, 2530-2537.
102. C. L. Covington and P. L. Polavarapu, *The Journal of Physical Chemistry A*, 2013, **117**, 3377-3386.
103. F. M. S. Junior, C. L. Covington, A. C. F. de Albuquerque, J. F. R. Lobo, R. M. Borges, M. B. de Amorim and P. L. Polavarapu, *Journal of Natural Products*, 2015, **78**, 2617-2623.
104. P. L. Polavarapu, C. L. Covington, K. Chruszcz-Lipska, G. Zajac and M. Baranska, *Journal of Raman Spectroscopy*, 2017, **48**, 305-313.
105. P. L. Polavarapu, C. L. Covington and V. Raghavan, *ChemPhysChem*, 2017, **18**, 2459-2465.
106. J. L. Johnson, V. Raghavan, A. Cimmino, A. Moeini, A. G. Petrovic, E. Santoro, S. Superchi, N. Berova, A. Evidente and P. L. Polavarapu, *Chirality*, 2018, **30**, 1206-1214.
107. J. L. Johnson, D. S. Nair, S. M. Pillai, D. Johnson, Z. Kallingathodi, I. Ibnusaud and P. L. Polavarapu, *ACS Omega*, 2019, **4**, 6154-6164.

108. J. Ren, D. Zhao, S.-J. Wu, J. Wang, Y.-J. Jia, W.-X. Li, H.-J. Zhu, F. Cao, W. Li, C. U. Pittman and X.-J. He, *Tetrahedron*, 2019, **75**, 1194-1202.
109. S. Cai, A. L. Risinger, C. L. Petersen, T. Grkovic, B. R. O'Keefe, S. L. Mooberry and R. H. Cichewicz, *Journal of Natural Products*, 2019, **82**, 928-936.
110. F. Cao, Z.-H. Meng, X. Mu, Y.-F. Yue and H.-J. Zhu, *Journal of Natural Products*, 2019, **82**, 386-392.
111. A. N. L. Batista, F. M. dos Santos, M. J. Batista and B. Q. Cass, *Molecules*, 2018, **23**.
112. L. A. Joyce, C. C. Nawrat, E. C. Sherer, M. Biba, A. Brunskill, G. E. Martin, R. D. Cohen and I. W. Davies, *Chemical Science*, 2018, **9**, 415-424.
113. E. F. Canzi, F. M. dos Santos, E. K. Meneghetti, B. H. L. N. Sales Maia and J. M. Batista, *Tetrahedron Letters*, 2018, **59**, 135-137.
114. F. Cao, T.-T. Sun, J.-K. Yang, G.-Z. Zhao, Q.-A. Liu, L.-D. Hu, Z.-Y. Ma and H.-J. Zhu, *Natural Product Research*, 2019, **33**, 2192-2199.
115. M. Masi, S. Meyer, M. Górecki, G. Pescitelli, S. Clement, A. Cimmino and A. Evidente, *Molecules*, 2018, **23**, 1734.
116. S. Vergura, E. Santoro, M. Masi, A. Evidente, P. Scafato, S. Superchi, G. Mazzeo, G. Longhi and S. Abbate, *Fitoterapia*, 2018, **129**, 78-84.
117. B. Esquivel, E. Burgueño-Tapia, C. Bustos-Brito, N. Pérez-Hernández, L. Quijano and P. Joseph-Nathan, *Chirality*, 2018, **30**, 177-188.
118. D. P. Demarque, D. R. Pinho, N. P. Lopes and C. Merten, *Chirality*, 2018, **30**, 432-438.
119. N. Ortlieb, K. Bretzel, A. Kulik, J. Haas, S. Lüdeke, N. Keilhofer, S. D. Schrey, H. Gross and T. H. J. Niedermeyer, *ChemBioChem*, 2018, **19**, 2472-2480.
120. Q. Yang, M.-M. Liang, H.-J. Wang, Q.-Q. Zhao, H.-J. Zhu, L. Liu and C. U. Pittman, *Tetrahedron*, 2017, **73**, 2432-2438.
121. H. E. Ortega, J. M. Batista, W. G. P. Melo, J. Clardy and M. T. Pupo, *Tetrahedron Letters*, 2017, **58**, 4721-4723.
122. H. E. Ortega, J. M. Batista, W. G. P. Melo, J. Clardy and M. T. Pupo, *Tetrahedron Letters*, 2018, **59**, 1239.
123. E. Burgueño-Tapia, K. Chávez-Castellanos, E. Cedillo-Portugal and P. Joseph-Nathan, *Tetrahedron: Asymmetry*, 2017, **28**, 166-174.
124. E. M. Melchor-Martínez, D. A. Silva-Mares, E. Torres-López, N. Waksman-Minsky, G. F. Pauli, S.-N. Chen, M. Niemitz, M. Sánchez-Castellanos, A. Toscano, G. Cuevas and V. M. Rivas-Galindo, *Journal of Natural Products*, 2017, **80**, 2252-2262.
125. G. V. Ccana-Ccapatinta, B. L. Sampaio, F. M. dos Santos, J. M. Batista and F. B. Da Costa, *Tetrahedron: Asymmetry*, 2017, **28**, 1823-1828.
126. F. Cao, C.-L. Shao, Y.-F. Liu, H.-J. Zhu and C.-Y. Wang, *Scientific Reports*, 2017, **7**, 12548.
127. D. Rossi, K. M. Ahmed, R. Gaggeri, S. Della Volpe, L. Maggi, G. Mazzeo, G. Longhi, S. Abbate, F. Corana, E. Martino, M. Machado, R. Varandas, M. D. C. Sousa and S. Collina, *Molecules*, 2017, **22**, 519.
128. V. Smyrniotopoulos, C. Merten, M. Kaiser and D. Tasdemir, *Marine Drugs*, 2017, **15**, 245.
129. G. Mazzeo, A. Cimmino, M. Masi, G. Longhi, L. Maddau, M. Memo, A. Evidente and S. Abbate, *Journal of Natural Products*, 2017, **80**, 2406-2415.
130. A. Evidente, L. Maddau, E. Spanu, A. Franceschini, S. Lazzaroni and A. Motta, *Journal of Natural Products*, 2003, **66**, 313-315.

131. E. Giorgio, L. Maddau, E. Spanu, A. Evidente and C. Rosini, *The Journal of Organic Chemistry*, 2005, **70**, 7-13.
132. S. Maity, S. Kanikarapu, K. Marumudi, A. C. Kunwar, J. S. Yadav and D. K. Mohapatra, *The Journal of Organic Chemistry*, 2017, **82**, 4561-4568.
133. M. Fusè, G. Mazzeo, G. Longhi, S. Abbate, M. Masi, A. Evidente, C. Puzzarini and V. Barone, *The Journal of Physical Chemistry B*, 2019, **123**, 9230-9237.
134. M. A. Aparicio-Cuevas, I. Rivero-Cruz, M. Sánchez-Castellanos, D. Menéndez, H. A. Raja, P. Joseph-Nathan, M. d. C. González and M. Figueroa, *Journal of Natural Products*, 2017, **80**, 2311-2318.
135. Z.-Q. Wang, C.-J. Wu, Z.-H. Wang, C. Huang, J. Huang, J.-H. Wang and T.-M. Sun, *Journal of Molecular Structure*, 2017, **1146**, 484-489.
136. S. M. Ryu, H. M. Lee, E. G. Song, Y. H. Seo, J. Lee, Y. Guo, B. S. Kim, J.-J. Kim, J. S. Hong, K. H. Ryu and D. Lee, *Journal of Agricultural and Food Chemistry*, 2017, **65**, 4273-4279.
137. L. F. Julio, E. Burgueño-Tapia, C. E. Díaz, N. Pérez-Hernández, A. González-Coloma and P. Joseph-Nathan, *Chirality*, 2017, **29**, 716-725.
138. C. Merten, M. Dirkmann and F. Schulz, *Chirality*, 2017, **29**, 409-414.
139. M. E.-A. Said, I. Bombarda, J.-V. Naubron, P. Vanloot, M. Jean, A. Cheriti, N. Dupuy and C. Roussel, *Chirality*, 2017, **29**, 70-79.
140. S.-S. Ding, C.-C. Zhang, W.-S. Shi, M.-M. Liang, Q. Yang, H.-J. Zhu and Y. Li, *Tetrahedron Letters*, 2016, **57**, 75-79.
141. C. Jiménez-Romero, J. E. Rode and A. D. Rodríguez, *Tetrahedron: Asymmetry*, 2016, **27**, 410-419.
142. R. Velázquez-Jiménez, J. M. Torres-Valencia, A. Valdez-Calderón, J. G. Alvarado-Rodríguez, J. D. Hernández-Hernández, L. U. Román-Marín, C. M. Cerda-García-Rojas and P. Joseph-Nathan, *Tetrahedron: Asymmetry*, 2016, **27**, 193-200.
143. A. Nakahashi, A. K. C. Siddegowda, M. A. S. Hammam, S. G. B. Gowda, Y. Murai and K. Monde, *Organic Letters*, 2016, **18**, 2327-2330.
144. R. F. Sprenger, S. S. Thomasi, A. G. Ferreira, Q. B. Cass and J. M. Batista Junior, *Organic & Biomolecular Chemistry*, 2016, **14**, 3369-3375.
145. Y. Matsuo, S. Maeda, C. Ohba, H. Fukaya and Y. Mimaki, *Journal of Natural Products*, 2016, **79**, 2175-2180.
146. J. C. Pardo-Novoa, H. M. Arreaga-González, M. A. Gómez-Hurtado, G. Rodríguez-García, C. M. Cerda-García-Rojas, P. Joseph-Nathan and R. E. del Río, *Journal of Natural Products*, 2016, **79**, 2570-2579.
147. Y. Zhang, M. R. Poopari, X. Cai, A. Savin, Z. Dezhahang, J. Cheramy and Y. Xu, *Journal of Natural Products*, 2016, **79**, 1012-1023.
148. F. Reinscheid and U. M. Reinscheid, *Journal of Molecular Structure*, 2016, **1106**, 141-153.
149. A. R. Ortega, M. Sánchez-Castellanos, N. Pérez-Hernández, R. E. Robles-Zepeda, P. Joseph-Nathan and L. Quijano, *Chirality*, 2016, **28**, 415-419.
150. M. E.-A. Said, P. Vanloot, I. Bombarda, J.-V. Naubron, E. M. Dahmane, A. Aamouche, M. Jean, N. Vanthuyne, N. Dupuy and C. Roussel, *Analytica Chimica Acta*, 2016, **903**, 121-130.

151. R. E. Cordero-Rivera, M. Meléndez-Rodríguez, O. R. Suárez-Castillo, C. I. Bautista-Hernández, N. Trejo-Carbajal, J. Cruz-Borbolla, L. E. Castelán-Duarte, M. S. Morales-Ríos and P. Joseph-Nathan, *Tetrahedron: Asymmetry*, 2015, **26**, 710-720.
152. C. M. Cerda-García-Rojas, M. A. Bucio, S. B. González, H. A. García-Gutiérrez and P. Joseph-Nathan, *Tetrahedron: Asymmetry*, 2015, **26**, 136-140.
153. E. Santoro, G. Mazzeo, A. G. Petrovic, A. Cimmino, J. Koshoubu, A. Evidente, N. Berova and S. Superchi, *Phytochemistry*, 2015, **116**, 359-366.
154. M. A. Muñoz, A. San-Martín and P. Joseph-Nathan, *Nat Prod Commun*, 2015, **10**, 1343-1344.
155. A. Krief, M. Dunkle, M. Bahar, P. Bultinck, W. Herrebout and P. Sandra, *Journal of Separation Science*, 2015, **38**, 2545-2550.
156. P. Bultinck, F. L. Cherblanc, M. J. Fuchter, W. A. Herrebout, Y.-P. Lo, H. S. Rzepa, G. Siligardi and M. Weimar, *The Journal of Organic Chemistry*, 2015, **80**, 3359-3367.
157. C. Casero, F. Machín, S. Méndez-Álvarez, M. Demo, Á. G. Ravelo, N. Pérez-Hernández, P. Joseph-Nathan and A. Estévez-Braun, *Journal of Natural Products*, 2015, **78**, 93-102.
158. C. Bustos-Brito, M. Sánchez-Castellanos, B. Esquivel, J. S. Calderón, F. Calzada, L. Yépez-Mulia, P. Joseph-Nathan, G. Cuevas and L. Quijano, *Journal of Natural Products*, 2015, **78**, 2580-2587.
159. Z. Wang, J. Chen, L. Li, Z. Zhou, Y. Geng and T. Sun, *Journal of Molecular Structure*, 2015, **1097**, 61-68.
160. P. G. Rodríguez Ortega, M. Montejo, F. Márquez and J. J. López González, *Journal of Molecular Graphics and Modelling*, 2015, **60**, 169-179.
161. M. Sánchez-Castellanos, M. A. Bucio, A. Hernández-Barragán, P. Joseph-Nathan, G. Cuevas and L. Quijano, *Chirality*, 2015, **27**, 247-252.
162. P. G. R. Ortega, M. Montejo and J. J. L. González, *ChemPhysChem*, 2015, **16**, 342-352.
163. P. G. Rodríguez Ortega, M. Montejo, F. Márquez and J. J. López González, *ChemPhysChem*, 2015, **16**, 1416-1427.
164. C. Merten, V. Smyrniotopoulos and D. Tasdemir, *Chemical Communications*, 2015, **51**, 16217-16220.
165. Y. Yaguchi, A. Nakahashi, N. Miura, T. Taniguchi, D. Sugimoto, M. Emura, K. Zaizen, Y. Kusano and K. Monde, in *Importance of Chirality to Flavor Compounds*, American Chemical Society, 2015, vol. 1212, ch. 3, pp. 35-56.
166. S. Chatterjee, S. Olsen, E. W. Blanch and F. Wang, *The Journal of Physical Chemistry B*, 2018, **122**, 2841-2850.
167. V. Raghavan, J. L. Johnson, D. F. Stec, B. Song, G. Zajac, M. Baranska, C. M. Harris, N. D. Schley, P. L. Polavarapu and T. M. Harris, *Journal of Natural Products*, 2018, **81**, 2654-2666.
168. V. Profant, A. Jegorov, P. Bouř and V. Baumruk, *The Journal of Physical Chemistry B*, 2017, **121**, 1544-1551.
169. P. Fagan, L. Kocourková, M. Tatarkovič, F. Králík, M. Kuchař, V. Setnička and P. Bouř, *ChemPhysChem*, 2017, **18**, 2258-2265.
170. G. Pescitelli and T. Bruhn, *ChemPhysChem*, 2017, **18**, 2549-2551.
171. Í. H. Calisto, M. Furlan, E. W. Blanch and J. M. Batista, *Vibrational Spectroscopy*, 2017, **91**, 136-140.
172. P. L. Polavarapu, C. L. Covington, K. Chruszcz-Lipska, G. Zajac and M. Baranska, *Journal of Raman Spectroscopy*, 2017, **48**, 777-777.

173. A. F. Monteiro, J. M. Batista, M. A. Machado, R. P. Severino, E. W. Blanch, V. S. Bolzani, P. C. Vieira and V. G. P. Severino, *Journal of Natural Products*, 2015, **78**, 1451-1455.
174. M. E. F. Pinto, J. M. Batista, J. Koehbach, P. Gaur, A. Sharma, M. Nakabashi, E. M. Cilli, G. M. Giesel, H. Verli, C. W. Gruber, E. W. Blanch, J. F. Tavares, M. S. d. Silva, C. R. S. Garcia and V. S. Bolzani, *Journal of Natural Products*, 2015, **78**, 374-380.
175. M. Roman, K. Chruszcz-Lipska and M. Baranska, *Journal of Raman Spectroscopy*, 2015, **46**, 1041-1052.
176. J. M. Batista, B. Wang, M. V. Castelli, E. W. Blanch and S. N. López, *Tetrahedron Letters*, 2015, **56**, 6142-6144.